UC Riverside

UC Riverside Electronic Theses and Dissertations

Title

Genetic and Environmental Causes of Obesity and Their Impact on Hypothalamic Function and Pituitary Plasticity

Permalink

https://escholarship.org/uc/item/1j07c84v

Author

Ruggiero, Rebecca Elizabeth

Publication Date

2023

Copyright Information

Peer reviewed|Thesis/dissertation

UNIVERSITY OF CALIFORNIA
RIVERSIDE

Genetic and Environmental Causes of Obesity and Their Impact on Hypothalamic
Function and Pituitary Plasticity

A Dissertation submitted in partial satisfaction
of the requirements for the degree of

Doctor of Philosophy

in

Biomedical Sciences

by

Rebecca E. Ruggiero

September 2023

Dissertation Committee:
        Dr. Djurdjica Coss, Chairperson
        Dr. Sika Zheng
        Dr. Iryna Ethell

The Dissertation of Rebecca E. Ruggiero is approved:

_____

_____

_____

                                                         Committee Chairperson

University of California, Riverside

ACKNOWLEDGEMENTS

"Science is a collaborative enterprise, spanning the generations. When it permits us to

see the far side of some new horizon, we remember those who prepared the way – seeing

for them also."

-Carl Sagan

The work in this dissertation would not be possible without the support of several people

involved:

To my advisor, Dr. Djurdjica Coss- Thank you for your unwavering support and

guidance these past five years. You have taught me to be a strong, mindful and

independent scientist. Without all that you have provided, I wouldn't be the scientist that

I am today.

To my Dissertation Committee, Dr. Sika Zheng and Dr. Iryna Ethell- Thank you for

your support and for always challenging and encouraging me in our committee meetings.

The work in Chapter Two would not be possible without the expertise and guidance from Dr. Sachiko Haga-Yamanaka, for advice on behavioral experiments and Dr. Nicholas DiPatrizio, for utilization of feeding chambers that helped characterize our phenotype and set a trajectory for this work.

In Chapter Three, I would like to acknowledge Dr. Brandon Le, for Bioinformatics help and expertise that helped push this project forward.

The work in Chapter Four would not be possible without the guidance, technical expertise and direction of Dr. Meera Nair and my advisor, Dr. Djurdjica Coss. To Dr. Jiang Li, thank you spearheading the project and for our technical discussions and collaboration.

Various colleagues have contributed to the success and experiments documented in this dissertation. Thank you to Pedro Villa, Dr. Nancy Lainez, Sarah Aby Hijleh, Bryant Avalos, Yuxin He, Xinru Qiu. Thank you to my friends and fellow-cohort members, Dr. Stefanie Sveiven, Samantha Sutley-Koury and Jeffery Koury, for your scientific advice, discussion and support that aided in the success of the experiments in this dissertation.

Lastly, I would like to acknowledge the input and guidance of faculty members that have been fruitful in my academic career and in the development of me as a scientist. Thank you to the members of my qualifying exam and guidance committee: Drs. Sika

Zheng, Sachiko Haga-Yamanaka, Marcus Kaul, Erica Heinrich, and Nicole Zur Nieden.
Thank you to Drs Meera Nair and Emma Wilson who were additional mentors in my
PhD training, from whom I have learned so much over the years. Your support and
guidance have aided in me becoming the scientist that I am today.

Acknowledgement of previous publications.

The text of this dissertation, in part, is a reprint of published material as it appears in:

1. Chapter Two:

Increased body weight in mice with *Fragile X messenger ribonucleoprotein 1* (*Fmr1*)
gene mutation is associated with hypothalamic dysfunction, August 2023, Scientific
Reports. The corresponding author, Djurdjica Coss, directed and supervised the research
in this chapter.

2. Chapter Four:

Sexual dimorphism in obesity is governed by RELMα regulation of adipose macrophages
and eosinophils, May 2023, eLife. The co-corresponding authors, Djurdjica Coss and
Meera Nair directed and supervised the research in this chapter.

DEDICATION

To my grandfather, Ralph Ruggiero

Thank you for instilling the love, passion, and curiosity for science in me at a young age.

To my husband, Troy Ruff

Thank you for always believing in me and for being my constant support system. You saved me from a dark and uncertain time in my life and always encouraged me to be my best. This dissertation wouldn't be possible without your support.

ABSTRACT OF THE DISSERTATION

Genetic and Environmental Causes of Obesity and Their Impact on Hypothalamic
Function and Pituitary Plasticity

by

Rebecca E. Ruggiero

Doctor of Philosophy, Graduate Program in Biomedical Sciences
University of California, Riverside, September 2023
Dr. Djurdjica Coss, Chairperson

Obesity is a chronic disease that is increasingly becoming a global public health concern. Obesity is associated with type 2 diabetes, cardiovascular disease, stroke and endocrine abnormalities. In addition, there are sex differences in obesity mediated pathologies, such as obese men are more at risk for developing metabolic syndrome and cardiovascular disease than obese women. The hypothalamus regulates a wide variety of homeostatic processes, including food intake and energy expenditure, which are tightly regulated in order to maintain proper energy homeostasis.

Genetic causes of obesity are largely hypothalamic in origin, however obesity is multifactorial, consisting of both genetic and environmental components that contribute to the steadfast increase in its prevalence. In addition, the hypothalamus regulates the pituitary gland, an endocrine organ that is responsible for the synthesis and secretion of hormones that are important in the regulation of basal metabolism, reproduction and

stress, all of which are dysregulated in obese patients. This work aims to elucidate genetic and environmental causes in hypothalamic and pituitary dysfunction in obesity.

Our studies identified a new genetic target, fragile X messenger ribonucleoprotein 1 (FMR1) in the regulation of energy expenditure in the hypothalamus and etiology of FMR1-linked obesity in mice. We proposed that FMR1 is critical in the regulation of pro-opiomelanocortin (POMC) neuron function in the regulation of food-foraging locomotor activity. We also investigated the effects of diet-induced obesity, as diet is a main environmental factor in obesity, in pituitary gland homeostasis. We determined that diet-induced obesity alters pituitary plasticity, primarily in somatotrope and lactotrope populations that secrete growth hormone (GH) and prolactin, respectively, altering downstream hormone production. In a separate study, we investigated sex differences in diet-induced obesity pathogenesis and demonstrated that macrophage secreted protein, resistin-like molecule alpha (RELMα), critically protects females against diet-induced obesity. Collectively, these studies implicate a new genetic target in hypothalamic regulation of energy homeostasis and that diet-induced obesity alters pituitary plasticity and hormone production, which could explain endocrine dysfunction in obesity.

TABLE OF CONTENTS

LIST OF FIGURES AND TABLES

CHAPTER ONE:

Introduction to genetic and environmental causes of obesity and their impact on the hypothalamus and pituitary gland

1.1 The Obesity Epidemic: a costly and deadly disease

Obesity is a chronic disease that is increasingly becoming a global public health concern. In the United States (U.S.) and worldwide, obesity is also associated with type 2 diabetes, heart disease, stroke, and some types of cancers, all of which are the leading causes of death. Over 50% of the global adult population will either become obese or overweight by 2030 [1]. In the U.S., over 60% of population are overweight, and over 33% are obese. The increase in obesity leads to significant economic burden of $173 billion yearly in the US [2]. The obesity epidemic has drastically increased in the last couple of decades and correlates with change in our environment and lifestyle including western diet, physical inactivity, sedentary lifestyle and lack of sleep [3, 4].

Obesity is a complex disease, arising from genetic and environmental contributions. Genetic variants in several genes or a single gene mutation can contribute to obesity by increasing huger and food intake, leading to dysregulated energy homeostasis. In addition, environmental changes and social determinants of health (SDOH), such as the condition in which an individual works, lives and learns, affect chronic disease outcomes and risks, including obesity. Racial, ethnic, socioeconomic groups, as well as physical and mental disabilities influence obesity.

Obesity-mediated pathologies result from an imbalance between energy intake and expenditure, leading to an accumulation of excess adipose tissue. The hypothalamus and pituitary gland are key components of the central nervous and endocrine systems that play a critical role in the regulation of energy homeostasis and metabolism and are sites of dysregulation in obesity.

Therefore, it is critical to understand the genetic and environmental contributors that give rise to disease progression and contribute to hypothalamic and pituitary gland dysfunction.

1.2 The Hypothalamic-Pituitary Axis

The hypothalamus functions in conjunction with the pituitary gland through the hypothalamic-pituitary axis. This axis contains intricate endocrine loops with a central role in maintaining homeostasis by integrating physiological and endocrine inputs with neuronal and hormonal outputs. The hypothalamus is a small area of the brain located underneath the thalamus. Among other functions, the hypothalamus functions as a complex neuroendocrine circuit, comprised of several nuclei containing neurons that produce a number of neuropeptides and neurohormones that are important for a variety of homeostatic processes, such as thermoregulation, food intake, energy expenditure, circadian rhythm and reproduction [5].

Hypothalamic neuronal cell bodies, located in different nuclei in the hypothalamus, synthesize a variety of hormones. Thyrotropin-releasing hormone (TRH), gonadotropin releasing hormone (GnRH), growth hormone-releasing hormone (GHRH) and corticotropin releasing hormone (CRH) are hormones that are produced and secreted from their respective neuronal populations and travel through an intricate hypophyseal portal system that is located at the base of the hypothalamus and connects to the anterior pituitary gland, in order to regulate pituitary function. In addition to hormones, several

other nuclei in the hypothalamus produce and secrete neuropeptides that are important in the regulation of food intake and energy expenditure. Neuropeptide Y (NPY), Agouti-related peptide (AgRP), pro-opiomelanocortin (POMC) and orexin are produced and secreted from their respective neuronal cell bodies in the arcuate (ARC) nucleus of the hypothalamus and act as the major control center in the hypothalamus in regulating energy homeostasis. These ARC neuronal populations are located near the median eminence (ME), which possess special vascularized arrangements of endothelial capillary cells, which allow them to sense nutrient signals coming from the periphery. Disruptions in the production and secretion of these neuropeptides are well characterized examples of monogenic and polygenic obesity, which will be described later in this text.

The pituitary gland is the master endocrine gland and plays a critical role in physiological homeostasis by integrating peripheral signals from the hypothalamus to regulate synthesis and secretion of pituitary hormones into the circulation. The pituitary gland comprises of the anterior (adenohypophysis) and posterior (neurohypophysis) lobes. There are six principal hormones that are synthesized and secreted by specialized cells of the anterior pituitary: prolactin, thyroid-stimulating hormone (TSH), adrenocorticotropin (ACTH), growth hormone (GH), luteinizing hormone (LH) and follicle-stimulating hormone (FSH). Synthesis and secretion of pituitary hormones are regulated at the level of the hypothalamus by the hypothalamic releasing hormones.

1.3 Sex differences in obesity-mediated pathologies

Obesity is state of chronic inflammation and increased adiposity. Obese adipose tissue is characterized by infiltration of pro-inflammatory macrophages, causing inflammation [5, 6]. This increase in macrophage infiltration is a consequence of increased adiposity and exposure to free fatty acids that are present in high fat diets (HFD). In humans and mice, male and females differ in their composition of their fat depots, as well as obesity-associated diseases. Males preferentially accumulate fat in visceral adipose tissue, whereas females accumulate their fat mass in subcutaneous adipose tissue. The accumulation of visceral adipose tissue in males has negative consequences for metabolic health, whereas accumulation of subcutaneous adipose tissue in females is thought to be protective [7]. Visceral depots contain a higher density of infiltrating macrophages and pro-inflammatory cytokines than do subcutaneous depots, suggesting that obese males are more likely to suffer from chronic inflammation and negative effects of metabolism, than females [8-10]. In addition, this increase in visceral adiposity in males has been highly correlated with increased cardiovascular disease, type 2 diabetes and metabolic syndrome. Since visceral adiposity is associated with metabolic syndrome, differential fat accumulation may explain why males have a higher propensity for obesity-mediated pathologies.

1.4 Genetic contributions to obesity

Twin studies revealed that the hereditability of body mass index (BMI) is between 40-70% [11]. Genetic contribution to obesity can be classified as: monogenic and polygenic obesity. Monogenic obesity is caused by mutations of a single gene, typically causing severe early onset-obesity. These mutations account for about 10% of obese patients with known genetic causes. Polygenic obesity, also known as "common obesity", is associated with single nucleotide polymorphism of 244 genes cited so far in mice and 253 quantitative trait loci in humans [4, 12]. While common, polymorphic variants have a modest effect in obesity, in comparison to monogenic obesity. Genome Wide Association Studies (GWAS) have been instrumental in identifying different variants that are associated with susceptibility to obesity [13-14]. Interestingly, many genes associated with obesity are involved in neural function, specifically in pathways that regulate appetite, food intake and energy homeostasis [13-14]. Most notable gene mutations in monogenic obesity are mutations in the leptin-melanocortin circuitry, including leptin (LEP), leptin receptor (LEPR), pro-opiomelanocortin (POMC) and melanocortin-4-receptor (MC4R), a circuit that is important in modulating mammalian appetite and energy expenditure. These were first identified in mice. In addition to genes involved in feeding circuitry, mutations in genes that have pleiotropic effects and cause syndromes are also associated with obesity. These syndromes that are associated with obesity include Prader-Willi syndrome (PWS), Bardet-Biedel syndrome (BBS), and Fragile X syndrome (FXS) are associated with obesity.

To study obesity, animal models have been exposed to high fat diet. However, different inbred mouse strains respond differently to diet. Strains including A/J, FBV/NJ and BALB/cJ strains are resistant to diet-induced obesity (DIO), whereas C57BL/6J strains gain weight [15-16]. In particular, the C57BL/6J mouse strain is a good model of human metabolic syndrome, because it develops obesity, hyperinsulinemia, hyperglycemia and hypertension when given *ad libitum* access to high fat diet (HFD) [17-19]. The C57BL6/J mouse strain exhibits slightly worse metabolic parameters in response to long HFD exposure due to mutation of the nicotinamide nucleotide transhydrogenase (*Nnt*) gene, versus the C57BL/6N strain [20]. Comparison on genetic makeup of these different strains may lead to the identification of additional genes that contribute to obesity.

1.5 Leptin (LEP) and leptin receptor (LEPR)

Leptin is an adipokine that is expressed, produced and secreted by white adipose tissue in proportion to fat mass [21]. Leptin is a product of the obese (ob) gene. Following synthesis and secretion from adipocytes in white adipose tissue, leptin crosses the blood-brain barrier and binds to its receptor, the leptin receptor (LEPR) in order to regulate body mass via negative feedback mechanisms between adipose tissue and the hypothalamus. Leptin also regulates food intake, energy expenditure and reproductive function and plays a role in proinflammatory immune responses, lipolysis and angiogenesis [22-23].

The role of leptin in obesity was identified in studies of severely obese ob/ob mice, which harbor mutation in the LEP gene, resulting in the complete lack of circulating leptin [24]. Mice deficient in leptin triggered other comorbidities aside from obesity, including hyperphagia, hyperinsulinemia, corticosterone excess and infertility [24]. The leptin receptor is encoded by the diabetes (db) gene and when deleted in db/db mice, are unresponsive to endogenous or exogenous leptin [25-28].

Leptin is essential for the regulation of satiety and energy balance in the melanocortin circuitry. Leptin regulates satiety by stimulating the expression of anorexigenic neuropeptides, pro-opiomelanocortin (POMC) that is processed to alpha-melanocyte stimulating hormone (aMSH). Leptin inhibits orexigenic neuropeptides, neuropeptide Y (NPY), agouti-related peptide (AgRP) and orexin [29-30]. When bound to its receptor on these neuronal populations in the arcuate (ARC) nucleus of the hypothalamus, it decreases food intake. In addition to leptin's role in modulating neuropeptide release, leptin has been shown to modulate innervation of these neuronal populations. Synaptic density of NPY/AgRP and POMC neurons differ between ob/ob and wild-type mice, and leptin treatment normalizes synaptic density hours before affecting food intake, suggesting that leptin can also act by modulating neuronal plasticity in the hypothalamus [31-32].

Recent studies suggested that leptin's anorexigenic effects are not brain region specific. Obese mice on high-fat diet (HFD) exhibit leptin resistance in the ARC and ventral tegmental area (VTA) while the lateral hypothalamus (LH), ventromedial hypothalamus (VM) and the dorsomedial hypothalamus (DMH) stayed sensitive to leptin

[33], suggesting that the ARC and VTA are leptin-responsive areas in the brain. In addition, lentiviral downregulation of the Ob gene in the ARC promoted diet-induced obesity in rats, demonstrating that the ARC has a role in leptin resistance in obesity [34].

Monogenic forms of childhood obesity due to mutations (point mutations, frameshift mutations and nonsense mutations) in the leptin gene result in congenital leptin deficiency, leading to defects in synthesis and/or secretion of leptin [35]. Individuals carrying one functional copy of the LEP gene exhibit diminished serum leptin levels and show normal birthweight followed by rapid weight gain, hyperphagia, hyperinsulinemia, immune dysfunction and hypogonadotropic hypogonadism [36-37]. A total of 67 congenital leptin deficiency cases have been identified, including 39 cases of frame-shift mutations, 20 missense mutation carriers and three individuals with nonsense mutations [38].

In patients and mice with diet-induced obesity, leptin expression and secretion are high, as these two parameters are correlated with body fat and adipocyte size [39-40]. Hyperleptinemia, and the inability for elevated leptin to sufficiently regulate appetite is coined "leptin resistance." Leptin resistance occurs due to reduced LEPR expression or disturbed leptin signaling [41]. Although loss of receptor function contributes to this resistance, more common mechanisms include defects in signaling pathways that regulate leptin signaling in addition to decreased transport of leptin across the blood-brain barrier [41-42].

1.6 The Melanocortin System

The melanocortin system is found in several nuclei of the hypothalamus and refers to a set of neural circuits and neuropeptide products that play a central role in the regulation of food intake and energy expenditure in mammals. This system is comprised of pro-opiomelanocortin (POMC) neurons, agouti-related peptide (AgRP)/neuropeptide Y (NPY)-expressing neurons and melanocortin receptors. POMC and AgRP neuronal cell bodies are found in the arcuate (ARC) nucleus of the hypothalamus. The ARC is located in the mediobasal hypothalamus and forms a morphological and functional entity with the median eminence. The ARC is an important nutrient sensor and integrates nutrient-state communicating signals from the periphery, which then act on AgRP/NPY or POMC neurons to facilitate changes in food intake and energy expenditure.

POMC and AgRP/NPY neurons have classically been shown to act in opposition to modulate appetite and energy expenditure [43]. POMC neurons are anorexigenic and when stimulated, POMC is processed into neuropeptide products that act on second-order neurons in the ventromedial hypothalamus (VMH) to induce satiety and the melanocortin-4- receptor (MC4R)-expressing neurons in the paraventricular nucleus (PVN) to increase energy expenditure. Conversely, AgRP/NPY neurons are orexigenic. AgRP that is released from AgRP/NPY neurons acts as a competitive antagonist of the MC4R receptor in PVN, where it inhibits energy expenditure and simulates rapid food intake. AgRP/NPY also sends projections to the lateral hypothalamus (LH), another major orexigenic nucleus in the hypothalamus, however the mechanisms by which AgRP neurons control LH neuronal subsets remain unresolved. AgRP/NPY neurons also

provides direct inhibitory input to POMC neurons via GABAergic receptors, to modulate neuronal activity and keep the regulation of the circuitry in a tight loop.

It has been well characterized that mutations in genes that make up the melanocortin circuitry lead to obesity in humans and mice. In 2020, the U.S. Food and Drug Administration (FDA) approved the MC4R agonist, setmelanotide, for chronic weight management in adult and pediatric patients with obesity due to mutations in the POMC and MC4R gene [44]. Briefly, we describe in detail mutations in this circuitry and their role in obesity pathologies.

1.7 Pro-opiomelanocortin (POMC)

Pro-opiomelanocortin (POMC) is a prohormone that is post-translationally processed into active neuropeptide hormones, melanocortin's (α- and γ melanocyte-stimulating hormones (MSHs)), endorphins (β-endorphin) in the hypothalamus and corticotropins (adrenocorticotropic hormone (ACTH)) in the anterior pituitary gland. POMC is highly expressed in the pituitary gland and the hypothalamus. Tissue-specific differences in POMC processing are important in neuropeptide production and downstream function. For example, ACTH is the major product in the anterior pituitary gland, while αMSH, γMSH and β-endorphin are the major products in the hypothalamus and intermediate lobe of the pituitary gland. ACTH production and secretion from the pituitary gland acts on the adrenal glands in order to facilitate cortisol production and secretion, which is important in the response to stress and regulation of glucose levels. Conversely,

melanocortin and endorphin neuropeptide products from POMC neurons in the hypothalamus are important in the stimulation of satiety and regulation of energy expenditure.

Processing of POMC prohormone into mature peptides is accomplished by a series of steps and cellular locations, involving the endoplasmic reticulum (ER), golgi, trans-golgi network and secretory granules. Specifically, POMC is cleaved and N-linked glycosylated in the ER, phosphorylated in the golgi, and broken down into peptides via peptidase activity in the trans-golgi and in secretory granules [45]. Two major endopeptidases, prohormone convertase 1/3 (PC1/3) and prohormone convertase 2 (PC2) are important in the processing of POMC into α-MSH, γ-MSH and ACTH [46]. Carboxypeptidase E is important in processing POMC to β-Endorphin that further undergoes additional post-translational modifications. Tissue-specific processing of POMC not only depends on location and expression of POMC but also specificity of prohormone convertase expression. For example, single-nucleus RNA sequencing of neurons in the mouse hypothalamus found that most POMC-positive cells express PC1/3 and PC2, while a smaller number express only PC1/3 [47-48]. Corticotropes in the anterior pituitary gland that process POMC into ACTH express PC1/3, whereas melanotropes in the intermediate lobe express both PC1/3 and PC2 to process ACTH into CLIP and a-MSH, thus specificity of endopeptidases are important in driving tissue-specific POMC processing.

POMC neuronal cell bodies are centrally located in the ARC of the hypothalamus, which is an important nutrient sensing area of the brain, and these neurons, along with

AgRP/NPY neurons are tightly regulated to maintain energy homeostasis. Nutrients, hormones and neurotransmitters have been studied and shown to play a role in modulating POMC neuronal activity and regulation of satiety and energy expenditure. The adipokine leptin, activates POMC neurons and acts on pre-synaptic GABAergic neurons, such as AgRP/NPY neurons, to reduce inhibitory tone to POMC neurons, leading to decreased food intake [49]. Leptin receptor (LEPR) deletion on POMC neurons throughout development has been shown to lead to mild obesity and hyperglycemia in mice, however deletion of the receptor from POMC neurons in adult mice doesn't lead to changes in body weight, food intake, or energy expenditure [50], suggesting that POMC neurons are not a direct target of leptin in obesity. Leptin has also been shown to depolarize POMC neurons and decrease GABA-tone onto POMC neurons [51]. Insulin has been shown to modulate POMC neuronal activity in the regulation of glucose metabolism, however its effects are controversial. Insulin has been classically thought to inhibit POMC neurons [52], however a recent report demonstrated that activation of insulin receptor on a subset of POMC neurons increases their firing rate [53]. Ghrelin, a hormone produced by enteroendocrine cells of the GI tract in response to hunger, strongly inhibits POMC neuronal activity, indirectly by activating AgRP/NPY neurons, which sends GABAergic synapses to POMC neurons [51, 54].

A majority of POMC neurons are found in the ARC of the hypothalamus, where they regulate satiety and energy expenditure. A small population (~10%) of POMC neurons are also found in the nucleus of the solitary tract (NTS) in the brainstem. Both neuronal populations are important in the regulation of satiety. Whole brain mapping studies

demonstrate distinct inputs to ARC POMC neurons and NTS POMC neurons. ARC POMC inputs primarily receive projections from AgRP neurons, as well as the brain stem and areas of the forebrain, whereas POMC NTS neurons receive inputs from other areas of the brainstem, such as the pons and medulla and visceral afferents from cholecystokinin neurons in the gastrointestinal tract [55-56]. While both populations regulate satiety, their mode of suppressing feeding behavior occurs at different time scales. Pharmacogenetic methods activating both neuronal populations individually demonstrate that ARC POMC neurons required chronic stimulation to suppress food intake, whereas NTS POMC neurons produced an acute inhibition of feeding behavior upon stimulation [57], suggesting that both neuronal populations act differentially to regulate satiety.

While both neuronal populations regulate satiety, ARC POMC neurons are the primary drivers in changes in energy expenditure. Recent single-cell RNA sequencing (scRNA-seq) have indicated that ARC POMC are functionally heterogeneous and could have various sub-populations with distinct functions, however further work needs to be done to better understand and characterize this heterogeneity [58]. In addition, neuronal projections from ARC POMC are the main signaling unit for POMC-derived peptides in the adult rodent brain. ARC POMC neuronal projections extend fibers to multiple regions in the brain, including the PVN, LH, NTS, central amygdala, periaqueductal grey, dorsal raphe nucleus and ventral tegmental area [59].

Humans and mice with loss of function mutations on the POMC gene are obese. *POMC* gene mutations leading to deficiency in humans presented severe, early onset

obesity associated with hyperphagia and altered skin and hair pigmentation [60-61]. Heterozygous loss of function and point mutations on the *POMC* gene predisposes obesity in humans [61-62]. In vivo mouse studies show that intracerebroventricular (i.c.v.) injection of MC4R agonists, such as a-MSH, blocks feeding, and antagonists, stimulate feeding [63]. When treated with a stable aMSH agonist, POMC mutant mice lost more than 40% of their excess body weight [60, 64]. Postnatal ablation of POMC neurons in mice lead to progressive obesity characterized by decreased energy expenditure [65]. The primary effects of POMC-derived neuropeptides on feeding and body weight are mediated by a-MSH acting on MC4R, and while POMC has been known to be a key regulator in the melanocortin system, other players in this circuitry have been implicated in obesity.

1.8 Agouti-Related Peptide (AgRP)

Agouti-related peptide (AgRP) is a neuropeptide produced in the ARC of the hypothalamus by AgRP/Neuropeptide Y (NPY) neurons. AgRP/NPY neurons co-express NPY and GABA and act to increase food intake and decrease energy expenditure. Similar to POMC neurons, AgRP neurons are located in close proximity to fenestrated capillaries in the median eminence, and thus have greater access to circulating hormones and nutrients to respond to these signals appropriately. Leptin and insulin inhibit AgRP neurons in order to suppress feeding in the fed state, whereas ghrelin, which is a hormone that is secreted in proportion to stomach emptying, activates AgRP neurons to promote food intake [54, 66-67].

AgRP neuropeptide is a competitive antagonist of melanocortin receptors, melanocortin-3-receptor (MC3R) and melanocortin-4 receptor (MC4R). When AgRP binds to these receptors, it stimulates food intake and decreases energy expenditure, opposing endogenous agonist, aMSH. NPY is the most potent orexigenic neuropeptide in the brain. Intracerebroventricular injection of NPY in the brain rapidly and robustly increases acute food intake within 1 hour and when administered chronically, induces obesity due to pronounced hyperphagia [68-69]. GABA is co-released with AgRP and is also important in stimulating food intake. Starvation induced by AgRP neuron ablation could not be rescued by chronic antagonism of MC4R receptors, however delivery of Bretazenil, a GABA mimetic, restored feeding [70], suggesting a critical role for GABA in mediating food intake. Projections from AgRP/NPY neurons synapse to MC4R-expressing neurons in the PVN to induce food intake and inhibit energy expenditure. AgRP/NPY neurons also project to POMC neurons in the ARC. These projections are GABAergic inhibitory synapses in order to inhibit POMC neurons and prevent the release of aMSH, which induces energy expenditure upon binding to MC4R in the PVN. AgRP/NPY neurons also project to the lateral hypothalamus (LH) to stimulate feeding.

Different sub-populations of AgRP/NPY neurons appear to be sufficient to promote food intake but does so using redundant pathways, suggesting heterogeneity within these neuronal populations. For example, different sub-populations of AgRP/NPY neurons in the ARC are responsible for slow and fast signals to induce feeding. Feeding responses measured by designer receptors exclusively activated by designer drugs (DREADD) technology, indicate that NPY and GABA released from AgRP/NPY neurons convey fast

signals to induce feeding, whereas AgRP induces slow and prolonged feeding [71]. In addition, ablation of AgRP/NPY neurons n adult mice lead to decreased food intake and body weight, where was there were no differences in neonatal mice [72-73], suggesting compensatory pathways that modulate food intake and energy homeostasis.

Mutations in *agouti,* a gene responsible for coat color in mice, was identified to cause adult-onset obesity syndrome in 1905 [74-75]. Mouse models studying its function and role in obesity have been well-studied. Over-expression of AgRP in transgenic mice or chronic i.c.v. injection into the brain causes hyperphagia and obesity [76]. Food deprivation induces increased gene expression of AgRP and NPY, increased firing rate of AgRP neurons, stimulating appetite and food-seeking behavior [77-78].

In obese males, AgRP plasma levels were reportedly higher in comparison to nonobese men [79]. SNP studies in the human AgRP gene promoter and coding regions have been associated with resistance to obesity and type 2 diabetes [80-84]. Mutation screening in human genes has revealed some SNPs in the AgRP gene, however, is not considered a main genetic contributor to obesity.

1.9 Melanocortin 4 receptor (MC4R)

Melanocortin receptors are G-protein coupled-receptors (GPCR) that are expressed throughout the central nervous system (CNS) and other regions. There are five melanocortin receptors: MC1R, MC2R, MC3R, MC4R and MC5R. MC1R is expressed in skin and hair follicles and is important in pigmentation. MC2R is expressed in the

adrenal cortex and is important in the regulation of cortisol production. MC3R and MC4R are expressed throughout the CNS and are the main regulators of food intake and energy expenditure. These receptors also regulate sympathetic outflow, heart rate and blood pressure. MC5R is expressed widely in exocrine glands and is important in their secretion.

MC3R and MC4R are important regulators in food intake and energy expenditure, however work understanding the effects of MC3R alone suggest that this receptor isn't critical in energy homeostasis regulation [85]. However, when MC4R is knocked-out in mice alone, there is increase adiposity, hyperphagia, glucose intolerance and obesity [85], thus work on understanding the role of MC4R in energy homeostasis has been well characterized. Although MC4R is widely expressed in the CNS, the PVN, dorsomedial nucleus and preoptic areas of the hypothalamus showed greatest response to AgRP, suggesting these areas where MC4R is expressed are important in energy homeostasis [86]. In the presence of endogenous agonist, αMSH, MC4R couples to Gas to induce GPCR-mediated signaling, which when induces downstream activation of adenylate cyclase and increase production of cAMP, which is then thought to increase transcription of cFOS, leading to neuronal activity [87]. AgRP antagonizes this signaling cascade in order to increase food intake. The PVN is the primary site for food intake and energy expenditure regulation. Although it is known that MC4R activation results in decreased food intake and increased energy expenditure, the downstream mediators of this signaling pathway are unknown.

Transcription factors have been shown to be important in mediated MC4R activation as well as development. Impairment of MC4R-expressing neuronal development, has been implicated in obesity. Single-minded homolog 1 (Sim1) is a transcription factor that is important in mediating development of MC4R-expressing neurons in PVN. Loss of Sim1 in mice leads to obesity due to impaired melanocortin signaling [88]. Humans with deletion of Sim1 have also been reported to develop early onset obesity [89-90]. Melanocortin receptor accessory protein 2 (MRAP2) is also required for MC4R-expressing neuronal function and has been shown to contribute to energy expenditure regulation [91-92]. In humans, 23 *MRAP2* heterozygous variants have been identified and associated with increased obesity risk in adults and children. Overall, this suggests that MC4R and transcription factors that are important in development and neuronal function have been implicated in obesity.

Mutations in the MC4R gene are the most prevalent genetic cause of obesity, accounting for 1 to 4% of cases of obesity [93]. *Mc4r* knockout mice display pronounced hyperphagia, hyperinsulinemia, hyperglycemia and obesity [94]. In both mice and humans, loss of one copy of the *MC4R* gene results in an intermediate obese phenotype, suggesting a gene dosage effect [94]. In addition to hyperphagia in the MC4R KO mouse, these mice also have impaired energy expenditure regulation, contributing to obesity [95]. In humans, there are 376 SNPs reported in the Mc4r gene that are associated with obesity and have a role in melanocortin ligand binding, cell surface receptor expression and GPCR signaling [96]. Setmelanotide, a synthetic MC4R agonist that is currently the first and only FDA approved drug to target the MC4R pathway, can effectively reduce

appetite, leading to weight loss without any adverse cardiovascular side effects. This drug is currently used for patients who are diagnosed with a variety of obesity syndromes, such as POMC deficiency, LEPR deficiency and Bardet-Bidel syndrome [97-98].

1.10 Fat Mass and Obesity Associated (FTO) Gene

The Fat Mass and Obesity Associated (FTO) gene was the first obesity associated susceptibility gene discovered using GWAS approaches. Since its discovery, multiple SNP variants within the first intron of the FTO gene were identified to be associated with human body mass and risk of obesity in a variety of population studies [99-103].

The mouse and human FTO gene are ubiquitously expressed, however its expression is highest in the brain, in particular, the hypothalamus [104]. Because of its high expression in the hypothalamus, it was suggested to play important roles in the regulation of food intake and energy expenditure [105]. When fasting wildtype mice, FTO mRNA expression was downregulated in the hypothalamus compared to fed controls [106]. In the context of several mouse models of obesity, such as LEP KO, LEPR KO and POMC KO, along with mice with DIO, hypothalamic FTO expression did not differ significantly than in WT mice, but there were differences in mesenteric fat in obese mice [106].

Further work elucidating the role of FTO in obesity was done using FTO deficient mice, as well as FTO heterozygotes. FTO KO animals weigh 30-40% less compared to WT littermates, while FTO het mutants, had a 10% weight loss compared to WT littermates, suggesting there is a gene dosage effect. When exposed to high fat diet, FTO

KO animals exhibited reduced weight gain and reduced white adipose tissue size compared to controls, suggesting that the disruption of FTO may serve as protection against DIO [107-108]. FTO KO also exhibited elevated levels of energy expenditure unrelated to locomotor activity, suggesting that these changes made be due to mechanisms in lipolysis and thermogenesis in adipose tissue and could explain reduced weight gain and adipose tissue size. Specifically in the hypothalamus, stereotaxic and AAV approaches indicate that over-expression of FTO in the ARC resulted in decreased food intake, while knocking down FTO increased food intake in rats [109].

While its role in food intake and energy expenditure regulation has been elucidated, how FTO regulates these two processes are unknown and are currently being studied. One recent study makes mention of FTO being an upstream modulator of Stat3 expression, which is important in leptin-mediated signaling [109].

1.11 Pleiotropic syndromes leading to obesity

Pleiotropic obesity syndromes are diseases that are complex with a long list of clinical symptoms in which obesity is only one out of a wide variety of physical and developmental anomalies. There are several pleiotropic syndromes with obesity as a dominant phenotype associated with other symptoms, such as mental retardation, endocrine dysfunction, limb or facial dysmorphisms.

The genetic basis of these syndromes is complex and although the etiology of many of these syndromes are known, their relationship to obesity is not clear. In this section we will focus on three syndromes that are all implicated in obesity.

1.11.1 Prader-Willi Syndrome (PWS)

Prader-Willi Syndrome (PWS) is the most common pleiotropic syndrome leading to obesity. PWS occurs in 1 in 10,000 to 1 in 29,000, affecting both males and females equally [110]. The molecular mechanism of this syndrome is a complex, multisystem chromosomal disorder that arises due chromosomal alterations on chromosome 15. The most common genetic etiology is deletion of the PWS segment of the paternally inherited chromosome 15 [111]. The other two subtypes are maternal uniparental disomy, when the patient inherits both copes of chromosome 15 from its mother, and imprinting errors. The disease is characterized by two clinical stages. Stage 1 occurs when patients have symptoms characterized by hypotonia, decreased muscle tone, extreme floppiness and failure to thrive in infants. Stage 2 progresses after infancy and is characterized by intense hyperphagia leading to obesity. PWS patients suffer from other endocrine deficits, such as growth hormone deficiency, hypothyroidism and central adrenal insufficiency.

The source of hyperphagia in PWS patients is thought to be due to changes in the hypothalamus, primarily through dysregulated hypothalamic satiety and feeding circuitry. Work has been done implicating that hypothalamic neuropeptide production, secretion

and neurocircuitries are altered in PWS. Among the genes that are deleted in the PWS segment of chromosome 15, MAGE family member L2 (Magel2), an E3 ubiquitin-protein ligase, has been identified as one of the players responsible for a majority of PWS symptoms, such as impaired growth, increased adiposity, obesity and altered metabolism.

Magel2 has been shown to be highly expressed in the hypothalamus. Unbiased proteomics studies of hypothalamic lysates of Magel2 KO mice showed significant decrease in secretory granule proteins, Scg2, Chgb as well as prohormone convertases, Pcsk1 and Pcsk2, which are important in processing POMC prohormone [112]. Neuropeptide production and release, such as αMSH, GnRH and oxytocin were significantly decreased in Magel2 KO mice. In addition, Magel2KO mice were shown to have altered POMC neuronal activity and decreased neuronal PVN projections, further suggesting that satiety regulation by POMC neurons is altered in PWS [113-114].

Functional magnetic resonance imaging (fMRI) studies in the hypothalamus and cortex of PWS patients reveal abnormal brain networks engaged in physiological control of eating as well as the motivational component of eating [115-116]. In a separate study, structural MRI scanning of PWS patients with age-matched controls indicated that all hypothalamic nuclei and volume were significantly smaller with impaired satiety score being correlated with hypothalamic white matter structural connectivity dysregulations [117]. αMSH levels in serum were also reported to be significantly decreased in PWS patients compared to obese and lean controls [118]. Overall, these studies implicate that the hypothalamic satiety center, composed of POMC neurons and processing to αMSH, is

altered in PWS patients and could explain the intense hyperphagia that is present in these patients.

1.11.2 Bardet-Bidel Syndrome (BBS)

Bardet-Bidel Syndrome (BBS) is an autosomal recessive disorder that affects multiple body systems, with obesity being a primary symptom alongside intellectual disability. The disease is rare, affecting 1 in 140,000 to 1 in 160,000 newborns. Several mutations (nonsense, deletions, missense, insertions/duplications) have been documented in all 12 BBS proteins, leading to the development of different clinical presentations of this disease, suggesting high genetic heterogeneity. Clinical findings associated with this disease include retinal degeneration, polydactyly, obesity, intellectual disability, hypertension and male and female reproductive tract abnormalities [119-120]. BBS patients have obesity that ranges from mild to severe and is reversible with proper diet and exercise. Rapid weight gain in these patients occurs during the first year of life due to extreme hyperphagia but there is no difference in metabolic rate between BBS patients and lean and obese controls, however there is decreased locomotor activity in BBS patients [121].

Not much is known or studied regarding how the hypothalamus is implicated in patients with BBS, however it is thought to play a role since BBS patients present with extreme hyperphagia and obesity. One study looked at the BBSome, a protein complex that is composed of seven highly conserved BBS proteins and one novel protein that is

important in primary cilium biogenesis, and how it is implicated in POMC and AgRP neurons. Targeted disruption of BBS1, the main core protein of the BBSome, in POMC and AgRP neurons separately lead to increase body weight, hyperinsulinemia, increased food intake, impaired glucose tolerance and adiposity in mice [122]. In a separate in vitro study, iPSC-derived hypothalamic neurons that had mutations in the BBSome complex had significant decreases in POMC expression and decreased production of neuropeptides [123]. These studies suggest that hypothalamic feeding circuitry is disrupted in BBS, leading to changes in food intake and consequently body weight, however more work needs to be done to understand the molecular mechanisms the BBSome complex has on AgRP and POMC neuronal function.

1.11.3 Fragile X Syndrome (FXS)

Fragile X Syndrome (FXS) is the most common monogenic cause of intellectual disability and autism. FXS is caused by CGG trinucleotide repeat expansion of the 5' untranslated region (UTR) of the fragile x messenger ribonucleoprotein 1 (FMR1) gene, which results in results in epigenetic silencing and thus, lack of its protein product, FMRP.

FMRP is an mRNA binding protein that plays a role in protein translation. mRNA metabolism and mRNA transport [124]. FMRP is encoded by the FMR1 gene and is ubiquitously expressed but its expression is highest in the brain [125]. Given the high expression of FMRP in the brain and the presence of intellectual disability and

impairment with those affected with FXS, targets of FMRP were investigated and involved in brain connectivity. Specifically, levels of neurotransmitters and their receptors have been examined in FXS mouse models in the cortex and hippocampus and determined a decrease in several GABA$_A$ receptor subunits, implicating a decrease in inhibitory signaling in FXS [126]. In addition, FMRP has also been shown to regulate neuronal excitability through impaired inhibition and altered neural circuits, leading to hyperexcitability [126]. While the role of FMRP in the regulation of cortical circuits has been addressed, the role of FMRP in the hypothalamus remains understudied.

Patients with FXS are more obese and the etiology of their increased prevalence with obesity is unknown. National survey data from 884 families indicate that the rate of obesity in adults with FXS is like the general population, while male children and adolescents with FXS having higher rates of obesity (31%) when compared to their developing same-aged peers [127]. Another recent longitudinal study conducted by Choo et al on 1233 FXS patients of different age groups found that FXS adults had increased BMI, supporting obesity as a clinical phenotype of FXS patients [128].

Very little work has been done in trying to elucidate the mechanism behind obesity in FXS patients. In particular, the role of FMR1 gene in the hypothalamus has not been studied and if hypothalamic dysfunction contributes to obesity in FXS patients. How FMR1 gene regulates food intake and energy expenditure and if the lack of FMR1 leads to hypothalamic dysfunction and increased body weight is addressed in Chapter two of this dissertation.

1.12 Environmental contributions to obesity

In addition to genetic contributions to obesity, rates of obesity are rising due to environmental factors such as diet, increased sedentary lifestyle, socioeconomic status, stress and exposure to endocrine disrupting chemicals (EDC). Modern lifestyle encourages individuals to live in an obesogenic environment, an environment that encourages individuals to eat more and exercise less. While the list goes on, this section will focus on three environmental contributors to obesity and how hypothalamus and pituitary gland are impacted.

1.13 Diet

Diet is one of the main environmental factors that influence obesity development. The link between diet and obesity is complex and is multidimensional, involving other aspects of lifestyle, such as physical activity, feeding times, smoking, alcohol consumption and genetic predispositions. Poor diet quality and increased exposure to foods high in fat and sugar can be due in part to populations that reside in food deserts, places where there is a scarcity of affordable, healthy food options. Food deserts are found in low-income communities, where residents may face additional barriers to access to healthier foods such as, transportation and financial constraints. Food deserts have been positively linked to obesity rates in the U.S. Switching from a non-food desert to a food desert region increases the odds of obesity to 30% alone, suggesting diet is an important contributor to

obesity, however, is multifactorial, and socioeconomic status is also an important variable to consider in diet-induced obesity [129].

The World Health Organization (WHO) published dietary recommendations, suggesting a diet focused on fruits, vegetables, whole grains and nuts while limiting sugar and fat consumption to 1%-30%, respectfully. Although these recommendations have been published, there exists several barriers to eating healthier food, such as socioeconomic status, location and eating behaviors. An accelerated lifestyle has also encouraged individuals to partake in processed foods and fast foods instead of home-cooked and prepared meals. A U.S. national survey reported that a home-consumed diet has decreased by 23% and most Americans have their calorie intake from processed foods, sit-down restaurants and fast-food restaurants [130]. Another review suggested that eating fried food four times per week gives a higher risk on developing obesity and other chronic diseases, such as type 2 diabetes, hypertension and coronary artery disease [131].

While there exists social barriers to diet-induced obesity, the question remains how diet impacts hypothalamic function and pituitary hormone production and secretion in obesity. Obesity is associated with peripheral tissue inflammation and neuroinflammation, such as hypothalamic inflammation. It has been implicated that hypothalamic neuronal function and synaptic plasticity are affected by neuroinflammation that is induced by diet-induced obesity (DIO). Hypothalamic inflammation is characterized by astrogliosis and infiltration of macrophages from adipose tissue [10, 132]. In animal models of DIO, signs of hypothalamic inflammation

are present as early as 3 days after high fat diet (HFD) consumption, occurring even before the onset of weight gain [133].

There are acute and chronic effects of HFD and how it affects hypothalamic function and feeding circuitry neurons. Acutely, DIO causes activation of pro-inflammatory cytokines, IL-1β, TNFα and IL-6, and recruitment of macrophages into the hypothalamus [17]. Saturated fatty acids from HFD trigger the activation of inflammatory signaling cascades via toll-like receptor 4 (TL4) signaling, leading to downstream nuclear factor kappa B (NF-κB) activation, leading to increased expression of inflammatory genes, such as suppressor of cytokine signaling 3 (Socs3) and pro-inflammatory cytokines [134]. Acute exposure to HFD leads to upregulated Socs3 in AgRP neurons, leading to hyperphagia and development of insulin and leptin resistance, and i.c.v. injection of unsaturated fatty acids restored leptin and insulin sensitivity in diet-induced obesity [135-136]. Chronic HFD feeding leads to changes in synaptic plasticity. Regarding feeding circuitry neurons, chronic HFD feeding impairs excitatory synaptic transmission in the ARC and decreases inhibitory synapses on POMC neuronal cell bodies [137-138]. POMC neurons are also subjected to apoptosis from chronic HFD [139]. However, since POMC neurons are heterogeneous, only partial signs of POMC neuronal alterations are observed in rodents exposed to chronic HFD. The number of POMC neurons with no spontaneous firing is increased in DIO by only 20% and chronic exposure to HFD leads to 20-50% loss of POMC-expression neurons in the ARC and decreased neuronal activity [133, 140].

In addition to damage to the hypothalamus, individuals with acquired hypothalamic obesity have damage to the pituitary gland, since the hypothalamus regulates pituitary gland hormone synthesis and secretion. This damage causes multiple hormone deficiencies in obesity. Thyrotropic, gonadotropic, somatotropic and corticotropic dysfunctions occur because of obesity-mediated pathologies in the hypothalamic-pituitary axis.

Thyroid gland function is involved in the control of thermogenesis and appetite and its dysfunction is associated with secondary changes in body weight, adiposity and resting energy expenditure independent of physical activity [141]. Obesity is linked to thyroid dysfunction. Obese patients have hypothyroidism, and this is clinically characterized with a moderate increase in thyroid-stimulating hormone (TSH) levels, due to negative feedback, which is associated with decreased thyroid hormone levels, increasing the resting energy expenditure [142-143]. Mechanisms underlying changes observed in hypothalamic-pituitary-thyroid axis in obesity are not well understood. It is not clear whether the extent of abnormalities observed in thyroid function are due to primary gland involvement, synthesis or secretion of TSH from the pituitary gland or both.

Growth hormone (GH) and insulin-like growth factor 1 (IGF-1) are important in the regulation of metabolism. GH stimulates lipolysis in adipose tissue and protein synthesis in muscle, thus decreased GH contributes to increased weight gain, adiposity and decreased muscle mass [144]. In obese patients, growth hormone (GH) secretion is blunted [145] and how GH production and secretion is dysregulated in obesity remains a mystery.

Obese patients have reproductive dysfunction. Obese males have androgen deficiency and hypogonadism due to increased visceral adiposity. Obese men also have low gonadotropins, luteinizing hormone (LH) and follicle-stimulating hormone (FSH) leading to infertility and reduced sperm count. Previous studies indicated that increased BMI and obesity are associated with the suppression of testosterone and reduced levels of sex hormone binding globulin [146-147]. Studies in humans were confirmed using rodent models demonstrating that male mice fed HFD had reduced LH, FSH, testosterone and sperm count [17].

While it is known that obesity causes hormonal deficiencies, the mechanisms behind altered hormone production and secretion are unknown. The pituitary gland is a master endocrine gland that is responsible for the production and secretion of GH, prolactin, TSH, adrenocorticotropic hormone (ACTH), LH and FSH. How diet-induced obesity impacts pituitary function, specifically hormone production and secretion are not known. Chapter three of this dissertation aims to answer this question and elucidate whether pituitary plasticity and changes in transcriptomics occurs due to chronic HFD in mice.

1.14 Stress

Stress is regulated by the hypothalamic-pituitary-adrenal (HPA) axis and the sympathetic nervous system (SNS) and is activated in acute and chronic stressful events. In response to stressors, corticotropin-releasing hormone (CRH) is secreted from neurons in the PVN and stimulates the synthesis and secretion of ACTH from the anterior

pituitary gland, which then acts on the adrenal gland in order to stimulate the production and secretion of cortisol. Stress response is characterized by acute adaptations, such as increased cognition, gluconeogenesis, lipolysis and inhibition of reproduction. When the HPA axis is chronically activated or dysregulated, it can contribute to the development of several diseases, including obesity and type 2 diabetes [148]. Disease pathology is thought to occur due to chronic exposure to stressors and subsequent prolonged secretion of glucocorticoids that can result in downstream gene expression changes that are important in the regulation of metabolism, such as adiposity, insulin resistance, hypertension, dyslipidemia and inflammation [149].

Traditional factors that are associated with obesity are related to hypercaloric, high fat diet, sedentary lifestyle and socioeconomic status (SES). Individuals with lower SES have more limited opportunities, leading to more stress and increase in stress hormone production, which can further predispose them to obesity. Dramatic effects of altered circulating cortisol levels on body weight are Cushing's syndrome, a state of hypercortisolism leading to central obesity, or Addison's disease which leads to hypocortisolism due to chronic adrenal insufficiency, leading to weight loss. In addition, increase in visceral adiposity also chronically hyper-activates the HPA axis.

The PVN is an important nucleus in the hypothalamus regarding the initiation of glucocorticoid secretion, as lesions to the PVN significantly decreased CRH and stress-induced ACTH levels [150]. The PVN receives major input from the ARC. AgRP/NPY neurons innervate CRH neurons in the PVN in order to stimulate CRH release. CRH is considered an anorexigenic signal, injection of CRH to the PVN inhibits NPY-induced

32

food intake in mice [151]. The ARC is an important sensor of glucocorticoids, as injection of glucocorticoids in the ARC resulted in hyperphagia and weight gain in rats [152]. In POMC-deficient mice, injection of corticosterone exacerbated hyperphagia, weight gain, adiposity and hyperleptinemia [153], suggesting that stress hormones have an important and functional role in the ARC and in feeding circuitry, and can be a mechanism in stress-induced obesity.

1.15 Endocrine Disrupting Chemicals (EDC)

Although obesity is largely fueled by genetic and environmental components, such as diet and stress, exposure to chemicals have been shown to have a role in its etiology. Interestingly, the current increase in obesity and other metabolic syndromes correlates with the increase in environmental chemical production and exposures of over the past few decades [154]. Endocrine disrupting chemicals (EDCs) are chemicals that mimic or interfere with actions of endocrine hormones, including estrogens, androgens, progestins, and hypothalamic and pituitary hormones. They do so by binding to or interfering with their receptors, which can disrupt signaling processes throughout the body.

EDCs or "obesogens", when in reference to obesity, are thought to be one of the factors that plays an important environmental contribution in obesity pathogenesis. EDCs are thought to pre-dispose individuals to weight gain by changing the metabolic "set point" in energy homeostasis. Some EDCs can increase the number of adipocytes or fat storage in existing adipocytes and promote obesity by shifting the balance in fat storage

versus fat catabolism [155]. Several studies show that EDCs such as, bisphenol A (BPA), tributyltin (TBT) and diethylstilbestrol (DES) can alter food intake but depend on dose and duration of the exposure [156-158].

One example of an EDC that has been largely studied in the context of obesity is BPA. BPA is a synthetic compound used to manufacturer plastics, food packaging, toys, canned foods, eyeglass lenses and medical equipment, such as tubing. BPA acts as an estrogen receptor agonist and its activity occurs through estrogen receptor alpha (ERα)-mediated signaling that leads to downstream MAPK-signaling of target genes. BPA can also act as an estradiol antagonist, preventing estrogen receptor beta (ERβ) to signal via its nuclear receptor to downstream MAPK targets [159-160].. BPA acts as an obesogen by changing early adipogenesis by modulating adipocyte hypertrophy and overexpression of lipogenic genes, such as peroxisome proliferator-activated receptor gamma (PPARγ), which has been implicated in the onset of diabetes and obesity, as well as lipoprotein lipase (LPL) and fatty acid synthase [161].

BPA exposure has been linked to changes in hypothalamic function and dysregulation of energy homeostasis in rodents. Neonatal exposure to BPA has been shown to downregulate protein levels of ERα in the ARC in adult female rats, leading to hyperphagia and metabolic syndrome [162]. Perinatal treatment of HFD-fed mice with BPA lead to sexually dimorphic changes in adulthood, primarily altered the level of expression of NPY, POMC and AgRP and decreased POMC fiber density in the PVN, suggesting that EDCs have important effects in ARC neural circuitry [163]. Lastly, BPA-exposed adult mice fed a HFD consumed more food and gained more weight than control

mice on HFD, suggesting that BPA may lead to changes in hypothalamic energy balance circuitry, leading to increased susceptibility to DIO [163].

1.16 Obesity as a chronic inflammatory state

Obesity is a state of chronic, low grade systemic inflammation and is a consequence of increased adiposity in white adipose tissue in humans and rodents [164-165]. Obese adipose tissue is characterized by the progressive infiltration of pro-inflammatory macrophages into the adipose tissue, causing inflammation [6, 164]. Macrophage number and size in adipose tissue correlates with increased adiposity in humans and mice, allowing them to become more activated and upregulate pro-inflammatory cytokine production, tumor necrosis factor alpha (TNFα), interleukin 6 (IL6) and interleukin 1 beta (IL-1β) [6,166]. Following increased adiposity in obesity, adipocytes produce monocyte chemoattractant protein-1 (MCP-1, or CCL2 chemokine), that is a ligand for CCR2 and recruits monocytes, leading to macrophage activation [167-168].

1.17 Macrophages in obese adipose tissue and resistin-like molecule alpha (RELMα)

Macrophages constitute an important fraction of the stromal vascular fraction within white adipose tissue. In lean individuals, adipose tissue macrophages consist of about 10% of the total cell population, and these macrophages possess an anti-inflammatory "M2" phenotype and perform tissue surveillance and remodeling functions that are associated with maintaining insulin sensitivity. In obesity, there is a change in

macrophage phenotype, from "M2" to a pro-inflammatory "M1" phenotype. Weight gain and increased adiposity induces local inflammation and cytokine production to promote the recruitment of circulating pro-inflammatory monocytes that then differentiation into M1 macrophages in the adipose tissue. This increase in pro-inflammatory cytokine production from M1 macrophages and reduced anti-inflammatory signals from M2 macrophages promotes adipose tissue dysfunction and impairs glucose tolerance.

There is evidence for the detrimental role of M1 macrophages in promoting adipose tissue insulin resistance. Specifically, macrophages in obese adipose tissue possess a CD11C+ M1 phenotype and gather around necrotic adipocytes in crown like structures [169-170]. Give the role of macrophages in obesity, sex differences in macrophages are of particular interest. Visceral adipose tissue contains more infiltrating macrophages and higher expression of pro-inflammatory cytokines than subcutaneous fat and male visceral adipose tissue accumulates more macrophages than females [6, 9-10]. Male macrophages are also more migratory, while protection in females is associated with higher production of anti-inflammatory cytokines, such as IL-10 and a T helper 2 (Th2) immune environment [9, 17].

Resistin-like molecule alpha (RELMɑ) is a highly cysteine rich M2 macrophage signature gene that is expressed predominantly in macrophages in response to a Th2 cytokine immune response. RELMɑ is present in various tissues and organs, such as heart, lung and white adipose tissues, especially in visceral fat followed by subcutaneous fat [171-172]. Several studies report the role of RELMɑ in metabolic disorders. Specifically, CD301+ phagocytes promote glucose metabolism through secretion of

RELMα and overexpression of RELMα promoted cholesterol homeostasis in low density

lipoprotein (LDL) receptor deficient mice [173-174]. Based on pervious findings of

males being susceptible to obesity mediated pathologies and adipose tissue dysfunction in

diet-induced obesity and females have protection that is driven by an Th2 immune

environment, chapter four of this dissertation will investigate how sex and RELMα

regulate diet-induced obesity and inflammation.

1.18 Concluding remarks

Understanding the genetic and environmental factors that contribute to hypothalamic

and pituitary dysfunction in obesity is critical in elucidating how energy homeostasis is

dysregulated in obesity and how obesity leads to multiple hormone imbalances that lead

to changes in physiology. This dissertation aims to identify new genetic and

environmental targets and mechanisms that are important in maintaining energy

homeostasis in the hypothalamus and tight control of pituitary gland hormone production

and secretion in maintaining tight physiological homeostasis. In addition, we investigate

the mechanisms of sex-differences in diet-induced obesity and identify a female specific

target that may be critical in maintaining adipose tissue homeostasis.

References for Chapter One

1. Kelly, T., et al. (2008). "Global burden of obesity in 2005 and projections to 2030." Int J Obes (Lond) 32(9): 1431-1437.

2. "Adult Obesity Facts." *Centers for Disease Control and Prevention*, Centers for Disease Control and Prevention, 17 May 2022, www.cdc.gov/obesity/data/adult.html.

3. Hruby, A., et al. (2016). "Determinants and Consequences of Obesity." Am J Public Health **106**(9): 1656-1662.

4. Flores-Dorantes, M. T., et al. (2020). "Environment and Gene Association With Obesity and Their Impact on Neurodegenerative and Neurodevelopmental Diseases." Front Neurosci **14**: 863.

5. Lainez, N. M. and D. Coss (2019). "Obesity, Neuroinflammation, and Reproductive Function." Endocrinology **160**(11): 2719-2736.

6. Weisberg, S. P., et al. (2003). "Obesity is associated with macrophage accumulation in adipose tissue." J Clin Invest **112**(12): 1796-1808.

7. Greenhill, C. (2016). "Adipose tissue: Sex differences in adipogenesis." Nat Rev Endocrinol **12**(9): 497.

8. Palmer, B. F. and D. J. Clegg (2015). "The sexual dimorphism of obesity." Mol Cell Endocrinol **402**: 113-119.

9. Chen, K. E., et al. (2021). "Visceral adipose tissue imparts peripheral macrophage influx into the hypothalamus." J Neuroinflammation **18**(1): 140.

10. Chen, K. E., et al. (2021). "Sex Differences in Macrophage Responses to Obesity-Mediated Changes Determine Migratory and Inflammatory Traits." J Immunol **206**(1): 141-153.

11. Stunkard, A. J., et al. (1986). "A twin study of human obesity." JAMA **256**(1): 51-54.

12. Rankinen, T., et al. (2006). "The human obesity gene map: the 2005 update." Obesity (Silver Spring) **14**(4): 529-644.

13. Locke, A. E., et al. (2015). "Genetic studies of body mass index yield new insights for obesity biology." Nature **518**(7538): 197-206.

14. Yengo, L., et al. (2018). "Meta-analysis of genome-wide association studies for height and body mass index in approximately 700000 individuals of European ancestry." Hum Mol Genet **27**(20): 3641-3649.

15. Montgomery, M. K., et al. (2013). "Mouse strain-dependent variation in obesity and glucose homeostasis in response to high-fat feeding." Diabetologia **56**(5): 1129-1139.

16. Farrell, G. C., et al. (2014). "Strain dependence of diet-induced NASH and liver fibrosis in obese mice is linked to diabetes and inflammatory phenotype." Liver Int **34**(7): 1084-1093.

17. Lainez, N. M., et al. (2018). "Diet-Induced Obesity Elicits Macrophage Infiltration and Reduction in Spine Density in the Hypothalami of Male but Not Female Mice." Front Immunol **9**: 1992.

18. Collins, S., et al. (2004). "Genetic vulnerability to diet-induced obesity in the C57BL/6J mouse: physiological and molecular characteristics." Physiol Behav **81**(2): 243-248.

19. Wang, C. Y. and J. K. Liao (2012). "A mouse model of diet-induced obesity and insulin resistance." Methods Mol Biol **821**: 421-433.

20. Fisher-Wellman, K. H., et al. (2016). "A Direct Comparison of Metabolic Responses to High-Fat Diet in C57BL/6J and C57BL/6NJ Mice." Diabetes **65**(11): 3249-3261.

21. Friedman, J. M. and J. L. Halaas (1998). "Leptin and the regulation of body weight in mammals." Nature **395**(6704): 763-770.

22. Saladin, R., et al. (1995). "Transient increase in obese gene expression after food intake or insulin administration." Nature **377**(6549): 527-529.

23. De Vos, P., et al. (1995). "Induction of ob gene expression by corticosteroids is accompanied by body weight loss and reduced food intake." <u>J Biol Chem</u> **270**(27): 15958-15961.

24. Zhang, Y., et al. (1994). "Positional cloning of the mouse obese gene and its human homologue." <u>Nature</u> **372**(6505): 425-432.

25. Tartaglia, L. A., et al. (1995). "Identification and expression cloning of a leptin receptor, OB-R." <u>Cell</u> **83**(7): 1263-1271.

26. Wauman, J., et al. (2017). "The Leptin Receptor Complex: Heavier Than Expected?" <u>Front Endocrinol (Lausanne)</u> **8**: 30.

27. Coleman, D. L. (1978). "Obese and diabetes: two mutant genes causing diabetes-obesity syndromes in mice." <u>Diabetologia</u> **14**(3): 141-148.

28. Coleman, D. L. and K. P. Hummel (1973). "The influence of genetic background on the expression of the obese (Ob) gene in the mouse." <u>Diabetologia</u> **9**(4): 287-293.

29. Jequier, E. (2002). "Leptin signaling, adiposity, and energy balance." <u>Ann N Y Acad Sci</u> **967**: 379-388.

30. Stephens, T. W., et al. (1995). "The role of neuropeptide Y in the antiobesity action of the obese gene product." <u>Nature</u> **377**(6549): 530-532.

31. Pinto, S., et al. (2004). "Rapid rewiring of arcuate nucleus feeding circuits by leptin." <u>Science</u> **304**(5667): 110-115.

32. Toda, C., et al. (2017). "POMC Neurons: From Birth to Death." <u>Annu Rev Physiol</u> **79**: 209-236.

33. Matheny, M., et al. (2011). "Region-specific diet-induced and leptin-induced cellular leptin resistance includes the ventral tegmental area in rats." <u>Neuropharmacology</u> **60**(2-3): 480-487.

34. Bian, J., et al. (2013). "Lentiviral vector-mediated knockdown of Lrb in the arcuate nucleus promotes diet-induced obesity in rats." <u>J Mol Endocrinol</u> **51**(1): 27-35.

35. Funcke, J. B., et al. (2014). "Monogenic forms of childhood obesity due to mutations in the leptin gene." Mol Cell Pediatr **1**(1): 3.

36. Farooqi, I. S., et al. (2001). "Partial leptin deficiency and human adiposity." Nature **414**(6859): 34-35.

37. Ozata, M., et al. (1999). "Human leptin deficiency caused by a missense mutation: multiple endocrine defects, decreased sympathetic tone, and immune system dysfunction indicate new targets for leptin action, greater central than peripheral resistance to the effects of leptin, and spontaneous correction of leptin-mediated defects." J Clin Endocrinol Metab **84**(10): 3686-3695.

38. Salum, K. C. R., et al. (2021). "When Leptin Is Not There: A Review of What Nonsyndromic Monogenic Obesity Cases Tell Us and the Benefits of Exogenous Leptin." Front Endocrinol (Lausanne) **12**: 722441.

39. Caro, J. F., et al. (1996). "Leptin: the tale of an obesity gene." Diabetes **45**(11): 1455-1462.

40. Paracchini, V., et al. (2005). "Genetics of leptin and obesity: a HuGE review." Am J Epidemiol **162**(2): 101-114.

41. Izquierdo, A. G., et al. (2019). "Leptin, Obesity, and Leptin Resistance: Where Are We 25 Years Later?" Nutrients **11**(11).

42. Obradovic, M., et al. (2021). "Leptin and Obesity: Role and Clinical Implication." Front Endocrinol (Lausanne) **12**: 585887.

43. Hill, J. W. and L. D. Faulkner (2017). "The Role of the Melanocortin System in Metabolic Disease: New Developments and Advances." Neuroendocrinology **104**(4): 330-346.

44. Clement, K., et al. (2020). "Efficacy and safety of setmelanotide, an MC4R agonist, in individuals with severe obesity due to LEPR or POMC deficiency: single-arm, open-label, multicentre, phase 3 trials." Lancet Diabetes Endocrinol **8**(12): 960-970.

45. Corbiere, A., et al. (2019). "Strategies for the Identification of Bioactive Neuropeptides in Vertebrates." Front Neurosci **13**: 948.

46. Ozawa, A., et al. (2010). "Modulation of prohormone convertase 1/3 properties using site-directed mutagenesis." Endocrinology **151**(9): 4437-4445.

47. Dowsett, G. K. C., et al. (2021). "A survey of the mouse hindbrain in the fed and fasted states using single-nucleus RNA sequencing." Mol Metab **53**: 101240.

48. Lam, B. Y. H., et al. (2017). "Heterogeneity of hypothalamic pro-opiomelanocortin-expressing neurons revealed by single-cell RNA sequencing." Mol Metab **6**(5): 383-392.

49. Vong, L., et al. (2011). "Leptin action on GABAergic neurons prevents obesity and reduces inhibitory tone to POMC neurons." Neuron **71**(1)

50. Caron, A., et al. (2018). "POMC neurons expressing leptin receptors coordinate metabolic responses to fasting via suppression of leptin levels." Elife **7**.

51. Cowley, M. A., et al. (2001). "Leptin activates anorexigenic POMC neurons through a neural network in the arcuate nucleus." Nature **411**(6836): 480-484.

52. Williams, K. W., et al. (2010). "Segregation of acute leptin and insulin effects in distinct populations of arcuate proopiomelanocortin neurons." J Neurosci **30**(7): 2472-2479.

53. Qiu, J., et al. (2014). "Insulin excites anorexigenic proopiomelanocortin neurons via activation of canonical transient receptor potential channels." Cell Metab **19**(4): 682-693.

54. Cowley, M. A., et al. (2003). "The distribution and mechanism of action of ghrelin in the CNS demonstrates a novel hypothalamic circuit regulating energy homeostasis." Neuron **37**(4): 649-661.

55. Wang, D., et al. (2015). "Whole-brain mapping of the direct inputs and axonal projections of POMC and AgRP neurons." Front Neuroanat **9**: 40.

56. Appleyard, S. M., et al. (2005). "Proopiomelanocortin neurons in nucleus tractus solitarius are activated by visceral afferents: regulation by cholecystokinin and opioids." J Neurosci **25**(14): 3578-3585.

57. Zhan, C., et al. (2013). "Acute and long-term suppression of feeding behavior by POMC neurons in the brainstem and hypothalamus, respectively." <u>J Neurosci</u> **33**(8): 3624-3632.

58. Quarta, C., et al. (2021). "POMC neuronal heterogeneity in energy balance and beyond: an integrated view." <u>Nat Metab</u> **3**(3): 299-308.

59. Mercer, A. J., et al. (2013). "Unraveling the central proopiomelanocortin neural circuits." <u>Front Neurosci</u> **7**: 19.

60. Krude, H., et al. (1998). "Severe early-onset obesity, adrenal insufficiency and red hair pigmentation caused by POMC mutations in humans." <u>Nat Genet</u> **19**(2): 155-157.

61. Farooqi, I. S., et al. (2006). "Heterozygosity for a POMC-null mutation and increased obesity risk in humans." <u>Diabetes</u> **55**(9): 2549-2553.

62. Farooqi, I. S. and S. O'Rahilly (2008). "Mutations in ligands and receptors of the leptin-melanocortin pathway that lead to obesity." <u>Nat Clin Pract Endocrinol Metab</u> **4**(10): 569-577.

63. Lindberg, I. and L. D. Fricker (2021). "Obesity, POMC, and POMC-processing Enzymes: Surprising Results From Animal Models." <u>Endocrinology</u> **162**(12).

64. Yaswen, L., et al. (1999). "Obesity in the mouse model of pro-opiomelanocortin deficiency responds to peripheral melanocortin." <u>Nat Med</u> **5**(9): 1066-1070.

65. Greenman, Y., et al. (2013). "Postnatal ablation of POMC neurons induces an obese phenotype characterized by decreased food intake and enhanced anxiety-like behavior." <u>Mol Endocrinol</u> **27**(7): 1091-1102.

66. Spanswick, D., et al. (1997). "Leptin inhibits hypothalamic neurons by activation of ATP-sensitive potassium channels." <u>Nature</u> **390**(6659): 521-525.

67. Spanswick, D., et al. (2000). "Insulin activates ATP-sensitive K+ channels in hypothalamic neurons of lean, but not obese rats." <u>Nat Neurosci</u> **3**(8): 757-758.

68. Stanley, B. G., et al. (1985). "Feeding and drinking elicited by central injection of neuropeptide Y: evidence for a hypothalamic site(s) of action." <u>Brain Res Bull</u> **14**(6): 521-524.

69. Stanley, B. G. and S. F. Leibowitz (1985). "Neuropeptide Y injected in the paraventricular hypothalamus: a powerful stimulant of feeding behavior." Proc Natl Acad Sci U S A **82**(11): 3940-3943.

70. Wu, Q., et al. (2009). "Loss of GABAergic signaling by AgRP neurons to the parabrachial nucleus leads to starvation." Cell **137**(7): 1225-1234.

71. Krashes, M. J., et al. (2013). "Rapid versus delayed stimulation of feeding by the endogenously released AgRP neuron mediators GABA, NPY, and AgRP." Cell Metab **18**(4): 588-595.

72. Gropp, E., et al. (2005). "Agouti-related peptide-expressing neurons are mandatory for feeding." Nat Neurosci **8**(10): 1289-1291.

73. Bewick, G. A., et al. (2005). "Post-embryonic ablation of AgRP neurons in mice leads to a lean, hypophagic phenotype." FASEB J **19**(12): 1680-1682.

74. Zemel, M. B. and H. Shi (2000). "Pro-opiomelanocortin (POMC) deficiency and peripheral melanocortins in obesity." Nutr Rev **58**(6): 177-180.

75. Barsh, G. (1999). "From Agouti to Pomc--100 years of fat blonde mice." Nat Med **5**(9): 984-985.

76. Graham, M., et al. (1997). "Overexpression of Agrt leads to obesity in transgenic mice." Nat Genet **17**(3): 273-274.

77. Swart, I., et al. (2002). "Hypothalamic NPY, AGRP, and POMC mRNA responses to leptin and refeeding in mice." Am J Physiol Regul Integr Comp Physiol **283**(5): R1020-1026.

78. Takahashi, K. A. and R. D. Cone (2005). "Fasting induces a large, leptin-dependent increase in the intrinsic action potential frequency of orexigenic arcuate nucleus neuropeptide Y/Agouti-related protein neurons." Endocrinology **146**(3): 1043-1047.

79. Katsuki, A., et al. (2001). "Plasma levels of agouti-related protein are increased in obese men." J Clin Endocrinol Metab **86**(5): 1921-1924.

80. Ilnytska, O. and G. Argyropoulos (2008). "The role of the Agouti-Related Protein in energy balance regulation." Cell Mol Life Sci **65**(17): 2721-2731.

81. Bai, F., et al. (2004). "Functional dimorphism of two hAgRP promoter SNPs in linkage disequilibrium." J Med Genet **41**(5): 350-353.

82. Argyropoulos, G., et al. (2003). "The agouti-related protein and body fatness in humans." Int J Obes Relat Metab Disord **27**(2): 276-280.

83. Mayfield, D. K., et al. (2001). "A role for the Agouti-Related Protein promoter in obesity and type 2 diabetes." Biochem Biophys Res Commun **287**(2): 568-573.

84. Argyropoulos, G., et al. (2002). "A polymorphism in the human agouti-related protein is associated with late-onset obesity." J Clin Endocrinol Metab **87**(9): 4198-4202.

85. You, P., et al. (2016). "Effects of Melanocortin 3 and 4 Receptor Deficiency on Energy Homeostasis in Rats." Sci Rep **6**: 34938.

86. Kim, M. S., et al. (2000). "Hypothalamic localization of the feeding effect of agouti-related peptide and alpha-melanocyte-stimulating hormone." Diabetes **49**(2): 177-182.

87. Glas, E., et al. (2016). "Exchange factors directly activated by cAMP mediate melanocortin 4 receptor-induced gene expression." Sci Rep **6**: 32776.

88. Michaud, J. L., et al. (2001). "Sim1 haploinsufficiency causes hyperphagia, obesity and reduction of the paraventricular nucleus of the hypothalamus." Hum Mol Genet **10**(14): 1465-1473.

89. Wang, J. C., et al. (2008). "A 5-Mb microdeletion at 6q16.1-q16.3 with SIM gene deletion and obesity." Am J Med Genet A **146A**(22): 2975-2978.

90. Faivre, L., et al. (2002). "Deletion of the SIM1 gene (6q16.2) in a patient with a Prader-Willi-like phenotype." J Med Genet **39**(8): 594-596.

91. Asai, M., et al. (2013). "Loss of function of the melanocortin 2 receptor accessory protein 2 is associated with mammalian obesity." Science **341**(6143): 275-278.

92. Novoselova, T. V., et al. (2016). "Loss of Mrap2 is associated with Sim1 deficiency and increased circulating cholesterol." J Endocrinol **230**(1): 13-26.

93. Vaisse, C., et al. (2000). "Melanocortin-4 receptor mutations are a frequent and heterogeneous cause of morbid obesity." J Clin Invest **106**(2): 253-262.

94. Huszar, D., et al. (1997). "Targeted disruption of the melanocortin-4 receptor results in obesity in mice." Cell **88**(1): 131-141.

95. Balthasar, N., et al. (2005). "Divergence of melanocortin pathways in the control of food intake and energy expenditure." Cell **123**(3): 493-505.

96. Fairbrother, U., et al. (2018). "Genetics of Severe Obesity." Curr Diab Rep **18**(10): 85.

97. Collet, T. H., et al. (2017). "Evaluation of a melanocortin-4 receptor (MC4R) agonist (Setmelanotide) in MC4R deficiency." Mol Metab **6**(10): 1321-1329.

98. Kuhnen, P., et al. (2019). "Melanocortin-4 Receptor Signalling: Importance for Weight Regulation and Obesity Treatment." Trends Mol Med **25**(2): 136-148.

99. Scuteri, A., et al. (2007). "Genome-wide association scan shows genetic variants in the FTO gene are associated with obesity-related traits." PLoS Genet **3**(7): e115.

100. Frayling, T. M., et al. (2007). "A common variant in the FTO gene is associated with body mass index and predisposes to childhood and adult obesity." Science **316**(5826): 889-894.

101. Dina, C., et al. (2007). "Variation in FTO contributes to childhood obesity and severe adult obesity." Nat Genet **39**(6): 724-726.

102. Do, R., et al. (2008). "Genetic variants of FTO influence adiposity, insulin sensitivity, leptin levels, and resting metabolic rate in the Quebec Family Study." Diabetes **57**(4): 1147-1150.

103. Hinney, A., et al. (2007). "Genome wide association (GWA) study for early onset extreme obesity supports the role of fat mass and obesity associated gene (FTO) variants." PLoS One **2**(12): e1361.

104.   Peters, T., et al. (1999). "Cloning of Fatso (Fto), a novel gene deleted by the Fused toes (Ft) mouse mutation." Mamm Genome **10**(10): 983-986.

105.   Fredriksson, R., et al. (2008). "The obesity gene, FTO, is of ancient origin, up-regulated during food deprivation and expressed in neurons of feeding-related nuclei of the brain." Endocrinology **149**(5): 2062-2071.

106.   Stratigopoulos, G., et al. (2008). "Regulation of Fto/Ftm gene expression in mice and humans." Am J Physiol Regul Integr Comp Physiol **294**(4): R1185-1196.

107.   Fischer, J., et al. (2009). "Inactivation of the Fto gene protects from obesity." Nature **458**(7240): 894-898.

108.   Church, C., et al. (2009). "A mouse model for the metabolic effects of the human fat mass and obesity associated FTO gene." PLoS Genet **5**(8): e1000599.

109.   Tung, Y. C., et al. (2010). "Hypothalamic-specific manipulation of Fto, the ortholog of the human obesity gene FTO, affects food intake in rats." PLoS One **5**(1): e8771.

110.   Butler, M. G. (2016). "Single Gene and Syndromic Causes of Obesity: Illustrative Examples." Prog Mol Biol Transl Sci **140**: 1-45.

111.   Bittel, D. C. and M. G. Butler (2005). "Prader-Willi syndrome: clinical genetics, cytogenetics and molecular biology." Expert Rev Mol Med **7**(14): 1-20.

112.   Chen, H., et al. (2020). "Loss of MAGEL2 in Prader-Willi syndrome leads to decreased secretory granule and neuropeptide production." JCI Insight **5**(17).

113.   Oncul, M., et al. (2018). "Impaired melanocortin pathway function in Prader-Willi syndrome gene-Magel2 deficient mice." Hum Mol Genet **27**(18): 3129-3136.

114.   Maillard, J., et al. (2016). "Loss of Magel2 impairs the development of hypothalamic Anorexigenic circuits." Hum Mol Genet **25**(15): 3208-3215.

115.   Holsen, L. M., et al. (2006). "Neural mechanisms underlying hyperphagia in Prader-Willi syndrome." Obesity (Silver Spring) **14**(6): 1028-1037.

116.   Shapira, N. A., et al. (2005). "Satiety dysfunction in Prader-Willi syndrome demonstrated by fMRI." J Neurol Neurosurg Psychiatry **76**(2): 260-262.

117.   Rybakova, N. I., et al. (1987). "[X-ray diagnosis of lung carcinoids]." Vestn Rentgenol Radiol(2): 35-42.

118.   Turkkahraman, D., et al. (2022). "Serum alpha-melanocyte-stimulating hormone (a-MSH), brain-derived neurotrophic factor (BDNF), and agouti-related protein (AGRP) levels in children with Prader-Willi or Bardet-Biedl syndromes." J Endocrinol Invest **45**(5): 1031-1037.

119.   Ranadive, S. A. and C. Vaisse (2008). "Lessons from extreme human obesity: monogenic disorders." Endocrinol Metab Clin North Am **37**(3): 733-751, x.

120.   Tobin, J. L. and P. L. Beales (2007). "Bardet-Biedl syndrome: beyond the cilium." Pediatr Nephrol **22**(7): 926-936.

121.   Grace, C., et al. (2003). "Energy metabolism in Bardet-Biedl syndrome." Int J Obes Relat Metab Disord **27**(11): 1319-1324.

122.   Guo, D. F., et al. (2019). "The BBSome in POMC and AgRP Neurons Is Necessary for Body Weight Regulation and Sorting of Metabolic Receptors." Diabetes **68**(8): 1591-1603.

123.   Wang, L., et al. (2021). "Bardet-Biedl syndrome proteins regulate intracellular signaling and neuronal function in patient-specific iPSC-derived neurons." J Clin Invest **131**(8).

124.   Sidorov, M. S., et al. (2013). "Fragile X mental retardation protein and synaptic plasticity." Mol Brain **6**: 15.

125.   Richter, J. D. and X. Zhao (2021). "The molecular biology of FMRP: new insights into fragile X syndrome." Nat Rev Neurosci **22**(4): 209-222.

126.   Rais, M., et al. (2018). "Sensory Processing Phenotypes in Fragile X Syndrome." ASN Neuro **10**: 1759091418801092.

127.   Raspa, M., et al. (2010). "Obesity, food selectivity, and physical activity in individuals with fragile X syndrome." Am J Intellect Dev Disabil **115**(6): 482-495

128.   Choo, T. H., et al. (2022). "Height and BMI in fragile X syndrome: A longitudinal assessment." Obesity (Silver Spring) **30**(3): 743-750.

129.   Chen, D., et al. (2016). "Food Environments and Obesity: Household Diet Expenditure Versus Food Deserts." Am J Public Health **106**(5): 881-888.

130.   Smith, L. P., et al. (2013). "Trends in US home food preparation and consumption: analysis of national nutrition surveys and time use studies from 1965-1966 to 2007-2008." Nutr J **12**: 45.

131.   Gadiraju, T. V., et al. (2015). "Fried Food Consumption and Cardiovascular Health: A Review of Current Evidence." Nutrients **7**(10): 8424-8430.

132.   Kalin, S., et al. (2015). "Hypothalamic innate immune reaction in obesity." Nat Rev Endocrinol **11**(6): 339-351.

133.   Thaler, J. P., et al. (2012). "Obesity is associated with hypothalamic injury in rodents and humans." J Clin Invest **122**(1): 153-162.

134.   Milanski, M., et al. (2009). "Saturated fatty acids produce an inflammatory response predominantly through the activation of TLR4 signaling in hypothalamus: implications for the pathogenesis of obesity." J Neurosci **29**(2): 359-370.

135.   Olofsson, L. E., et al. (2013). "Modulation of AgRP-neuronal function by SOCS3 as an initiating event in diet-induced hypothalamic leptin resistance." Proc Natl Acad Sci U S A **110**(8): E697-706.

136.   Cintra, D. E., et al. (2012). "Unsaturated fatty acids revert diet-induced hypothalamic inflammation in obesity." PLoS One **7**(1): e30571.

137.   Wang, X. and H. Li (2022). "Chronic high-fat diet induces overeating and impairs synaptic transmission in feeding-related brain regions." Front Mol Neurosci **15**: 1019446.

138.   Horvath, T. L., et al. (2010). "Synaptic input organization of the melanocortin system predicts diet-induced hypothalamic reactive gliosis and obesity." Proc Natl Acad Sci U S A **107**(33): 14875-14880.

139.   Moraes, J. C., et al. (2009). "High-fat diet induces apoptosis of hypothalamic neurons." PLoS One **4**(4): e5045.

140.   Paeger, L., et al. (2017). "Energy imbalance alters Ca(2+) handling and excitability of POMC neurons." Elife **6**.

141.   Fontenelle, L. C., et al. (2016). "Thyroid Function in Human Obesity: Underlying Mechanisms." Horm Metab Res **48**(12): 787-794.

142.   Reinehr, T. (2010). "Obesity and thyroid function." Mol Cell Endocrinol **316**(2): 165-171.

143.   Laurberg, P., et al. (2012). "Thyroid function and obesity." Eur Thyroid J **1**(3): 159-167.

144.   Moller, N. and J. O. Jorgensen (2009). "Effects of growth hormone on glucose, lipid, and protein metabolism in human subjects." Endocr Rev **30**(2)

145.   Rasmussen, M. H. (2010). "Obesity, growth hormone and weight loss." Mol Cell Endocrinol **316**(2): 147-153.

146.   Corona, G., et al. (2013). "Body weight loss reverts obesity-associated hypogonadotropic hypogonadism: a systematic review and meta-analysis." Eur J Endocrinol **168**(6): 829-843.

147.   Lee, Y., et al. (2019). "Impact of Bariatric Surgery on Male Sex Hormones and Sperm Quality: a Systematic Review and Meta-Analysis." Obes Surg **29**(1): 334-346.

148.   Kyrou, I., et al. (2006). "Stress, visceral obesity, and metabolic complications." Ann N Y Acad Sci **1083**: 77-110.

149.   Nicolaides, N. C., et al. (2015). "Stress, the stress system and the role of glucocorticoids." Neuroimmunomodulation **22**(1-2): 6-19.

150.   Makara, G. B. (1992). "The relative importance of hypothalamic neurons containing corticotropin-releasing factor or vasopressin in the regulation of adrenocorticotropic hormone secretion." Ciba Found Symp **168**: 43-51.

151.   Heinrichs, S. C., et al. (1993). "Corticotropin-releasing factor in the paraventricular nucleus modulates feeding induced by neuropeptide Y." Brain Res **611**(1): 18-24.

152.   Izzi-Engbeaya, C., et al. (2020). "Effects of corticosterone within the hypothalamic arcuate nucleus on food intake and body weight in male rats." Mol Metab **36**: 100972.

153.   Smart, J. L., et al. (2006). "Glucocorticoids exacerbate obesity and insulin resistance in neuron-specific proopiomelanocortin-deficient mice." J Clin Invest **116**(2): 495-505.

154.   Casals-Casas, C. and B. Desvergne (2011). "Endocrine disruptors: from endocrine to metabolic disruption." Annu Rev Physiol **73**: 135-162.

155.   Heindel, J. J., et al. (2015). "Endocrine disruptors and obesity." Nat Rev Endocrinol **11**(11): 653-661.

156.   Mackay, H., et al. (2013). "Organizational effects of perinatal exposure to bisphenol-A and diethylstilbestrol on arcuate nucleus circuitry controlling food intake and energy expenditure in male and female CD-1 mice." Endocrinology **154**(4): 1465-1475.

157.   Batista, T. M., et al. (2012). "Short-term treatment with bisphenol-A leads to metabolic abnormalities in adult male mice." PLoS One **7**(3): e33814.

158.   Garcia-Arevalo, M., et al. (2014). "Exposure to bisphenol-A during pregnancy partially mimics the effects of a high-fat diet altering glucose homeostasis and gene expression in adult male mice." PLoS One **9**(6): e100214.

159.   Acconcia, F., et al. (2015). "Molecular Mechanisms of Action of BPA." Dose Response **13**(4): 1559325815610582.

160.   De Coster, S. and N. van Larebeke (2012). "Endocrine-disrupting chemicals: associated disorders and mechanisms of action." J Environ Public Health **2012**: 713696.

161.   Somm, E., et al. (2009). "Perinatal exposure to bisphenol a alters early adipogenesis in the rat." Environ Health Perspect **117**(10): 1549-1555.

162.   Monje, L., et al. (2010). "Exposure of neonatal female rats to bisphenol A disrupts hypothalamic LHRH pre-mRNA processing and estrogen receptor alpha expression in nuclei controlling estrous cyclicity." Reprod Toxicol **30**(4): 625-634.

163.   Mackay, H., et al. (2013). "Organizational effects of perinatal exposure to bisphenol-A and diethylstilbestrol on arcuate nucleus circuitry controlling food intake and energy expenditure in male and female CD-1 mice." Endocrinology **154**(4): 1465-1475.

164.   Xu, H., et al. (2003). "Chronic inflammation in fat plays a crucial role in the development of obesity-related insulin resistance." J Clin Invest **112**(12): 1821-1830.

165.   Hotamisligil, G. S., et al. (1993). "Adipose expression of tumor necrosis factor-alpha: direct role in obesity-linked insulin resistance." Science **259**(5091): 87-91.

166.   Olefsky, J. M. and C. K. Glass (2010). "Macrophages, inflammation, and insulin resistance." Annu Rev Physiol **72**: 219-246.

167.   Kanda, H., et al. (2006). "MCP-1 contributes to macrophage infiltration into adipose tissue, insulin resistance, and hepatic steatosis in obesity." J Clin Invest **116**(6): 1494-1505.

168.   Kaplan, J. L., et al. (2015). "Adipocyte progenitor cells initiate monocyte chemoattractant protein-1-mediated macrophage accumulation in visceral adipose tissue." Mol Metab **4**(11): 779-794.

169.   Lumeng, C. N., et al. (2007). "Obesity induces a phenotypic switch in adipose tissue macrophage polarization." J Clin Invest **117**(1): 175-184.

170.   Lumeng, C. N., et al. (2008). "Phenotypic switching of adipose tissue macrophages with obesity is generated by spatiotemporal differences in macrophage subtypes." Diabetes **57**(12): 3239-3246.

171.   Steppan, C. M., et al. (2001). "A family of tissue-specific resistin-like molecules." <u>Proc Natl Acad Sci U S A</u> **98**(2): 502-506.

172.   Bing, C., et al. (2002). "Resistin and RELM-alpha gene expression in white adipose tissue of lactating mice." <u>Biochem Biophys Res Commun</u> **296**(2): 458-462.

173.   Kumamoto, Y., et al. (2016). "CD301b(+) Mononuclear Phagocytes Maintain Positive Energy Balance through Secretion of Resistin-like Molecule Alpha." <u>Immunity</u> **45**(3): 583-596.

174.   Lee, M. R., et al. (2014). "The adipokine Retnla modulates cholesterol homeostasis in hyperlipidemic mice." <u>Nat Commun</u> **5**: 4410

CHAPTER TWO:

Increased body weight in mice with *Fragile X messenger ribonucleoprotein 1* (*Fmr1*) gene mutation is associated with hypothalamic dysfunction

Rebecca E. Ruggiero-Ruff[1], Pedro A. Villa[1], Sarah Abu Hijleh[1], Bryant Avalos[1], Nicholas V. DiPatrizio[1], Sachiko Haga-Yamanaka[2], and Djurdjica Coss[1]*

[1]Division of Biomedical Sciences; School of Medicine, University of California, Riverside; [2]Department of Molecular, Cell, and Systems Biology; College of Natural and Agricultural Sciences, University of California, Riverside

2.1 Abstract

Mutations in the *Fragile X Messenger Ribonucleoprotein 1* (*FMR1*) gene are linked to Fragile X Syndrome, the most common monogenic cause of intellectual disability and autism. People affected with mutations in *FMR1* have higher incidence of obesity, but the mechanisms are largely unknown. In the current study, we determined that male *Fmr1* knockout mice (KO, *Fmr1$^{-/y}$*), but not female *Fmr1$^{-/-}$*, exhibit increased weight when compared to wild-type controls, similarly to humans with *FMR1* mutations. No differences in food or water intake were found between groups; however, male *Fmr1$^{-/y}$* display lower locomotor activity, especially during their active phase. Moreover, *Fmr1$^{-/y}$* have olfactory dysfunction determined by buried food test, although they exhibit increased compulsive behavior, determined by marble burying test. Since olfactory brain regions communicate with hypothalamic regions that regulate food intake, including POMC neurons that also regulate locomotion, we examined POMC neuron innervation and numbers in *Fmr1$^{-/y}$* mice. POMC neurons express Fmrp, and POMC neurons in *Fmr1$^{-/y}$* have higher inhibitory GABAergic synaptic inputs. Consistent with increased inhibitory innervation, POMC neurons in the *Fmr1$^{-/y}$* mice exhibit lower activity, based on cFOS expression. Notably, *Fmr1$^{-/y}$* mice have fewer POMC neurons than controls, specifically in the rostral arcuate nucleus, which could contribute to decreased locomotion and increased body weight. These results suggest a role for *Fmr1* in the regulation of POMC neuron function and the etiology of *Fmr1*-linked obesity.

2.2 Rationale for elucidating the role of *FMR1* gene in obesity

Mutations in the *Fragile X Messenger Ribonucleoprotein 1* (*FMR1*) gene cause Fragile X Syndrome (FXS), the most common genetic form of intellectual disability [1, 2]. People affected with this disorder have mental impairment, autism and higher incidence of obesity [3-7]. Mutation entails expansion of the unstable CGG trinucleotide repeats, which leads to hypermethylation, silencing of the gene and the loss of protein product, FMRP. FMRP is an mRNA binding protein that regulates protein levels of its targets [8, 9]. In the brain, where it is most highly expressed, FMRP binds mRNAs that encode synaptic proteins, contributing to cognitive dysfunctions in FXS [10-12]. While the mechanisms of intellectual impairments following FMRP loss are beginning to emerge, mechanisms of increased weight are not known. The effect of FMRP loss on the cortex and hippocampus have been analyzed [13, 14], however, how mutations affect hypothalamic functions has not been examined. Herein, we investigated the effects of FMRP loss in the regulation of body weight and food intake, using the *Fmr1* knock-out (*Fmr1$^{-/y}$*, KO) mouse model. Due to differential methylation between human and mouse genes, the *Fmr1* KO is a widely used mouse model to study Fragile X Syndrome and is considered a better model than putative mimics of the CGG repeat expansion [15, 16]. We analyzed effects of the lack of Fmrp on food intake and specifically on a population of hypothalamic neurons that regulate feeding, satiety and energy expenditure.

FMR1 mutations are associated with increased obesity particularly in children. 34% of pediatric patients with FXS experience obesity compared to 18% of unaffected children [3-6]. Obesity, especially in childhood, leads to an increased risk of cardiovascular

disease, metabolic syndrome, dementia, and stroke. The causes of increased obesity in

FXS are not clear. Food intake and energy expenditure are regulated by the

hypothalamus, which also controls other homeostatic processes, such as circadian

rhythms, thermoregulation, stress response, and reproductive function. Our previous

study analyzed the role of the *Fmr1* gene in reproduction, since women with *FMR1*

mutation experience early cessation of reproductive function and males have

macroorchidism [17, 18]. We demonstrated increased innervation of ovarian follicles

and of GnRH neurons in the hypothalamus that regulate reproduction [19]. The

hypothalamus receives information on availability of energy stores from the periphery to

regulate food intake [20, 21]. Metabolic cues are integrated primarily by anorexigenic

proopiomelanocortin (POMC) neurons and orexigenic neuropeptide Y (NPY) / agouti-

related protein (AgRP) neurons located in the arcuate nucleus (ARC) of the mediobasal

hypothalamus [22]. AgRP neurons in the satiated state lower GABA tone that normally

inhibits POMC neurons [23, 24]. This disinhibition leads to activation of POMC neurons

and synthesis of the POMC peptide. POMC is cleaved to several neuropeptides, most

importantly to alpha-melanocyte stimulating hormones (αMSH) that plays a role in

weight regulation by binding to melanocortin 4 receptor (MC4R). Signaling through this

receptor, located in several nuclei, including paraventricular nucleus (PVN),

ventromedial hypothalamus (VMH) and brainstem, in the brain helps maintain the

balance between food intake and energy expenditure [25-27]. Given that *FMR1* gene

mutations are associated with increased obesity, it is critical to examine *FMR1* role in the

regulation of energy balance.

Individuals with FXS exhibit abnormal sensory information processing leading to hypersensitivity to a variety to sensory inputs, which results in a wide array of behavioral symptoms [13]. This may be a result of alteration in several neurotransmitter receptor levels resulting in decreased inhibitory/excitatory synaptic balance and the diminished synaptic plasticity [28]. Mutations of the *FMR1* gene may affect olfaction, but the results are not clear. *Fmr1* KO mice have decreased ability to detect smell, but no differences from controls in distinguishing between different odorants [29]. Olfaction in animals is critical for food detection and intake, and the olfactory bulb projects to the hypothalamus and feeding circuitry to stimulate hunger and food intake [30, 31]. However, exact mechanisms and pathways that connect olfactory brain regions with the hypothalamus to stimulate hunger, or to the regions that regulate locomotion to increase foraging for food, are not clear. In this study, we analyzed feeding and energy expenditure in *Fmr1* KO mice, and hypothalamic neurons that regulate these processes. We determined that male KO mice are heavier than controls, but lack differences in food intake, while locomotion was affected. We identified profound effects on olfaction and POMC neurons that regulate energy expenditure. Therefore, olfaction and alterations in activity of POMC neurons likely contribute to the dysregulation of energy balance and increased obesity in people affected with *FMR1* mutations.

2.3 Materials and Methods

2.3.1 Animals

All animal procedures were performed with the approval from the University of California (Riverside, CA) Animal Care and Use Committee and in accordance with the National Institutes of Health Animal care and Use Guidelines. Breeding pairs of FVB.129P2-Fmr1tm1Cgr/J (*Fmr1* KO) and their congenic controls (WT) mice were obtained from Jackson Laboratories and bred in-house. Mice were maintained under a 12-h light, 12-h dark cycle and received food and water *ad libitum*. *Fmr1* KO mice have larger litters [19] and to prevent litter size influence on pup weight, litter sizes were normalized to 8 mice per litter. Previous studies using FXS mouse models demonstrated that these mice have heightened response to stress and altered levels of glucocorticoids [32]. To reduce stress, animals were acclimated by daily handling.

2.3.2 Feeding behavior and locomotor activity

WT and *Fmr1* KO mice between 8-10 weeks of age were individually housed in Phenomaster feeding chambers (TSE Systems, Chesterfield, MO, USA) to analyze food intake and locomotion, and received access to standard chow and water *ad libitum* throughout behavioral testing. These chambers allow for continuous monitoring of food and water intake, and rigorous analysis of locomotor activity given that frames are equipped with light-beam grid and infrared sensors in 3 dimensions.

Animals were allowed 72 hours to acclimate, after which food intake, water intake, and locomotion were recorded. Food weight, water, and continuous locomotor activity were measured in real time and recorded using the TSE Phenomaster Software.

2.3.3 Behavioral tests

2.3.3.1 Buried and Unburied Food Test

Buried and unburied food tests were performed as previously described [33, 34]. Male and female mice, 8-12 weeks of age, after 24-hour fasting period, were used to locate buried or unburied standard chow pellet, starting at 7 pm, at the start of their active cycle and dark period in our colony. Polycarbonate cages with clean bedding material at a depth of 5 cm were used for testing. A single mouse was placed at the center of a test cage and allowed to acclimate for 5 minutes. After acclimatization, the mouse was placed in a clean holding cage, the pellet was buried, and the mouse was placed back in the test cage and allowed to recover the buried food pellet within a 10 min test time. Separate holding and test cages were used for each mouse. Latency, defined as the time between placing the mouse into the cage and the mouse grasping the food pellet with its forepaws, was recorded. Latency of animals that did not recover the food pellet within 10 min was recorded as 600 sec. One week after the buried food test was performed, the mice underwent the unburied food test. The acclimation and testing conditions were identical to the buried food test, except the mice were timed in grasping the food pellet that was left on the top of bedding.

2.3.3.2 Marble Burying Test

Marble burying test was performed as previously described [35]. Briefly, Male and female mice, 8-12 weeks of age were tested at 7pm, as described above. Polycarbonate cages with fitted filter tops were filled with fresh unscented mouse bedding to a depth of 5 cm. Standard glass marbles were washed in mild laboratory detergent, rinsed with distilled-deionized water and dried, and then spaced out evenly in five rows of four marbles on the top of bedding. Test recording started immediately after the animal was placed in the cage, far away from the marbles as possible. The animals were left to explore undisturbed for 30 min. Marbles were counted and scored as buried if two-thirds of its surface was covered by bedding.

2.3.4 Histological analyses and immunohistochemistry

WT controls and *Fmr1* KO mice were anesthetized, perfused with 20 ml PBS and 20 ml 4% paraformaldehyde; and tissues were collected. Hypothalami were sectioned to 50 μm coronal sections. Sections containing paraventricular nucleus (PVN) and arcuate nucleus (ARC) where MC4R or POMC neurons are located, respectively, were blocked and stained for β-endorphin for POMC neuron detection (1:10,000 dilution, rabbit anti-β-endorphin, Phoenix Pharmaceuticals H-022-33), MC4R (1:1,000 dilution, rabbit anti-MC4R, Abcam ab24233), GABAγ2 receptor subunit (1:10,000 dilution, guinea pig anti-GABAγ2, Synaptic systems 224 004), VGAT (1:5,000, mouse anti-VGAT, Synaptic systems 131 011) or cFOS (1:10,000, guinea pig anti-cFOS, Synaptic systems 226 308)

for 48 hours at 4°C. After PBST washes, sections were incubated overnight at 4°C with secondary antibodies: goat anti-rabbit IgG-Alexa Fluor 488 (1:5000, Invitrogen, A11034,); anti-mouse IgG-Alexa Fluor 594 (1:1000, A11032, Invitrogen); anti-guinea pig–biotin (1:1000, BA-7000, Vector Laboratories, Burlingame, CA) followed by streptavidin-Cy5 (1:1000, 434316, Vector Laboratories, Burlingame, CA). Secondary antibody-only controls were performed to determine antibody specificity. MC4R neurons in the PVN were quantified by mean fluorescent intensity (MFI) using Fiji ImageJ. Numbers of POMC neurons were quantified by counting β-endorphin/POMC stained cell bodies in the coronal sections throughout the arcuate nucleus of the hypothalamus. To quantify the number of cFOS-expressing POMC neurons, 50um coronal sections of the arcuate nucleus were stained for POMC and cFOS, and results represented as a percentage of cFOS-positive POMC neurons. All sections were imaged using Leica microscope (DM6000) and analyzed using Fiji ImageJ.

Immunostaining for FMRP was performed using free-floating 50um sections spanning PVN (for MC4R-FMRP) or ARC (POMC/β-endorphin-FMRP). Sections were stained for 48 hours with primary antibodies, mouse anti-FMRP (1:1000; Developmental Studies Hybridoma Bank, catalog #2F5-1-s, RRID: AB_10805421) and POMC or MC4R antibodies as above. After PBST washes, sections were incubated overnight at 4°C with secondary antibodies: goat anti-rabbit IgG-Alexa Fluor 488 (1:5000, Invitrogen, A11034,); anti-mouse biotin (1:1000, BA-9200, Vector Laboratories, Burlingame, CA) followed by streptavidin-Cy5 (1:1000, 434316, Vector Laboratories, Burlingame, CA).

Slices were mounted on slides with Vectashield mounting medium containing DAPI (Vector Laboratories, H-1200).

To determine puncta density, we followed our established protocol as previously published [19, 36, 37]. Puncta were counted in the individual neurons using z-stacks acquired by confocal Leica SP2 microscope. Images were encoded for blind analysis. At least 15-20 individual neurons from 3 different sets of mice were counted. 3D reconstruction was performed by Imaris software (Bitplane, Inc; Concord, MA).

2.3.5 Western blot

Whole cell lysates were obtained from the dissected hypothalami from WT controls and FMR1 knockout mice and after protein determination, the same amount of protein from each sample was resolved on SDS-PAGE, transferred on nitrocellulose membrane and probed for: GABAγ2 receptor subunit (1:1000, 14104-1-AP, Proteintech), VGAT (1:1000, 131 011, Synaptic Systems), MC4R (1:1000, ab24233, Abcam) or β-tubulin (1:1000, sc-9104, Santa Cruz Biotechnology). Bands were quantified using ChemiDoc imaging system (Bio-Rad, Hercules, CA).

2.3.6 Statistical analyses

Statistical differences between WT control and *Fmr1* KO mice ($p < 0.05$) were determined by t-test, or ANOVA when appropriate, followed by Tukey's post-hoc test for multiple comparisons using Prism software (GraphPad, CA).

2.4 Results

2.4.1 *Fmr1* knockout male mice are heavier

Children and adolescents with FXS are heavier than age-matched controls, but it is not clear if this is due to food preference or due to the effects of the *FMR1* gene mutation on the hypothalamic feeding circuitry. To address this question, we monitored the weight of *Fmr1* KO mice and compared them to WT controls. Given that *Fmr1* KO mice have larger litters {Villa, 2023 #10046}, we controlled for the number of pups per litter on the day of birth, since litter size affects early food intake and consequently weight. We normalized litter sizes to 8 pups per litter, and 4 different litters were analyzed. We monitored pups' weight from postnatal day 7 (p7), when we can distinguish males and females, to p90, and determined that *Fmr1* KO male mice were heavier than WT controls (Fig. 2.1a, top). Female homozygous *Fmr1* KO mice did not show differences in weight (Fig. 2.1a, bottom), consistent with the observations that homozygous FXS females have less severe outcomes than males [34-37]. We determined that from p10, *Fmr1* KO male mice were heavier (p11 WT=6.82g, KO=7.67g, p=0.012). The weight difference was lost for 10 days after weaning, from p21-p30, likely due to increased anxiety of *Fmr1* KO mice after separation from their mothers, that has been demonstrated [37, 43]. At p35 and after, until p90, *Fmr1* KO male mice were again significantly heavier than WT mice (p42 for example, WT=22.9g, KO=25.8g, p=0.00023). We then investigated if weight gain stems from increased food intake, and we individually housed WT and KO mice in two-hopper feeding chambers. After a three-day acclimation period, food intake, water consumption, and locomotor activity were measured in real time for another 3 days.

Animals received *ad libitum* access to standard chow and water throughout testing. There was no difference in food or water intake, in males or females KO mice compared to controls (Fig. 2.1b. left). To determine if there are differences in blood glucose levels, we measured circulating glucose at p42, at random and after a 12-hour fast, but did not detect any differences in either males or females (Fig 2.1b, right). Using Phenomaster chambers to monitor locomotor activity, we determined that there was a decrease in movement of *Fmr*1 KO male mice compared to WT (Fig. 2.1c). This decrease was significant during the dark cycle, which is consistent with previous reports [44]. WT controls exhibited increased locomotion at the onset of the dark phase, when mice normally experience their active period and initiate foraging for food. *Fmr1* KO males exhibited smaller increase in this circadian locomotive activity. Area under the curve (AUC) was calculated to demonstrate overall significantly reduced locomotion, WT=4330 compared to KO=3223 (p=0.015; Fig. 2.1c, right). Females did not show a significant difference in locomotion, and in fact, KO females exhibited a trend of moving more, which may correspond to hyperactivity [45]. AUC for female mice was WT=3234 compared to KO=3949 (Fig. 2.1d, right). Therefore, *Fmr1* KO males exhibit increased weight, no difference in food intake, and reduced locomotor activity compared to controls, which likely contributes to increased weight [46].
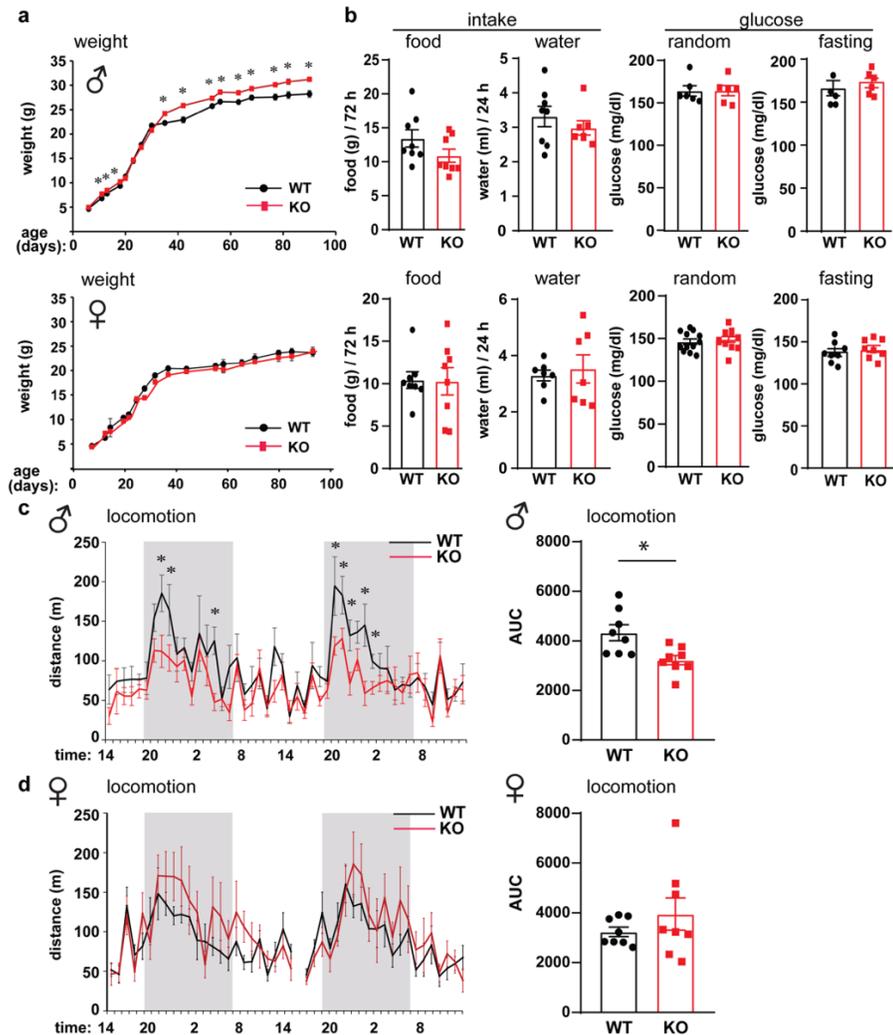
Fig 2.1. *Fmr1* knockout (KO) male mice are heavier than controls. a, Litter sizes were normalized to 8 mice per litter, weight of 4 litters per genotype monitored from p7-p90, and *Fmr1* KO mice compared to wild-type FVB controls (WT) (KO, red; WT controls, black; males, top; females, bottom). n=12-16 mice, points represent group mean +/- standard error. Statistical significance between weight at each age is represented with * ($p < 0.05$, ANOVA followed by Tukey's post hoc test). b, Food (left) and water (right) intake were not different (cumulative, n=8 per genotype); glucose levels (random, left; measured after overnight fasting, right) were not different (WT, black bars represent group mean +/- standard error, each black circle represents one animal; KO, red bars represent group mean +/- standard error, each red square represents one animal). c, Locomotor activity of male mice measured continuously with Phenomaster for 48 hours. Left, x-axis indicates time of day, when monitoring started at 14:00 or 2pm, shaded area represents dark cycle, lights off in our vivarium from 7 pm – 7 am; black line, WT; red line, *Fmr1* KO; n=8 mice, points represent group mean +/- standard error; WT, black; KO, red. Right, area under the curve (AUC), WT, black bars represent group mean +/- standard error, each black circle represents one animal; KO, red bars represent group mean +/- standard error, each red square represents one animal. d, Locomotor activity, female mice. Statistical significance (*, $p < 0.05$) was determined with t-test followed by Tukey's post hoc test.

Given that mice increase locomotion at the beginning of their active period, in order to reach the food pellets and eat, we investigated if *Fmr1* KO mice exhibit decreased locomotion due to the inability to smell food. The buried food test measures the latency to uncover a small piece of chow and is a reliable method to assess olfaction, since it uses animals' natural propensity to use olfactory cues when foraging for food [47, 48, 49]. We determined that *Fmr1* KO male mice showed significant delay in reaching the food pellet. WT males uncovered the food pellet at 136.5 seconds, while KO reached the pellet at 458.8 seconds (Fig. 2.2a, p=0.0263). There was no difference in latency of female mice to reach the buried food pellet, which may be consistent with lack of differences in locomotion.

As a control to assess motivation to eat, we performed an unburied food test, where the food pellet was left on the top of the bedding, after which the mouse was introduced to the cage in the opposite corner. There was no difference in the latency to reach the pellet and start eating between KO and WT mice when the food is visible, in male or female mice (Fig. 2.2b). We concluded that KO mice experience hunger signals, consistent with food intake analyses reported in Fig 1b. Given that KO mice exhibited a delay in digging for food, we wanted to determine whether *Fmr1* KO mice have aversion to digging and performed a marble burying test [50]. Although *FMR1* mutations are associated with autism-spectrum disorders, which is characterized by repetitive or compulsive behaviors, we considered the marble burying test adequate to control for the willingness to dig, since these are natural and spontaneous behaviors in mice. We determined that *Fmr1* KO male and female mice buried significantly more marbles (Fig.

2.2c). WT male mice buried 7.5 marbles out of 20 during the 30-minute test period, while KO male mice buried 15.8 marbles (Fig. 2c, left; p=0.0135). WT female mice buried 10.8 marbles, compared to KO female mice that buried 16.2 marbles (Fig. 2.2c, right; p= 0.0004). These results demonstrate that *Fmr1* KO mice exhibit increased repetitive behaviors consistent with models of autism. Significantly for our studies, *Fmr1* KO male mice have an affinity to dig and therefore, delay in obtaining a food pellet stems from reduced olfaction.
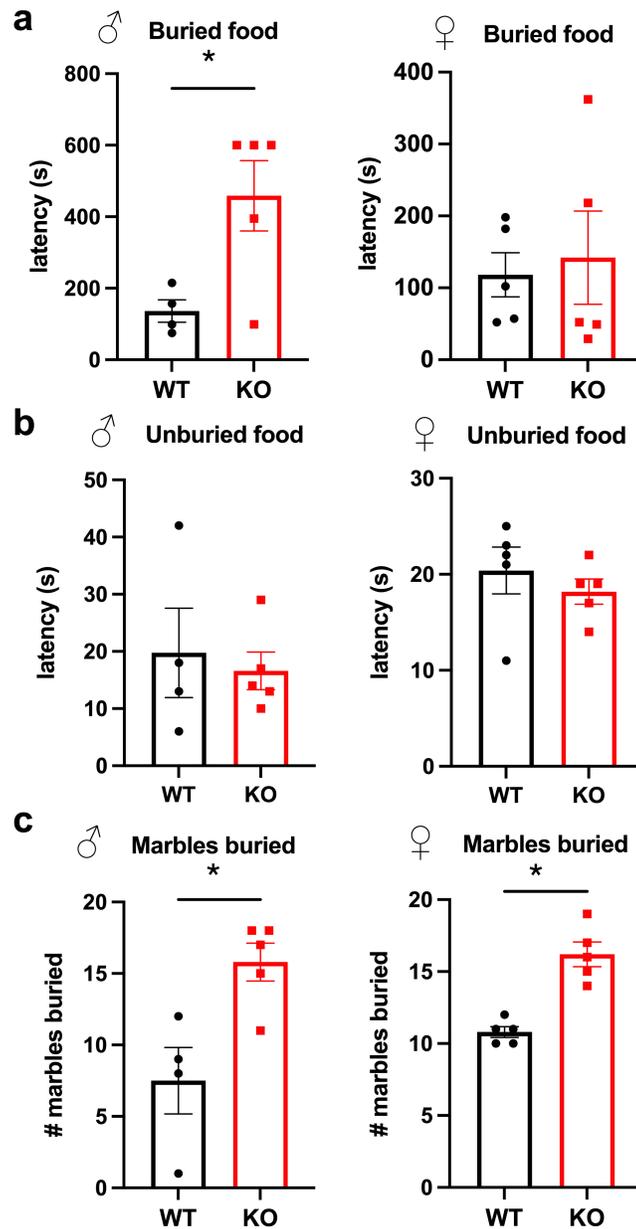
Fig 2.2 Buried food test demonstrates olfactory impairment in *Fmr1* KO male mice. a, Left, WT male mice reached buried food pellet faster than KO mice (p=0.0263; WT, black bars represent group mean +/- standard error, each black circle represents one animal; KO, red bars represent group mean +/- standard error, each red square represents one animal). Right, no difference in latency to uncover buried food pellet in female mice. b, No difference in latency to retrieve unburied food pellet between KO and WT mice (left, male; right, female). c, Left, WT males buried fewer marbles than KO male mice (p=0.0135). Right, WT females buried fewer marbles than KO females (p= 0.0004). Statistical significance, indicated with * was determined with t-test followed by Tukey's post hoc test.

2.4.2 *Fmr1* gene deletion causes increased GABAergic innervation and less activity in POMC neurons

To answer if olfactory impairment in males regulates locomotion via feeding circuitry in the hypothalamus, we examined POMC neurons in male mice, since POMC neurons regulate energy expenditure [51, 52], and ablation of POMC neurons reduces locomotion in the dark phase [53]. POMC neurons regulate energy expenditure by targeting MC4R neurons, primarily in the paraventricular nucleus (PVN) of the hypothalamus [54]. POMC neurons also target MC4R expressing neurons in the premotor network, that stimulate locomotion [55]. We determined that 84% of POMC neurons expressed FMRP, while only 9% of MC4R expressing neurons in the PVN contained FMRP (Fig. 2.3). Therefore, we concentrated on POMC neurons and examined their innervation.
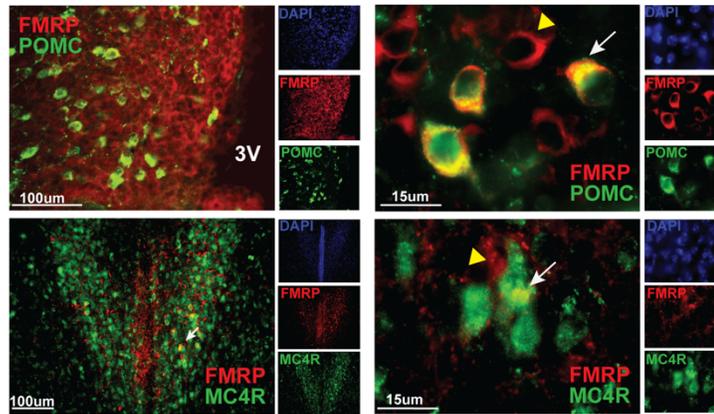
Fig 2.3 POMC neurons express FMRP. Top, POMC neurons in arcuate nucleus stained with anti-β-endorphin (green) and anti-FMRP (red). Representative images using 20x objective (3V, third ventricle, left); and 63X objective (right). Bottom, MC4R neurons in the PVN stained with anti-MC4R (green) and FMRP (red). DAPI was included to detect the nuclei (separate channels on the side) but omitted in overlay to better visualize co-localization of FMRP with neurons of interest.

We then analyzed MC4R protein levels, as targets of POMC neurons via αMSH, we examined MC4R protein levels on whole hypothalamic protein lysates using western blotting and determined that there are no differences in MC4R protein levels between WT and KO males (Fig. 2.4). Activation of POMC neurons occurs via their disinhibition through reduced GABA innervation. Hence, we examined levels of GABA$_A$ receptors and VGAT in the hypothalami of *Fmr1* KO compared to WT. GABARγ2 is the obligatory subunit of the pentameric GABA$_A$ receptor [56], while vesicular GABA transporter (VGAT), is a presynaptic marker of GABAergic terminals [57, 58]. There was a significant increase in the levels of GABARγ2 protein in the hypothalami of *Fmr1* KO male mice, consistent with our previous observations in female mice {Villa, 2023 #10046}. However, VGAT levels were not different (Fig. 2.4).
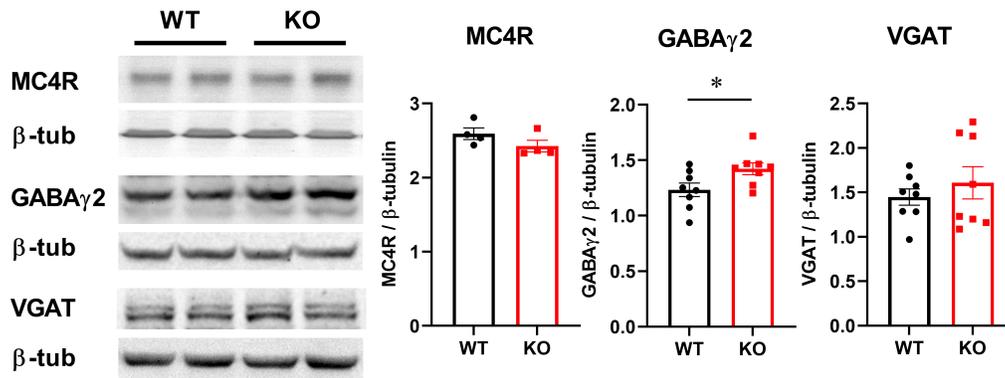
Fig 2.4 Western blots of the hypothalami whole cell lysates determined changes in synaptic proteins in *Fmr1* KO male mice. Hypothalami were dissected and protein levels were analyzed by western blotting. Protein levels of 4-8 mice per group were quantified using ChemiDoc and amount of the protein of interest normalized to the amount of β-tubulin. Each point represents one animal, while bars represent group means +/- standard error. Statistical significance, indicated with a * ($p < 0.05$) was determined with t-test followed by Tukey's post hoc test.

Since GABA can regulate POMC neuron activity (PMID 18272480, PMID 11373681) and we determined increases in GABARγ2 in the whole hypothalamus of male KO animals, we next analyzed the GABAergic innervation of POMC neurons. First, we counted the number of GABA$_A$ receptors in the POMC neuron soma and determined a significant increase in *Fmr1* KO mice to 154% from WT (Fig. 2.5a). To determine the number of synaptic GABA$_A$ receptors we performed triple stain for VGAT, GABA$_A$ and POMC, since VGAT is located in GABAergic presynaptic terminal. We stained for b-endorphin to detect POMC neurons, GABAγ2 and VGAT and counted the number of puncta where VGAT was located in a close opposition to GABAγ2 in POMC neurons. At least 15 neurons per mouse, 3 mice per group, were counted (Fig. 2.5b). We determined more than a 4-fold increase (to 409%) in GABAergic innervation of POMC neurons in *Fmr1* KO mice.
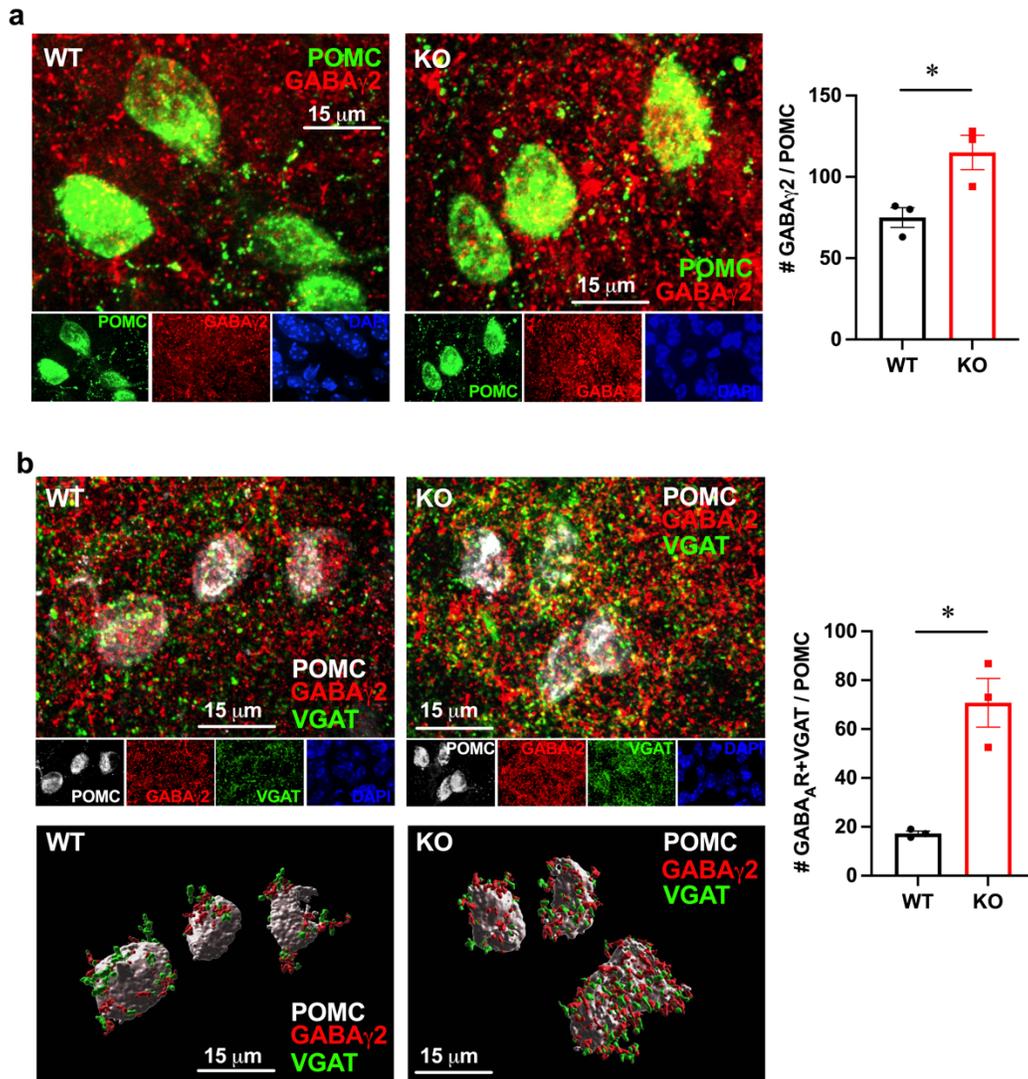
Fig 2.5 *Fmr1* KO males have increased GABAergic innervation. a, GABA$_A$ receptors in the POMC neuron soma were quantified; b, Synaptic GABA$_A$ receptors were quantified as appositions of GABAγ2 and VGAT in POMC neurons. GABA$_A$ (red), VGAT (green), POMC (grey). At least 20 neurons per mouse were quantified and the average for each mouse was represented with a point, while bars present genotype average. Bottom, 3D reconstruction of confocal images using Imaris. Statistical significance, indicated with a * (p < 0.05) was determined with t-test followed by Tukey's post hoc test.

To determine functional significance of changes in innervation, we counted the numbers of MC4R neurons in the PVN and POMC neurons throughout ARC in *Fmr1* KO and WT mice (Fig. 2.6). We determined that there was no change in the number of MC4R neurons in the PVN (Fig. 2.6a). We then assessed the activity of POMC neurons by staining for cFOS and counting the percentage of cFOS-positive POMC neurons. KO mice had significantly lower fraction of cFOS-positive POMC neurons (Fig. 2.6b, arrowheads indicate cFOS-positive neurons; cFOS is located in the nucleus (magenta), while b-endorphin is cytoplasmic (green); inset, higher magnification of the positive neurons indicated by arrows). *Fmr1* KO mice also had fewer POMC neurons in the arcuate nucleus of the hypothalamus (Fig. 2.6c). Given the functional and regional heterogeneity of POMC neurons, we counted POMC neurons separately in the rostral region of the arcuate nucleus and in the caudal region. We determined that rostral region specifically had 24% fewer POMC neurons in *Fmr1* KO than WT controls, while caudal region lacked significant difference (Fig. 2.6d). Given that POMC neurons regulate locomotion via αMSH activation of MC4R-neurons in the premotor area [59, 60], we postulate that this decrease in POMC neuron number causes decreased energy expenditure due to lower innervation of premotor area, which leads to increased weight gain.
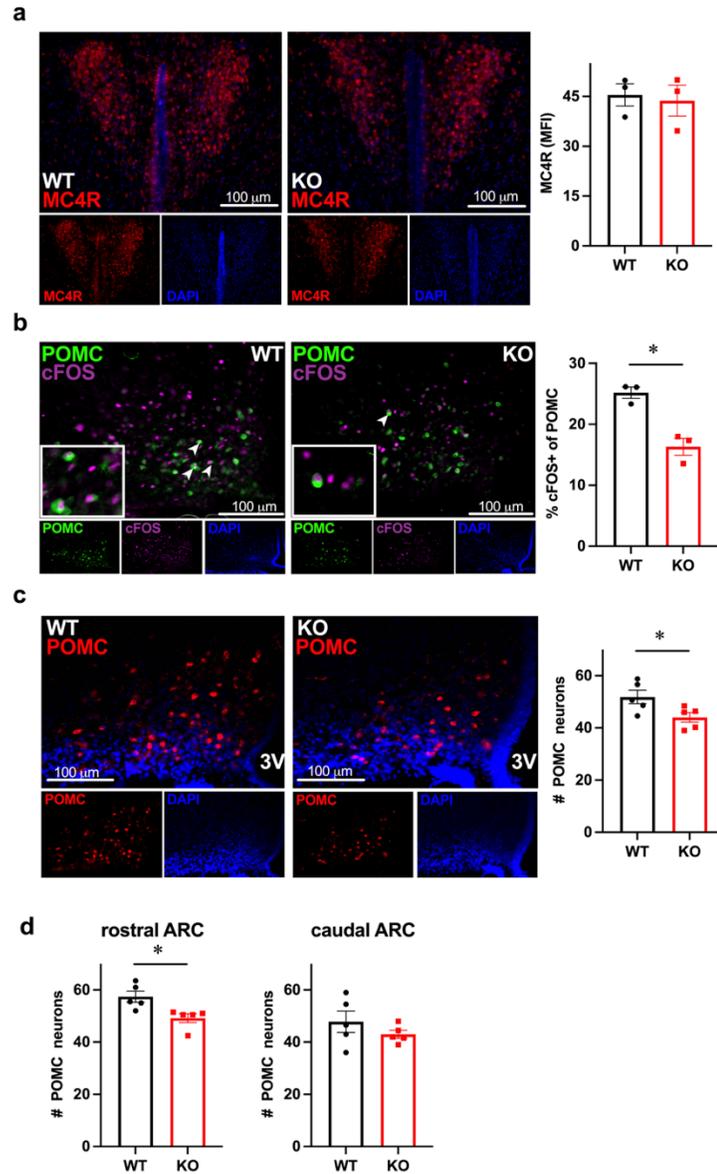
Fig 2.6. Decreased activity and numbers of POMC neurons in the arcuate nucleus of the hypothalamus in *Fmr1* KO male mice. a, no difference in the MC4R neuron number in the PVN between WT and KO male mice, quantified as MFI using ImageJ; MFIs of 5-7 coronal sections per mouse were averaged; each dot represents one animal, bar represents group mean +/- SEM. b, KO males have fewer active POMC neurons compared to WT, determined by co-staining of POMC (green, cytoplasmic) and cFOS (magenta, nuclear). cFOS-positive POMC neurons are indicated with arrowheads, inserts contain higher magnification of double positive neurons. Right, numbers of cFOS positive POMC, shown as percentage. c, KO males have fewer POMC neurons, determined by counting β-endorphin/POMC cell bodies throughout the arcuate nucleus in at least 6 sections per mouse and averaged; each dot represents one animal, bar represents group mean +/- SEM. d, Counts for the rostral and caudal regions demonstrated separately to indicate regional heterogeneity. Statistical significance, indicated with a * ($p < 0.05$) was determined with t-test followed by Tukey's post hoc test.

2.5 Discussion

We sought to uncover the effects of the loss of FMRP on hypothalamic neurons and energy expenditure, which may help elucidate the mechanisms of weight gain in people affected by FXS due to a mutation in the *FMR1* gene. Additionally, our studies uncovered a significant factor, the *FMR1* gene, in weight homeostasis and regulation of feeding circuitry. Our studies determined increased weight without increased food intake in *Fmr1* KO mice. We further determined that the weight gain, specifically in male mice, may be due to lower locomotion during the dark cycle, which in turn may be due to impaired olfaction and the inability to smell food. These results point to the critical role of FMRP in the olfactory-feeding circuitry axis. Furthermore, we determined that POMC neurons that regulate energy expenditure receive higher GABAergic innervation and exhibit lower activity and fewer numbers in *Fmr1* KO mice. Therefore, we posit that POMC neurons are the linchpin between olfaction, hunger signals, and locomotion when foraging for food.

Our results may explain reasons for the increased prevalence of obesity in people affected with FXS. Body weight increase of *Fmr1* KO mice to 115% of controls is similar to what was observed in mice with a deletion of leptin receptor specifically in POMC neurons causes, which experienced 120% weight gain compared to controls [61]. The increase in body weight in *Fmr1* KO mice of the FVB background that we observed here, is consistent with an increase in body weight of *Fmr1* KO mice on C57 background reported before [62]. Report by Leboucher, et al., postulated that the increase in body weight is due to the changes in body composition, specifically an increase in muscle mass

and bone volume, while we provide additional possibilities, such as decreased locomotion or POMC neuron dysfunction that may contribute to weight gain. An earlier study by the same group analyzed metabolic indicators in *Fmr1* KO mice [63] and found a lack of differences in glucose levels, which is in agreement with our study, but reported differences in serum lipid profile, leptin and insulin. Our study may be in agreement with a study using a zebrafish model of *Fmr1* deletion, that determined developmental defects in the motor cortex, which may lead to changes in locomotion [64]. Also in agreement with our results here, decreased locomotion in the *Fmr1* KO mice on the C57 background was reported before, in a report that demonstrated that reduced movement is due to reduced forward locomotion and bout onsets [44]. This study also did not find any differences in food intake similar to our results, but contrary to our study and studies by Lebousher, et al., did not find differences in weight or body composition either. Another study using slightly older mice, did not detect differences in weight {Uutela, 2012 #10078}, either because of differences in age, or because we normalized the litter size, which may explain different results concerning body weight.

We detected an increase in $GABA_A$ receptor levels in the hypothalami of *Fmr1* KO mice. A number of studies determined a decrease in several $GABA_A$ receptor subunits, in the cortex and hippocampus of KO mice, implicating a decrease in inhibitory signaling in the neuropathology of the disease {El Idrissi, 2005 #9668;Adusei, 2010 #9667;Zhang, 2017 #9666;D'Hulst, 2006 #9665}. Indeed, *Fmr1* KO mice show cortical hyperexcitability similar to FXS individuals {Gibson, 2008 #10072;Contractor, 2015 #9681}. However, these differences in $GABA_A$ receptor levels were brain region specific

and were not observed in the cerebellum {D'Hulst, 2006 #9665;D'Hulst, 2009 #10071}. We show increased GABA$_A$ receptor levels in the hypothalami of *Fmr1* KO mice, indicating additional regional differences. GABA is the dominant neurotransmitter in the hypothalamus {Decavel, 1990 #10069} and GABAergic neurons are first order neurons that receive information from periphery {Delgado, 2013 #10070}, indicating the importance of inhibitory circuits in the hypothalamus. Based on findings of decreased GABA$_A$ receptor levels in several brain areas, GABA$_A$ receptor agonists were proposed as possible pharmacological treatments for FXS symptoms {Olmos-Serrano, 2010 #10073;Olmos-Serrano, 2011 #10074;El Idrissi, 2009 #10075}. Given our results, this pharmacological approach may increase incidence of obesity in individuals affected by FXS. Of note, GABA$_A$ receptor agonists cause weight gain and a decrease in locomotor activity when administered to rats {Murphy, 2011 #10076}.

We detected lower neuronal activity and fewer POMC neurons in *Fmr1* KO mice. POMC neurons regulate locomotion and energy expenditure. An increase in energy expenditure occurs via αMSH binding to the MC4R receptors [53]. However, mechanisms whereby POMC neurons regulate locomotion are less clear. Animals increase locomotion to locate food and POMC neurons may be involved in this anticipatory behavior [52]. POMC neurons directly innervate spinal cord regions of the premotor networks via long-range projections to MC4R-expressing V2a interneurons [55]. Furthermore, leptin via leptin receptor expression exclusively in POMC neurons of leptin receptor KO mice is sufficient to stimulate locomotion [65]. AgRP neurons may also be involved, since DREADD-mediated acute activation of AgRP neurons decreased

locomotor activity during the dark cycle [66]. Due to the inability to examine AgRP neurons in *Fmr1* KO mice, without crossing to an AgRP-reporter strain, we examined POMC neurons, since AgRP neurons regulate feeding and satiety, in part, via GABAergic innervation of POMC neurons [20, 21]. We determined a decrease in the activity and number of POMC neurons, which may contribute to decreased locomotion.

POMC neurons are a heterogeneous population [51, 52]. In addition to the population in the arcuate nucleus of the hypothalamus with about 5000 neurons, there is a small population of about 200 POMC neurons in the nucleus of solitary tract (NTS), whose function is not clear. Diphtheria toxin–mediated ablation of POMC neurons in the ARC but not the NTS, increased food intake, reduced energy expenditure, and decreased locomotor activity in the dark stage [53]. For that reason, we focused on POMC neurons in the arcuate nucleus. However, there is further functional and regional heterogeneity within the hypothalamic POMC neurons. Addressing regional heterogeneity, rostral arcuate nucleus POMC neurons project mostly to autonomic areas in the brainstem, such as the dorsal vagal complex [67, 68]. POMC neurons in the caudal part of the arcuate nucleus project to hypothalamic areas, including the PVH. Due to this regional heterogeneity, we counted POMC neurons in the rostral and caudal portions of the arcuate nucleus, separately, and detected a decrease in the rostral POMC population. Findings that POMC neurons from the rostral part of the arcuate nucleus project to the brainstem, which controls locomotion [59, 60], may correspond to our results or decreased locomotion and fewer rostral POMC neurons in *Fmr1* KO male mice. Functional heterogeneity of POMC neurons within the arcuate nucleus may indicate

subpopulations with different roles in the regulation of energy balance, locomotion, food intake, glucose metabolism, and lipid levels {Quarta, 2021 #10004}. Further studies are needed to explain if differences in connectivity, neurotransmitter and neuropeptide receptor composition cause the functional heterogeneity.

Foraging for food is guided by olfactory cues and is accompanied by increased locomotion. *FMR1* is expressed throughout the brain regions associated with olfaction [69]. *Fmr1* KO mice exhibit olfactory dysfunctions and decreased ability to detect an odorant, but lack differences in the ability to habituate to odorants or to discriminate between them [26]. Study in flies determined that FMRP expression is required to process olfactory information and create context-dependent memories [70]. Structural and morphological changes in olfactory brain regions have also been reported in *Fmr1* KO mice [13, 69]. Our results using food pellet detection in the buried food test and marble burying test identified an olfactory deficit. The buried food-seeking test, which tests whether the food-deprived mice can find the food pellet hidden beneath the bedding, determined that KO male mice exhibit a delay, likely due to inability to smell food. Controls for motivation to eat, such as unburied food test, and for burying ability, such as marble burying test, determined that KO mice have the same motivation to eat as WT, consistent with lack of differences in food intake; and that KO mice buried more and thus, exhibit increased repetitive behavior, consistent with *Fmr1*-associated compulsive disorders. Important for our studies, this control determined that KO mice have the ability to dig the bedding. Although it is clear that smelling food increases appetite, the connections between olfactory circuits and feeding circuits are not completely elucidated.

Several studies demonstrated the connectivity between olfactory brain regions and the hypothalamic regions that regulate food intake [71]. Specifically, connections between the olfactory bulb and the hypothalamic arcuate nucleus where POMC neurons are located have been described [71-73]. Sensory detection of food after pellet presentation to mice activated POMC neurons [74], indicating that POMC neurons may be involved in anticipatory behavior in preparation for food intake [52].

Therefore, it is possible that olfactory dysfunction dysregulates POMC neurons, which in turn decrease locomotion in the form of food seeking behavior. This decrease in locomotion reduces energy expenditure and contributes to weight gain, despite the lack of differences in overall food intake.

References for Chapter Two

1. Lieb-Lundell, C. C. E. Three faces of fragile X. Phys. Ther. 96(11), 1782–1790 (2016).

2. Lozano, R. et al. Fragile X syndrome: A review of clinical management. Intract. Rare Dis. Res. 5(3), 145–157 (2016).

3. Raspa, M. et al. Obesity, food selectivity, and physical activity in individuals with fragile X syndrome. Am. J. Intellect. Dev. Disabil.115(6), 482–495 (2010).

4. Butler, M. G. Single gene and syndromic causes of obesity: Illustrative examples. Prog. Mol. Biol. Transl. Sci. 140, 1–45 (2016).

5. Fryns, J. P. et al. A peculiar subphenotype in the fra(X) syndrome: Extreme obesity-short stature-stubby hands and feet-diffuse hyperpigmentation. Further evidence of disturbed hypothalamic function in the fra(X) syndrome?. Clin. Genet. 32(6), 388–392 (1987).

6. Mart.nez-Cerde.o, V. et al. FMR1 premutation with Prader-Willi phenotype and fragile X-associated tremor/ataxia syndrome. Clin. Case Rep. 5(5), 625–629 (2017).

7. de Vries, B. B. et al. Clinical and molecular studies in fragile X patients with a Prader-Willi-like phenotype. J. Med. Genet. 30(9), 761–766 (1993).

8. Edbauer, D. et al. Regulation of synaptic structure and function by FMRP-associated microRNAs miR-125b and miR-132. Neuron 65(3), 373–384 (2010).

9. Feng, Y. et al. Translational suppression by trinucleotide repeat expansion at FMR1. Science 268(5211), 731–734 (1995).

10. Ascano, M. et al. FMRP targets distinct mRNA sequence elements to regulate protein expression. Nature 492, 382 (2012).

11. Darnell, J. C., Mostovetsky, O. & Darnell, R. B. FMRP RNA targets: Identification and validation. Genes Brain Behav. 4(6), 341–349 (2005).

12. Darnell, J. C. et al. FMRP stalls ribosomal translocation on mRNAs linked to synaptic function and autism. Cell 146(2), 247–261 (2011).

13. Rais, M. et al. Sensory processing phenotypes in fragile X syndrome. ASN Neuro 10, 1759091418801092 (2018).

14. Booker, S. A. & Kind, P. C. Mechanisms regulating input–output function and plasticity of neurons in the absence of FMRP. Brain Res. Bull. 175, 69–80 (2021).

15. Berman, R. F. et al. Mouse models of the fragile X premutation and fragile X-associated tremor/ataxia syndrome. J. Neurodev. Disord. 6(1), 25 (2014).

16. Mientjes, E. J. et al. The generation of a conditional Fmr1 knock out mouse model to study Fmrp function in vivo. Neurobiol. Dis. 21(3), 549–555 (2006).

17. Welt, C. K., Smith, P. C. & Taylor, A. E. Evidence of early ovarian aging in fragile X premutation carriers. J. Clin. Endocrinol. Metab. 89(9), 4569–4574 (2004).

18. Berkovitz, G. D. et al. Gonadal function in men with the Martin-Bell (fragile-X) syndrome. Am. J. Med. Genet. 23(1–2), 227–239 (1986).

19. Villa, P. A. et al. Altered GnRH neuron and ovarian innervation characterize reproductive dysfunction linked to the fragile X messenger ribonucleoprotein (Fmr1) gene mutation. Front. Endocrinol. (Lausanne) 14, 1129534 (2023).

20. Morton, G. J., Meek, T. H. & Schwartz, M. W. Neurobiology of food intake in health and disease. Nat. Rev. Neurosci. 15(6), 367–378 (2014).

21. Zhan, C. et al. Acute and long-term suppression of feeding behavior by POMC neurons in the brainstem and hypothalamus, respectively. J. Neurosci. 33(8), 3624–3632 (2013).

22. Bellefontaine, N. et al. Leptin-dependent neuronal NO signaling in the preoptic hypothalamus facilitates reproduction. J. Clin. Invest. 124(6), 2550–2559 (2014).

23. Vong, L. et al. Leptin action on GABAergic neurons prevents obesity and reduces inhibitory tone to POMC neurons. Neuron 71(1), 142–154 (2011).

24. Meng, F. et al. New inducible genetic method reveals critical roles of GABA in the control of feeding and metabolism. Proc. Natl. Acad. Sci. 113(13), 3645–3650 (2016).

25. Balthasar, N. et al. Divergence of melanocortin pathways in the control of food intake and energy expenditure. Cell 123(3), 493–50 (2005).

26. Girardet, C. & Butler, A. A. Neural melanocortin receptors in obesity and related metabolic disorders. Biochem. Biophys. Acta. 1842(3), 482–494 (2014).

27. Dores, R. M. et al. 60 YEARS OF POMC: Melanocortin receptors: Evolution of ligand selectivity for melanocortin peptides. J. Mol. Endocrinol. 56(4), T119–T133 (2016).

28. Antoine, M. W. et al. Increased excitation–inhibition ratio stabilizes synapse and circuit excitability in four autism mouse models. Neuron 101(4), 648-661.e4 (2019).

29. Schilit Nitenson, A. et al. Fragile X mental retardation protein regulates olfactory sensitivity but not odorant discrimination. Chem. Senses 40(5), 345–350 (2015).

30. Russo, C. et al. Ghrelin-containing neurons in the olfactory bulb send collateralized projections into medial amygdaloid and arcuate hypothalamic nuclei: Neuroanatomical study. Exp. Brain Res. 236(8), 2223–2229 (2018).

31. Gascuel, J. et al. Hypothalamus-olfactory system crosstalk: Orexin a immunostaining in mice. Front. Neuroanat. 6, 44 (2012).

32. Hardiman, R. L. & Bratt, A. Hypothalamic–pituitary–adrenal axis function in fragile X syndrome and its relationship to behaviour: A systematic review. Physiol. Behav. 167, 341–353 (2016).

33. Yang, M. & Crawley, J. N. Simple behavioral assessment of mouse olfaction. Curr. Protoc. Neurosci. 8, Unit 8.24 (2009).

34. Machado, C. F. et al. Buried food-seeking test for the assessment of olfactory detection in mice. Bio Protoc. 8(12), e2897 (2018).

35. Angoa-P.rez, M. et al. Marble burying and nestlet shredding as tests of repetitive, compulsive-like behaviors in mice. J. Vis. Exp. JoVE 82, 50978–50978 (2013).

36. Lainez, N. M. & Coss, D. Leukemia inhibitory factor represses GnRH gene expression via cFOS during inflammation in male mice. Neuroendocrinology 108(4), 291–307 (2019).

37. Lainez, N. M. et al. Diet-induced obesity elicits macrophage infiltration and reduction in spine density in the hypothalami of male but not female mice. Front. Immunol. 2018(9), 1992 (1992).

38. Lee, C.H. et al. Neuroanatomical profile of young females with fragile X syndrome: A voxel-based morphometry analysis. Cereb. Cortex (2021).

39. Smith, E. G. et al. Sex differences in resting EEG power in fragile X syndrome. J. Psychiatr. Res. 138, 89–95 (2021).

40. Wall, C. A. et al. Early negative affect in males and females with fragile X syndrome: Implications for anxiety and autism. J. Neurodev. Disord. 11(1), 22 (2019).

41. Nolan, S. O. et al. Deletion of Fmr1 results in sex-specific changes in behavior. Brain Behav. 7(10), e00800 (2017).

42. Reyes, S. T. et al. Effects of the sigma-1 receptor agonist blarcamesine in a murine model of fragile X syndrome: Neurobehavioral phenotypes and receptor occupancy. Sci. Rep. 11(1), 17150 (2021).

43. Bonasera, S. J. et al. Decreased home cage movement and oromotor impairments in adult Fmr1-KO mice. Genes Brain Behav. 16(5), 564-573 (2017).

44. Bailey, D. B. Jr. et al. Co-occurring conditions associated with FMR1 gene variations: Findings from a national parent survey. Am. J. Med. Genet. A 146A(16), 2060–2069 (2008).

45. Bjursell, M. et al. Acutely reduced locomotor activity is a major contributor to Western diet-induced obesity in mice. Am. J. Physiol. Endocrinol. Metab. 294(2), E251–E260 (2008).

46. Rattazzi, L. et al. Impaired sense of smell and altered olfactory system in RAG-1−⁄− immunodeficient mice. Front. Neurosci. 9, 318 (2015).

47. Toda, C. et al. POMC neurons: From birth to death. Annu. Rev. Physiol. 79, 209–236 (2017).

48. Quarta, C. et al. POMC neuronal heterogeneity in energy balance and beyond: An integrated view. Nat. Metab. 3(3), 299–303 (2021).

49. Garfield, A. S. et al. A neural basis for melanocortin-4 receptor-regulated appetite. Nat. Neurosci. 18(6), 863–871 (2015).

50. Reino., P. et al. Hypothalamic pomc neurons innervate the spinal cord and modulate the excitability of premotor circuits. Curr. Biol. 30(23), 4579-4593.e7 (2020).

51. Spergel, D. J. Modulation of gonadotropin-releasing hormone neuron activity and secretion in mice by non-peptide neurotransmitters, gasotransmitters, and gliotransmitters. Front. Endocrinol. (Lausanne) 10, 329 (2019).

52. Lin, W. et al. Distribution of vesicular glutamate transporter-2 messenger ribonucleic acid and protein in the septum-hypothalamus of the rat. Endocrinology 144(2), 662–670 (2003).

53. Yin, W. et al. Expression of vesicular glutamate transporter 2 (vGluT2) on large dense-core vesicles within GnRH neuroterminals of aging female rats. PLoS ONE 10(6), e0129633 (2015).

54. Leiras, R., Cregg, J. M. & Kiehn, O. Brainstem circuits for locomotion. Annu. Rev. Neurosci. 45, 63–85 (2022).

55. Takakusaki, K. et al. Brainstem control of locomotion and muscle tone with special reference to the role of the mesopontine tegmentum and medullary reticulospinal systems. J. Neural Transmiss. 123(7), 695–729 (2016).

56. Balthasar, N. et al. Leptin receptor signaling in POMC neurons is required for normal body weight homeostasis. Neuron 42(6), 983–991 (2004).

57. Leboucher, A. et al. Fmr1-deficiency impacts body composition, skeleton, and bone microstructure in a mouse model of fragile X syndrome. Front. Endocrinol. 10(678) (2019).

58. Leboucher, A. et al. The translational regulator FMRP controls lipid and glucose metabolism in mice and humans. Mol. Metab. 21, 22–35 (2019).

59. Barker, C. M., Miles, K. D. & Doll, C. A. Fmrp regulates neuronal balance in embryonic motor circuit formation. Front. Neurosci. 16, 962901 (2022).

60. Uutela, M. et al. Reduction of BDNF expression in Fmr1 knockout mice worsens cognitive deficits but improves hyperactivity and sensorimotor deficits. Genes Brain Behav. 11(5), 513–523 (2012).

61. El Idrissi, A. et al. Decreased GABA(A) receptor expression in the seizure-prone fragile X mouse. Neurosci. Lett. 377(3), 141–146 (2005).

62. Adusei, D. C. et al. Early developmental alterations in GABAergic protein expression in fragile X knockout mice. Neuropharmacology 59(3), 167–171 (2010).

63. Zhang, N. et al. Decreased surface expression of the δ subunit of the GABA(A) receptor contributes to reduced tonic inhibition in dentate granule cells in a mouse model of fragile X syndrome. Exp. Neurol. 297, 168–178 (2017).

64. D'Hulst, C. et al. Decreased expression of the GABAA receptor in fragile X syndrome. Brain Res. 1121(1), 238–245 (2006).

65. Gibson, J. R. et al. Imbalance of neocortical excitation and inhibition and altered UP states reflect network hyperexcitability in the mouse model of fragile X syndrome. J. Neurophysiol. 100(5), 2615–2626 (2008).

66. Contractor, A., Klyachko, V. A. & Portera-Cailliau, C. Altered neuronal and circuit excitability in fragile X syndrome. Neuron 87(4), 699–715 (2015).

67. D'Hulst, C. et al. Expression of the GABAergic system in animal models for fragile X syndrome and fragile X associated tremor/ ataxia syndrome (FXTAS). Brain Res. 1253, 176–183 (2009).

68. Decavel, C. & Van den Pol, A. N. GABA: A dominant neurotransmitter in the hypothalamus. J. Comp. Neurol. 302(4), 1019–1037 (1990).

69. Delgado, T. Glutamate and GABA in appetite regulation. Front. Endocrinol. 4 (2013).

70. Olmos-Serrano, J. L. et al. Defective GABAergic neurotransmission and pharmacological rescue of neuronal hyperexcitability in the amygdala in a mouse model of fragile X syndrome. J. Neurosci. 30(29), 9929–9938 (2010).

71. Olmos-Serrano, J. L., Corbin, J. G. & Burns, M. P. The GABA(A) receptor agonist THIP ameliorates specific behavioral deficits in the mouse model of fragile X syndrome. Dev. Neurosci. 33(5), 395–403 (2011).

72. El Idrissi, A. et al. Taurine improves congestive functions in a mouse model of fragile X syndrome. Adv. Exp. Med. Biol. 643, 191–198 (2009).

73. Murphy, H. M., Ihekoronze, C. & Wideman, C. H. Zolpidem-induced changes in activity, metabolism, and anxiety in rats. Pharmacol. Biochem. Behav. 98(1), 81–86 (2011).

74. Huo, L. et al. Leptin-dependent control of glucose balance and locomotor activity by POMC neurons. Cell Metab. 9(6), 537–547 (2009).

75. Jiang, J. et al. Activation of hypothalamic AgRP and POMC neurons evokes disparate sympathetic and cardiovascular responses. Am. J. Physiol.-Heart Circ. Physiol. 319(5), H1069–H1077 (2020).

76. Zheng, H. et al. Brain stem melanocortinergic modulation of meal size and identification of hypothalamic POMC projections. Am. J. Physiol. Regul. Integr. Comp. Physiol. 289(1), R247–R258 (2005).

77. King, C. M. & Hentges, S. T. Relative number and distribution of murine hypothalamic proopiomelanocortin neurons innervating distinct target sites. PLoS ONE 6(10), e25864 (2011).

78. Bodaleo, F. et al. Structural and functional abnormalities in the olfactory system of fragile X syndrome models. Front. Mol. Neurosci. 12(135) (2019).

79. Kanellopoulos, A. K. et al. Learning and memory deficits consequent to reduction of the fragile X mental retardation protein result from metabotropic glutamate receptor-mediated inhibition of cAMP signaling in Drosophila. J. Neurosci. 32(38), 13111–13124 (2012).

80. Peris-Sampedro, F. et al. The orexigenic force of olfactory palatable food cues in rats. Nutrients 13(9) (2021).

81. Yeomans, M. R. Olfactory influences on appetite and satiety in humans. Physiol. Behav. 87(4), 800–804 (2006).

82. Jovanovic, P. & Riera, C. E. Olfactory system and energy metabolism: a two-way street. Trends Endocrinol. Metab. 33(4), 281–291 (2022).

83. Chen, Y. et al. Sensory detection of food rapidly modulates arcuate feeding circuits. Cell 160(5), 829–841 (2015).

CHAPTER THREE:

Single-Cell Transcriptomics Identifies Pituitary Gland Changes in Diet-Induced Obesity

Rebecca E. Ruggiero-Ruff [#1], Brandon H. Le [#2], Nancy M. Lainez[1] and Djurdjica Coss[*1]

[1]Division of Biomedical Sciences; School of Medicine, University of California, Riverside; [2]Institute for Integrative Genome Biology Bioinformatics Core Facility, University of California, Riverside; Riverside, CA 92521

# equal contribution

3.1 Abstract

Obesity is a chronic disease with increasing prevalence worldwide. Obesity leads to increased risk of heart disease, stroke, and diabetes; as well as endocrine alterations, linked to reproductive disorders, changes in basal metabolism, and stress hormone production, all of which are regulated by the pituitary. In this study, we performed single cell RNA sequencing (scRNA-seq) of pituitary glands from male mice fed control (CTRL) and high-fat diet (HFD), to determine obesity-mediated changes in pituitary cell populations and gene expression. We determined that HFD induced dramatic changes in somatotrope and lactotrope populations, by increasing the proportion of somatotropes and decreasing the proportion of lactotropes. Cell numbers of other hormone-producing cell populations remained unaffected. Gene expression changes demonstrated that in HFD, somatotropes became more metabolically active, with increased expression of genes associated with cellular respiration, and downregulation of genes and pathways associated with cholesterol biosynthesis. Despite a lack of changes in gonadotrope numbers, genes important in the regulation of gonadotropin hormone production were significantly downregulated. Corticotropes and thyrotropes were the least affected in HFD, while melanotropes exhibited reduced cell number. Lastly, we determined that changes in plasticity and gene expression caused changes in hormone levels. Serum prolactin was decreased corresponding to fewer lactotropes, while lower luteinizing hormone (LH) and follicle-stimulating hormone (FSH) in the serum corresponded to a decrease in transcription and translation. Taken together, our study highlights diet-

induced changes in pituitary gland populations and gene expression that play a role in altered hormone levels in obesity.

3.2 Rationale to elucidating diet-induced obesity changes in the pituitary gland

Obesity is a significant public health concern, since the number of obese people has steadily increased over the last 30 years (1). Currently, over a third of US population is obese, which causes $147 billion a year economic burden to the US healthcare system (2). This increase in obesity has coincided with an increase in co-morbidities, such as metabolic disorders, type 2 diabetes, cardiovascular disease, stroke, and diminished reproductive function (3-7). The pituitary gland secretes hormones that control metabolism, growth, stress response, and reproduction. Thus, pituitary may respond to increased caloric intake in diet-induced obesity to maintain homeostasis. Furthermore, pituitary hormone synthesis and secretion is under control of hypothalamic releasing hormones, that also exhibit gene expression changes in response to obesity (8, 9), since hypothalamus regulates feeding and satiety, in addition to other homeostatic functions. To investigate population changes and gene expression changes in the pituitary during obesity, we analyzed pituitary cells using single cell RNA sequencing (scRNA-seq).

Pituitary gland can be divided into posterior pituitary, a collection of axonal projections whose cell bodies are located in the hypothalamus that secrete oxytocin and vasopressin, and anterior pituitary, an endocrine gland. Anterior pituitary comprises the main portion of the pituitary gland and is composed of five secretory cell types that

secrete six hormones (10-12). Hormone-producing cells encompass the largest fractions of anterior pituitary cells: growth hormone (GH)-producing somatotropes are the most abundant, followed by prolactin (Prl)-producing lactotropes, while thyroid stimulating hormone (TSH)-producing thyrotropes, luteinizing hormone (LH) and follicle-stimulating hormone (FSH)-producing gonadotropes, and adrenocorticotropin (ACTH)-producing corticotropes each comprise smaller percentages of cells. Stem cells, endothelial cells, and immune cells are also present in the pituitary and although scarce, may regulate the function of hormone-producing cells (13, 14). These different cell populations develop sequentially under the control of lineage-defining transcription factors (15, 16). Given such mixed lineage, scRNA-seq provides an ability to determine changes within one population of cells, and compare changes at a population level leading to altered cell number, to transcriptional level leading to gene induction or repression.

Herein, we investigated pituitary changes after a 12-week exposure to a high fat diet. We previously analyzed gene expression changes in the hypothalamus using a custom Nanostring probe panel, and reported changes in *Gnrh*, *Dat* dopamine transporter, *Pomc* mRNA levels in the hypothalamus, in addition to obesity-mediated gene expression alterations of other neuropeptides and synaptic molecules (8, 9). We also reported inflammatory changes that stem from activation of resident immune cells and infiltration of peripheral myeloid cells into the hypothalamus. Since pituitary endocrine cells respond to hypothalamic releasing peptides, in this study we focused on changes in the anterior pituitary cells in response to obesity.

We used the 10x Genomics platform for scRNA-seq to analyze obesity-mediated changes in gene expression and in different populations of pituitary endocrine cells. scRNA-seq (17-22) and single nuclei RNA-sequencing (snRNA-seq) (23, 24) of the pituitary gland was performed previously and we first compared our studies to these previous studies to classify cell types. We chose the 10X platform that was demonstrated to have highly consistent performance for high throughput analyses compared to other methods (25). Given that the pituitary can be relatively easily dissociated into single cells, compared to other tissues, such as brain, muscle, or adipose, we opted for scRNA-seq rather than snRNA-seq. Although cell dissociation may change select mRNA levels, scRNA-seq allowed detection of a total cellular RNAs of which nuclear RNAs are only a portion (25, 26). We then compared different pituitary cell type changes in response to obesity. We determined changes in pituitary population and gene expression that correspond to changes in hormone levels in the circulation.

3.3 Materials and Methods

3.3.1 Mice

All experiments were performed with approval from the University of California (Riverside, CA) Animal Care and Use Committee and in accordance with the National Institutes of Health Animal care and Use Guidelines. C57BL/6J mice were maintained under a 12-hour light, 12-hour dark cycle and received food and water *ad libitum*. C57BL/6J male mice were obtained from Jackson labs at weaning age. After a week of

acclimatization on normal chow, mice were placed on either high fat diet (HFD, D12492, 60% kcal from fat; 5.21 kcal/g; carbohydrate 20% kcal, protein 20% kcal, fat 60% kcal (lard 0.32 g/g diet, soybean oil 0.03 g/g); Research Diet, New Brunswick, NJ) or control diet (CTRL, D12450J, 10% kcal from fat; matching sucrose levels to HFD; 3.82 kcal/g; carbohydrate 70% kcal, protein 20% kcal, fat 10% kcal (lard 0.02 g/g diet, soybean oil 0.025 g/g); Research Diet, New Brunswick, NJ) for 12 weeks.

3.3.2 Pituitary gland dispersion

Pituitary glands from each animal were processed separately. Pituitary glands from 16-week old male C57BL/6J mice were dissected, rinsed in ice cold 1X PBS, and placed into an enzyme cocktail containing 0.25% collagenase and 0.25% Trypsin-EDTA in HBSS with 25 mM HEPES pH 7.2 for 30 minutes at 37 C. Enzymatic reaction was stopped with 10% Fetal Bovine Serum (FBS) in DMEM and 1% Penicillin-Streptomycin. DNAse1 at a final concentration of 25 µg/ml was added to each pituitary suspension for 10 minutes at 37 C, Debris was removed by passing through a 70 µM filter and cells were gently pelleted at 180 g for 5 minutes and resuspended at ~1200 cells per µL in DMEM for 10x Genomics gel beads-in-emulsion (GEM) preparation.

3.3.3 Single cell capture and library preparation using 10x Chromium platform

Single cell 3' library generation was performed using the 10x Genomics Chromium Controller, following the manufacturer's protocol for the v3.1 reagent kit (10x Genomics,

Pleasanton, CA, CG000204). Single cells RNA-sequencing (scRNA-seq) was performed using four lanes on the 10x Genomics Chromium, providing two biological and technical replicates for each diet. Individual pituitary suspensions were loaded onto a Chromium Single Cell A Chip, one suspension per lane, with a master mix of reverse transcription (RT) reagents, single cell 3' v3.1 gel beads, and partitioning oil into respective wells. Each sample contained a total of 16,560 cells with cell viabilities between 90-95% at a concentration of 1200 cells/µl with a targeted cell recovery of 10,000 cells per channel at a multiplet rate of 7.6%. Following GEM creation, RT was performed to generate barcoded cDNA. The resulting post-GEM RT product was cleaned up using DynaBeads MyOne SILANE beads (Thermofisher Scientific) and SPRIselect Reagent kit (Beckman Coulter). Full-length barcoded cDNA was amplified, cleaned, and fragmented, to generate sequencing libraries. 3' single cell gene expression libraries were generated using a fixed proportion (25%) of the total cDNA per sample), with unique indices per sample to allow for multiplexing (Chromium Dual Index Kit TT, Set A, PN-1000215, 10x Genomics). Libraries were quantified by Qubit 3 fluorometer (Invitrogen) and quality assessed by the 2100 Agilent High Sensitivity BioAnalyzer (UC Riverside Genomics Core Facility, Riverside, CA). Equivalent molar concentrations of libraries were pooled and sequenced using Novaseq 6000 (Illumina) using 10x Genomics recommended sequencing depth and run parameters (sequencing depth of 50,000 read pairs per cell) at the UC San Diego (UCSD) Institute for Genomics Medicine (IGM) Center.

3.3.4 Data processing and Quality Control

Demultiplexed FASTQ files were aligned to the mouse mm10-2020-A genome with
Cell Ranger v6.1.2 with default setting using STAR aligner in the Cell Ranger count
pipeline. The Cell Ranger count pipeline uses FASTQ files to perform alignment,
filtering, barcode counting, and UMI counting, to determine clusters and gene expression
analysis. The Cell Ranger-generated gene expression matrices were imported into R
(v4.2.2) (R Core Team 2022: *R: A Language and Environment for Statistical Computing.*
Vienna, Austria: R Foundation for Statistical Computing. https://www.R-project.org/)
with the Seurat (v4.3) package (27) using the convenience function Read10X. The
function imports individual samples processed through the Cell Ranger pipeline as a
Seurat Object. All the samples (i.e., Seurat objects) were aggregated into one with the
Seurat merge function. Quality control analysis was carried out on the aggregated object
to identify and remove low-quality cells. Specifically, cells were selected for further
downstream analysis on the following criteria: gene counts > 1000, UMI counts per cell >
1000, log10GenesPerUMI > 0.8; fraction of reads in cells was between 86%-91%, cells
with mitochondrial genes > 20% were filtered out to eliminate dead cells. Included cells
were further subjected to doublet detection using Chord with default settings, which were
also filtered out (28). (Supplemental Figure 3.1 and Supplemental Table 3.1 demonstrate
quality control parameters).
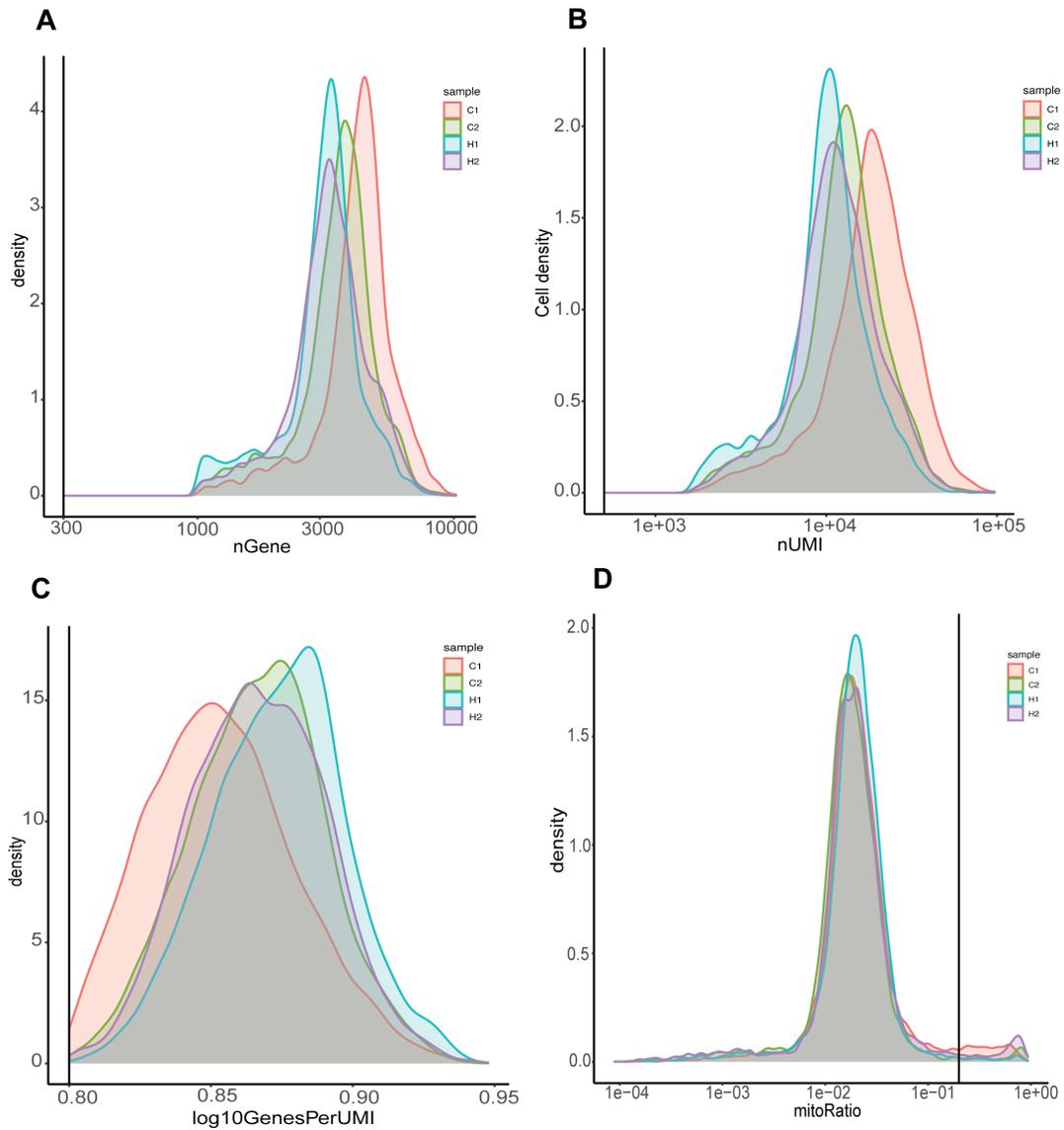
Supplemental Fig 3.1 Quality Control of scRNA-seq datasets. A. Gene counts; B. UMI counts per cell; C. Log10GenesPerUMI; D. Percent mitochondrial genes, vertical line indicates 20% of mitochondrial genes set as a cutoff for inclusion (left of line) or exclusion (right).

100

	Ctrl 1	Ctrl 2	HFD 1	HFD 2
Number of cells	7,463	8,173	10,921	8,180
Total sequence reads	770,377,703	676,466,100	617,667,548	718,862,907
Sequencing saturation	79.7%	75.7%	78.6%	78.8%
Fraction of reads in cells	86.0%	90.1%	86.3%	90.7%
Total genes detected	23,199	23,216	22,759	23,265
Mean reads per cell	103,226	82,768	56,558	87,881
Median genes detected per cell	3,004	3,468	1,707	3,139
Median UMI per cell	9,9433	11,771	4,822	10,490
Reads mapped to genome	94.5%	94.2%	93.1%	95.3%
Reads mapped uniquely to transcriptome	73.9%	72.6%	70.6%	74.3%

Supplemental Table 3.1 Cell Capture and Sequencing Metrics for scRNA-seq of C57BL/6J mouse pituitary gland fed either control (CTRL) or high fat diet (HFD).

3.3.5 Normalization, Dimensional Reduction and Clustering

Data were normalized using the Seurat SCTransform (v0.3.5) package (29, 30) with

parameters method = "glmGamPoi", vst.flavor="v2" and regression of the percentage of

mitochondrial genes mapping. Principal component analysis (PCA) within the Seurat

package was performed using RunPCA with n = 30. Cell clusters were generated using

the 30 principal components with the FindNeighbors and FindClusters functions within

Seurat and visualization in a two-dimensional space using the UMAP algorithm. To

identify markers for each cluster, the FindAllMarkers function within Seurat was applied

with the Wilcox likelihood-ratio test and p-value adjustments using the Bonferroni

correction. Markers were defined as genes with expression in more than 25% of the cells

within the cluster and having a positive log2 fold change >= 0.25 against all other

clusters and an adjusted p-value < 0.05.

3.3.6 Differential gene expression (DEG) and gene ontology (GO) enrichment analysis

Differentially-expressed genes (DEGs) between conditions (CTRL and HFD) for each

cluster were identified using the Seurat FindMarkers function with parameters

"min.pct=0.25 logfc.threshold=0.25". Specifically, the Seurat object containing all the

clusters and normalized data was subset by cluster and the FindMarkers function was

applied to each cluster. DEGs, presented in the volcano plots, were defined as genes with

expression in more than 25% of the cells within the cluster and having log2 fold change

threshold more than 25% between CTRL and HFD with a p-value <0.05. Gene ontology

(GO) enrichment analysis was carried out using ShinyGo v0.77 platform (South Dakota State University) (31). All significant genes that were up or downregulated (Upregulated: Log2FC $\geq$ 0.25, -Log10 (p-value) >1.3, Downregulated: Log2FC $\leq$ 0.25, -Log10 (p-value) >1.3) for each relative comparison were visualized using a dotplot chart, plotting fold enrichment for each respective GO term for Biological Processes. For each GO enrichment analysis, FDR of <0.05 was applied, with the pathway minimum set to 10.

3.3.7 Sub-cluster analysis

To identify sub-clusters within the annotated cell cluster (e.g., somatotrope), cells within a cluster were first extracted using the base R subset function. The reduced dataset (containing only cells within the cluster) was subjected to normalization, PCA dimensional reduction, and clustering using the same parameters and settings as before for all the data. Differential expression analysis within each sub-cluster was determined as described above.

3.3.8 Pseudotime trajectory analysis

Trajectory analyses were implemented using the Monocle3 packages (32) with default parameters. For the somatotrotope - progenitor - lactotrope lineages, Pou1f1 expressing cells were set as the trajectory root. For the gonadotrope - thyrotrope trajectories, Cga expressing cells were set as the root**.**

3.3.9 Hormone analysis

CTRL and HFD males were sacrificed between 9 am and 11 am by isoflurane inhalation and blood was obtained from the inferior *vena cava.* Blood was left to coagulate for 15 min at room temperature and centrifuged at 2000g for 15 min to obtain serum. Hormone levels were measured using Luminex MagPix instrument using the Milliplex MAP Mouse Pituitary Magnetic Bead Panel (MPTMAG-49K, Millipore Sigma, Burlington, MA). Given that LH antibody from the Millipore panel did not pass quality control, we performed the ultra-sensitive, in-house LH ELISA to measure LH in serum (33). The capture monoclonal antibody (anti-bovine LH beta subunit, 518B7, RRID:AB_2665514) was provided by Janet Roser (University of California, Davis). The detection polyclonal antibody (rabbit LH antiserum, AFP240580Rb, RRID:AB_2665533) was provided by the National Hormone and Peptide Program (NHPP). HRP-conjugated polyclonal antibody (goat anti-rabbit) was purchased from DakoCytomation (Glostrup, Denmark; D048701-2). Mouse LH reference prep (AFP5306A; NHPP) was used as the assay standard. The assay sensitivity is 0.016 ng/ml and the intra-assay coefficient of variation is 2.2% and inter assay coefficient of variation was 7.3% at the low end of the standard curve. Statistical analysis was performed by GraphPad Prism 9. Each animal is presented with a dot, while group average was presented as a bar ± standard error. Statistical differences between CTRL and HFD male mice were determined using t-test and Tukey's posthoc analysis ($p < 0.05$).

3.4 Results

3.4.1 scRNA-seq of pituitary glands identified pituitary cell types

Pituitary single-cell suspensions from control (CTRL) or high fat diet (HFD) male C57BL/6J mice were processed separately and loaded on the Chromium Next GEM Chip, each into a separate well to account for biological and technical variability (Supplemental Table 3.1). Single cell libraries were aggregated, and quality control (QC) performed using Seurat. A total of 23,888 cells were recovered: 4,151 and 6,813 cells for CTRL and 5,940 and 6,984 cells for HFD. Uniform Manifold Approximation and Projection (UMAP) plots of each biological replicate were highly similar, and all cell populations were common to each sample in the aggregated data set (Supplemental Figure 3.2), demonstrating low variability between samples.
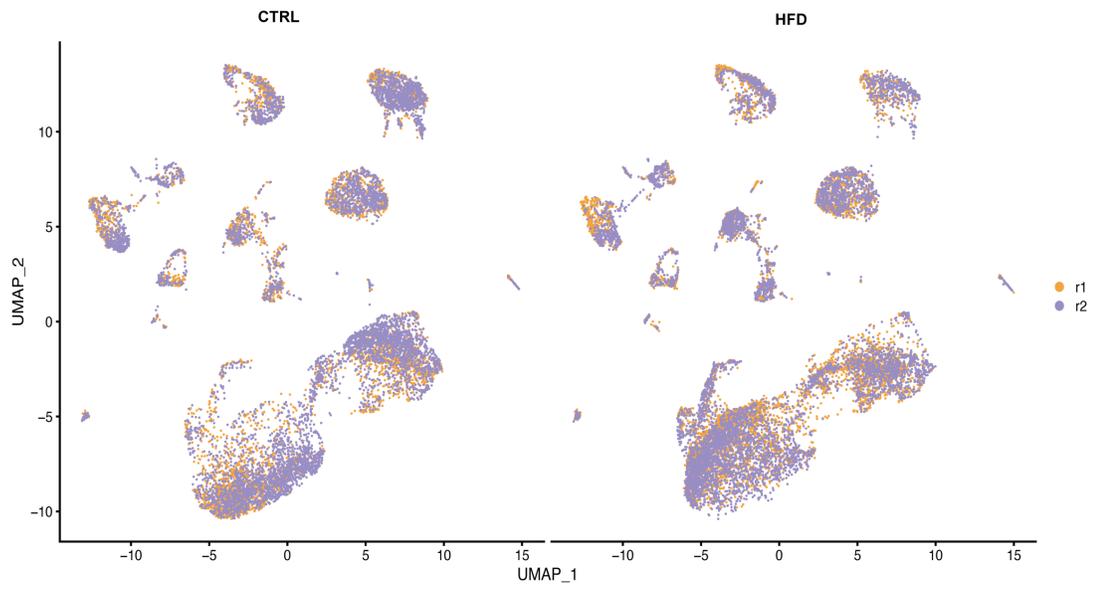
Supplemental Figure 3.2 UMAP plot of aggregate cells from CTRL and HFD mice.

Seurat was used to identify cell clusters presented in UMAP of aggregated data set (Fig. 3.1A). Sixteen separate population clusters were identified (Fig. 3.1A). Pituitary populations were initially identified with known marker genes (Fig. 3.1B). Somatotropes (#1, green), characterized by high expression of *Gh,* were the most abundant cell population comprising 36% of cells. *Prl*-expressing lactotropes (#2, magenta) were the second most abundant cell type comprising 18%. Corticotrope (#4, yellow, 9%) and intermediate lobe melanotropes (#5, orange, 7%) were identified by high expression of *Pomc.* Melanotropes were distinguished from corticotropes by expression o*f Oacyl,* which was previously described as a novel marker of melanotropes (17) (Fig. 3.1B). Melanotropes (#5, orange) also demonstrated significant differences from a population exhibiting melanotrope progenitor markers, such as *Pax7* and *Tbx19* (#15, silver, melano-progen, 0.3% of all cells), that they separated into different clusters. Gonadotropes (#8, purple), representing 5% of cells, were identified by *Lhb* and *Fshb*, and thyrotropes (#9, brown), representing 2% of cells, were identified by *Tshb* expression. Lineage-specific transcription factors, such as *Pou1f1* and *Nr5a1* were highly expressed in their respective cell types. *Pou1f1* was expressed in somatotropes and lactotropes and their progenitors (#3, darker blue, 4% of cells), while *Nr5a1,* a SF1 transcription factor that marks committed gonadotropes, was expressed highly in the gonadotrope population (Fig. 3.1B). We also identified double-positive Pou1f1+Nr5a1+ population (#14, pink, 0.3% of cells) that exhibited lower expression of hormonal genes, *Gh*, *Prl*, *Lhb*, *Fshb*, than fully differentiated somatotropes, lactotropes or gonadotropes, respectively (Fig 3.1B). This population was previously described (22) and proposed to be a new developmental

trajectory. Co-expression of *Pou1f1* and *Nr5a1* was also previously described in pituitary tumors (34). Endothelial cells (#7, blue), representing 5% of cells, were defined by expression of *Plvap*; stem cells (#6, red) representing 6% of cells, by the expression of *Mia*; myeloid cells (#12, orange) representing 2.8% of cells, by the expression of *Cx3cr1* and *Trem2*, and lymphoid cells (#13, lavender) representing 0.7% of cells, by the expression of *Cd3g* (Fig. 3.1B).

To further characterize clusters and identify top differentially expressed genes that define each cluster, top six markers for each hormone-producing cell type, endothelial and stem cells were plotted in a heatmap (Fig. 3.1C). Unsurprisingly, the top marker in each hormone-producing cluster was the specific hormone it produces and secretes, such as *Gh* for somatotropes, *Prl* for lactotropes, *Pomc* for corticotropes and melanotropes, *Lhb and Fshb* for gonadotropes and *Tshb* for thyrotropes (Fig. 3.1C). Most of other cluster-defining genes were previously characterized (17), such as *Pappa2* and *Rad18* in somatotropes, *Angpt1* and *Edil3* in lactotropes, *Tnnt1* for corticotropes, *Oacyl, Esm1 and Pkib* in melanotropes and *Tgfbr3l, Spp1 and Grem1* in gonadotropes (Fig. 3.1C). Adult pituitary stem cells, the largest non-hormonal producing population, were enriched in markers such as *Mia, Lcn2,* in addition to *Sox2*; while endothelial cells were enriched in *Igfbp3* and *Igfbp7*, in addition to *Plvap* (Fig. 3.1C). These most highly enriched genes per cluster support our classification of the 16 identified populations.
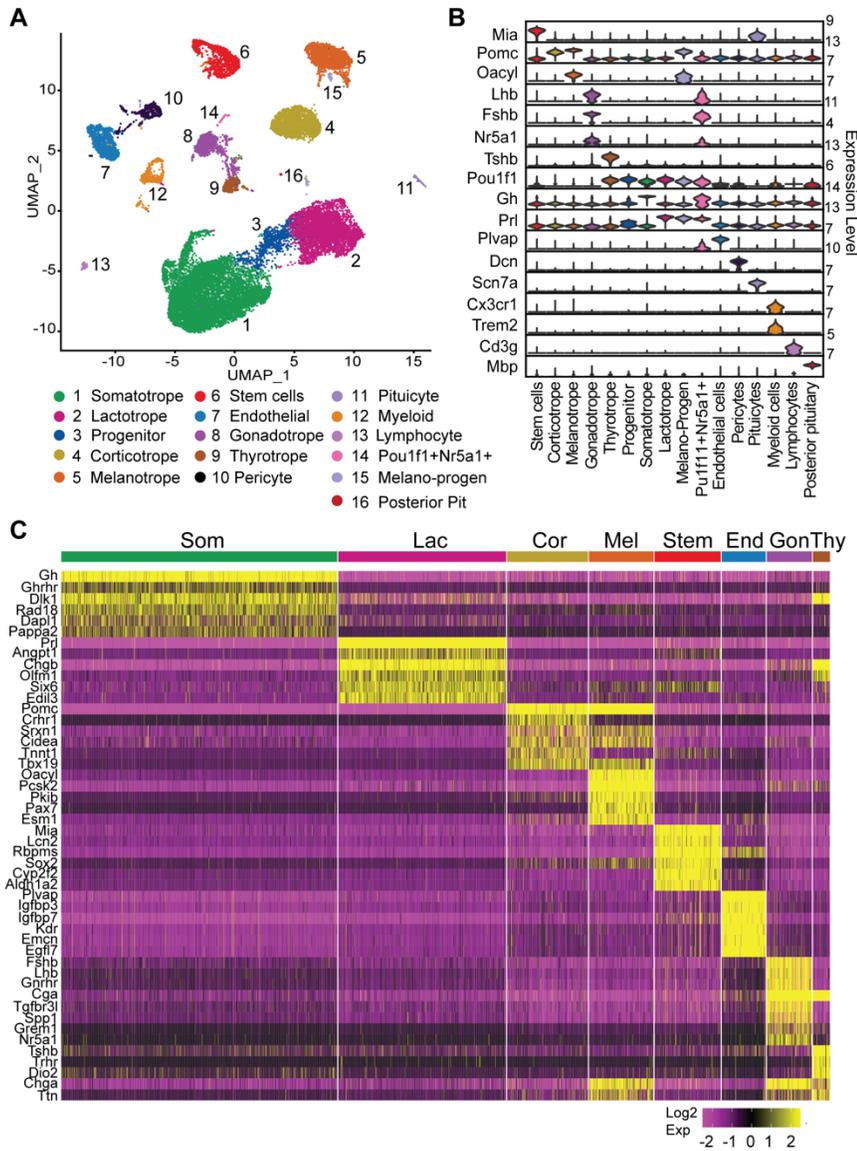
Fig 3.1 Identification of mouse pituitary cell types using scRNA-seq. A. UMAP representation of 23,888 male pituitary cells from the merged data sets from CTRL and HFD. Cells of the same type were color-coded, while each dot represents a single cell; B. Violin plot representation of expression levels of marker genes for each cell type (same colors as in A); C. Heat map demonstrates expression of the top 6 enriched genes in somatotropes (Som), lactotropes (Lac), corticotropes (Cor), melanotropes (Mel), gonadotropes (Gon), thyrotropes (Thy), stem cells (Stem) and endothelial cells (End).

3.4.2 High fat diet induced population changes in the pituitary gland

Given that obesity causes significant homeostatic changes, we determined whether HFD induced population changes in the pituitary hormone-producing cell clusters (Fig. 3.2). We performed clustering analysis and compared pituitary populations in CTRL and HFD diet male mice (Fig. 3.2A). The same populations were detected in HFD as in CTRL, however there was a significant shift in several of the clusters, specifically in somatotropes (green) and lactotropes (magenta) (Fig. 3.2A). To easier observe these differences, we overlapped UMAP projections of CTRL and HFD (Fig. 3.2B). The somatotrope fraction increased from 30.2% in CTRL to 41.1% in HFD, while lactotrope fraction decreased from 21.6% to 14.4% (Fig. 3.2C). Melanotrope population also changed, and its proportion decreased in HFD, from 11.2% in CTRL to 4.5% in HFD. We previously analyzed obesity-mediated inflammation in the hypothalamus (7-9, 35, 36), and determined obesity-induced infiltration and increased numbers of immune cells of myeloid lineage. In the pituitary, as well, myeloid cell numbers increased from 2.5% in CTRL to 2.8% in HFD. Other populations did not demonstrate significant differences in cell numbers between HFD and CTRL (Fig. 3.2C). Because HFD induced population changes in somatotropes and lactotropes, we determined if these population changes were due to altered differentiation from *Pou1f1*-progenitor populations. A pseudotime trajectory analysis was performed, with *Pou1f1* gene expression set as the root, to determine the developmental progression of somatotrope and lactotrope populations (Fig. 3.2D). In CTRL, the pseudotime trajectory indicated a normal differentiation pattern, with *Pou1f1*-expressing cells beginning at the progenitor population and from there, these

cells either adopted a somatotrope or lactotrope fate (Fig. 3.2D). By contrast, this

developmental progression was impaired in HFD. Consistent with increased numbers of

somatotrope, *Pou1f1*-progenitors differentiated faster into the somatotrope population,

while a subset of cells became lactotropes slower (Fig. 3.2D). This change in

developmental progression could indicate reasons for a larger somatotrope cluster in

HFD and for fewer lactotropes in HFD compared to CTRL (Fig. 3.2C). Overall, this data

suggests that HFD induced population changes in the pituitary gland, primarily in the

somatotrope and lactotrope populations, and that these changes may arise due to

alterations in differentiation of *Pou1f1*-progenitor populations to somatotrope or

lactotrope lineages.
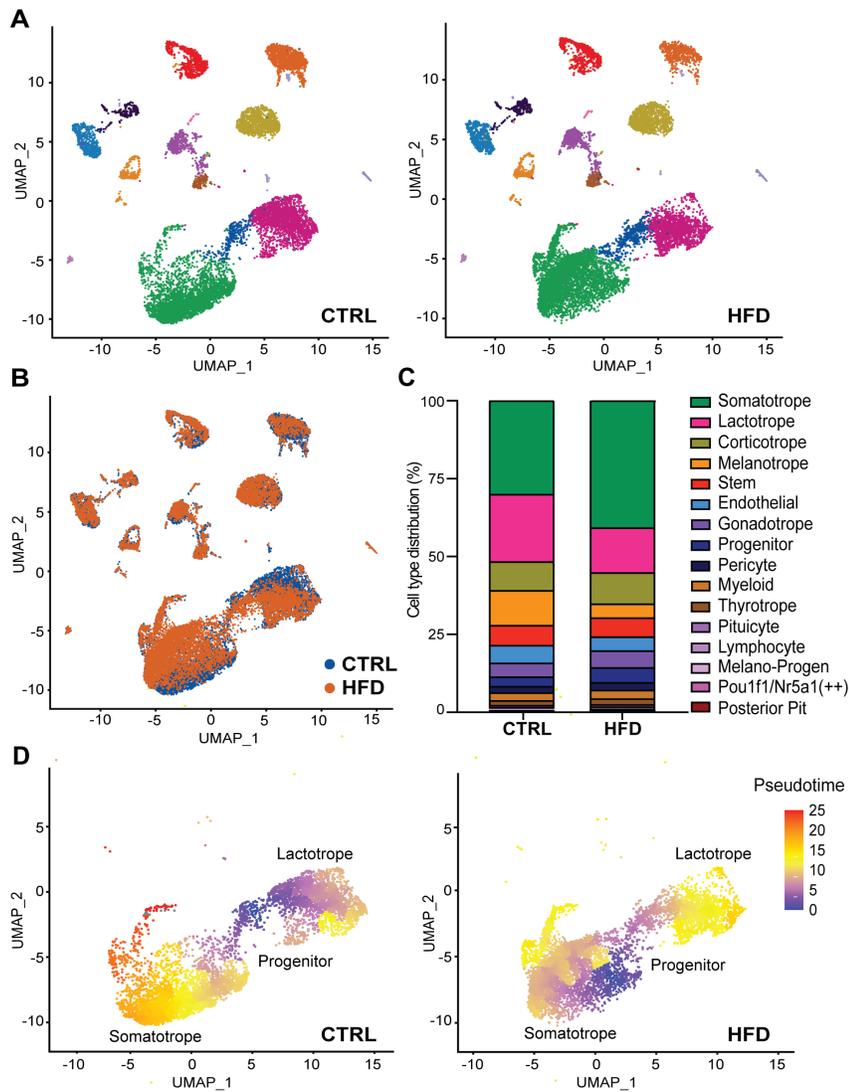
Fig 3.2 HFD induces population changes in somatotropes and lactotropes. A. UMAP representation of CTRL (10,964 cells total, left) and HFD (12,924 cells total, right); B. Overlaid UMAP representation of cells from CTRL (blue) and HFD (orange); C. Stacked bar graphs representation of cell type distribution; D. UMAP of pseudotime trajectory analysis of somatotropes, Pou1f1-expressing progenitors, and lactotropes, with Pou1f1 expression set as a root, CTRL (left), HFD (right).

3.4.3 Gene expression and sub-cluster population changes in somatotropes and lactotropes

After determining the most significant population shifts occurred in the somatotrope and lactotrope populations (Fig. 3.2), we performed sub-cluster analysis of somatotropes (Fig. 3.3) and lactotropes (Fig. 3.4), to determine which sub-populations contribute to HFD-induced changes in these populations. Additionally, we analyzed gene expression changes in response to HFD. Sub-cluster analysis of the somatotropes identified seven sub-clusters (Fig. 3.3A). We analyzed expression of genes that are important for somatotrope differentiation and specification to define sub-clusters (Fig. 3.3B). *Gh* expression was the highest in sub-clusters 0 and 2, while *Ghrhr* expression was uniform across all sub-clusters (Fig. 3.3B). Committed somatotrope markers, *Neurod4* and *Pou1f1,* were also expressed highly in all sub-clusters, demonstrating that all sub-clusters were indeed somatotropes (Fig. 3.3B). Markers of previously characterized sub-population of somatotropes expressing sterol/cholesterol biosynthesis genes (17), *Ldlr* and *Hmgcs1* were expressed highly in sub-clusters 1 and 2, in addition to *Socs3* (Fig. 3.3B). Sub-cluster 3 comprised somatotropes enriched in fatty-acid metabolism genes that have high expression of the fatty acid-binding protein 5 (*Fabp5)*, apolipoprotein E (*Apoe*), uncoupling protein 2 (*Ucp2*), and malate dehydrogenase (*Mdh2*) (data not shown). Sub-cluster 5 contained metabolically active somatotropes with high levels of mitochondrial electron transport genes and cytochrome genes, *mt-Co1*, *mt-Co2*, *mt-Co3*, *mt-Cytb*, *mt-Nd* genes (not shown). Somatotrope sub-cluster comparison between HFD and CTRL, demonstrated striking differences in cell number, namely an increase in sub-

clusters 0 (8.5% in CTRL and 39% in HFD) and sub-cluster 3 (2.4% in CTRL and 20.3% in HFD) in HFD compared to CTRL and a decrease in sub cluster 1 (42% in CTRL and 16% in HFD) and sub-cluster 2 (38% in CTRL and 3% in HFD) in HFD compared to CTRL (Fig 3.3C-D).

We performed differential gene expression (DEG) analysis between HFD and CTRL somatotropes and identified 88 upregulated DEGs and 81 downregulated DEGs (Fig. 3.3E). *Fabp5,* the top marker of subcluster 3, that had significantly more cells in HFD compared to CTRL, was up-regulated in HFD (Fig 3.3C-E). During QC analyses, we filtered out cells whose mitochondrial gene expression count was higher than 20% to filter out dead or dying cells. After filtering, HFD somatotropes still demonstrated upregulation of *mt-Cytb* and *mt-Co2,* enriched in sub-cluster 5, which indicated that respiration electron transport chain and proton transmembrane pump pathways were significantly upregulated (Fig. 3.3E). Glycoprotein metabolic and biosynthetic GO pathways were among the top GO terms that were upregulated in HFD (Fig. 3.3E). Genes enriched in these pathways include *Itm2b, Itm2c* and *Tmem59.* Genes and pathways that were down-regulated in HFD compared to CTRL include genes involved in sterol biosynthesis and cholesterol biosynthesis pathways, such as *Hmgcs1* and *Hmgcsr* (Fig. 3.3E). Significant decrease of these genes corresponds to changes in sub-cluster size in HFD, since these genes are top markers for sub-clusters 1 and 2, both of which are decreased In HFD (Fig. 3.3C-D). *Socs3,* a negative regulator of the Janus kinase/signal transducer and activator of transcription (JAK/STAT) pathway, was also significantly decreased in HFD somatotropes (Fig. 3.3E). *Socs3* regulates several hormones involved

114

in metabolism, including insulin, growth hormone, and insulin-like growth factor-1 signaling. *Socs3* is also highly expressed in sub-clusters 1 and 2, which are decreased in HFD (Fig. 3.3B-3.3D). In addition, genes and GO pathways that were enriched in cell stress response, such as *Hsp90aa1* and *Pappa2* were downregulated in HFD (Fig. 3.3E). *Rad18* expression, an E3 ubiquitin protein ligase that was highly enriched in somatotropes (Fig. 1C), significantly decreased in HFD somatotropes compared to CTRL (Fig. 3.3E). Overall, this data suggests that HFD induced somatotrope population changes and that these population changes correspond to changes in gene expression in obesity. Expression of *Gh*, *Ghrhr*, and other genes highlighted in feature plots in Fig. 3.3B (except for *Socs3* and *Hmgcs1*, discussed above), did not change in HFD.
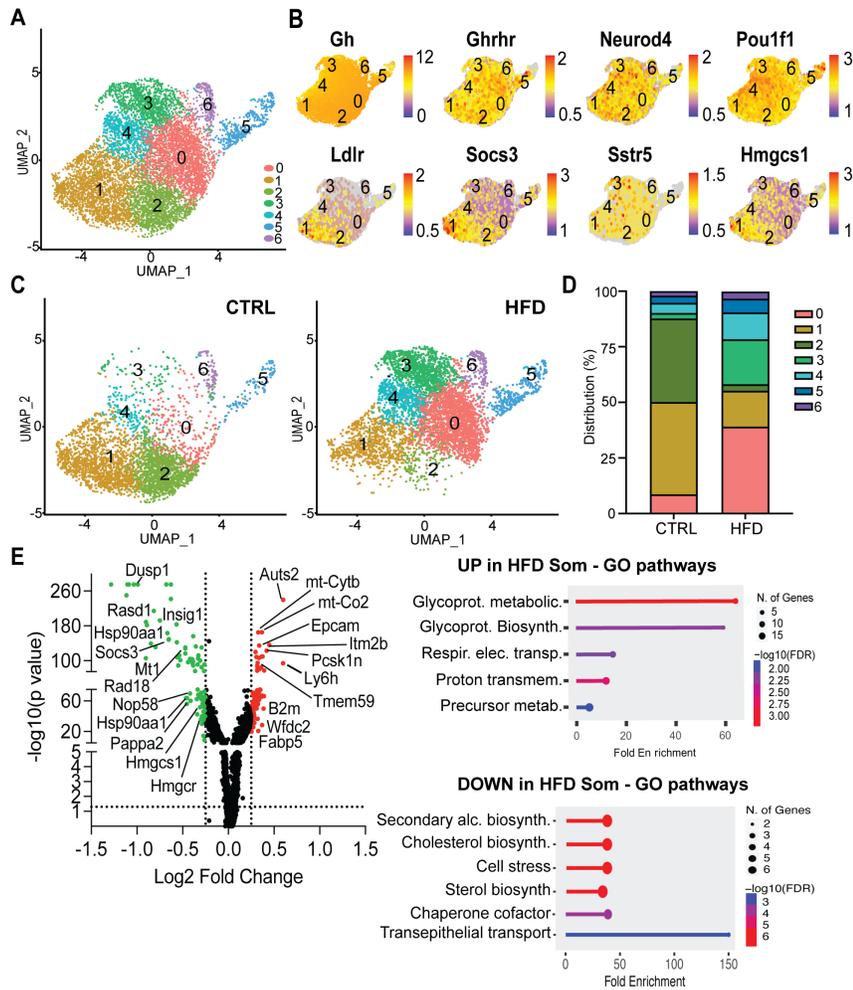
Fig 3.3 Somatotrope sub-cluster analysis identifies HFD-induced population changes. A. UMAP representation of all somatotrope sub-clusters (CTRL and HFD combined); B. Feature plots of somatotrope enriched genes, expression scale represents Log2 expression; scales differ for each gene depending on an expression level; C. UMAPS of CTRL (left) and HFD (right) sub-cluster plots; D. Sub-cluster cell number proportions in CTRL and HFD; E. Volcano plot demonstrating differentially expressed genes (DEGs) in somatotropes from CTRL and HFD (left). Genes depicted as red dots represent significantly up-regulated genes in HFD (Log2FC ≥0.25, -Log10(p-value) >1.3) and genes depicted as green dots represent significantly down-regulated genes in HFD (Log2FC ≤0.25, -Log10(p-value) >1.3). Genes depicted as black dots are genes that did not meet significance threshold. Gene ontology (GO) analyses demonstrate enriched pathways for significantly up-regulated and down-regulated genes.

116

Lactotrope sub-cluster analysis revealed six sub-clusters (Fig. 3.4A). Top markers in sub-clusters reveal that *Prl* was highly expressed in sub-clusters 0 and 4, while lineage-commitment marker, *Pou1f1* was expresses the highest in sub-clusters 1 and 2, indicating that sub-clusters 1 and 2 were immature lactotropes (Fig. 3.4B). Galanin (*Gal),* a peptide that is important in regulating prolactin release and lactotrope proliferation, was highly expressed in sub-cluster 1 (Fig. 3.4B). Sub-cluster proportions rated significant plasticity between CTRL and HFD (Fig. 3.4C-D). There was a significant decrease in sub-cluster 1 in HFD compared to CTRL (51% in CTRL compared to 8% in HFD), and a significant increase in sub-cluster 2 in HFD (6% in CTRL compared to 44% in HFD) (Fig. 3.4C-D). DEG analysis in lactotropes between HFD and CTRL indicated 47 significantly up-regulated genes in HFD, and 78 down-regulated genes in HFD (Fig. 3.4E). Decrease in *Prl*, *Drd2*, *Esr1*, and *Ets2* mRNAs did not reach 25% change cutoff (data not shown), while *Pou1f1* mRNA levels did not change at all. Expression of heat shock protein genes (*Hspa1a, Hspa1b* and *Hspb1*) was significantly up-regulated, which correlated with protein refolding and peptide hormone processing as most changed pathways (Fig. 3.4E). *Hspb1* expression was highest in sub-clusters 0, 2, and 5, all of which were increased in HFD (Fig. 3.4B-D), suggesting that increased gene expression in heat shock proteins in HFD corresponded with changes in lactotropes population dynamics. Peptide hormone processing and insulin metabolic processing were also significantly up-regulated GO pathways, marked by significant increases in *Cpe* and *Pcsk2* (Fig. 3.4E). Down-regulated genes in HFD lactotropes belong to stress response and nitric oxide mediated signaling pathways (Fig. 3.4E) such as *Mt1, Mt2* and *Rasd1.* Ablation of *Mt1* and *Mt2* have been

implicated in obesity pathogenesis, as a potential link in the regulation of energy balance, however their role in the pituitary gland and in lactotropes remains unknown (37). Galanin (*Gal)* was significantly down-regulated, and had the highest expression in sub-cluster 1, which was significantly decreased in HFD (Fig. 3.4B-E). Galanin that colocalizes with prolactin in the same secretory granule, facilitates the secretion of prolactin and acts as a growth factor for the lactotrope (38). Because galanin expression is decreased in lactotropes on HFD, we hypothesize that low galanin expression could contribute to lower lactotrope number (Fig. 3.4C-E). Taken together, these data suggest that somatotrope and lactotrope populations undergo dramatic sub-cluster population changes in response to HFD, and these population changes correspond to changes in gene expression induced by HFD.
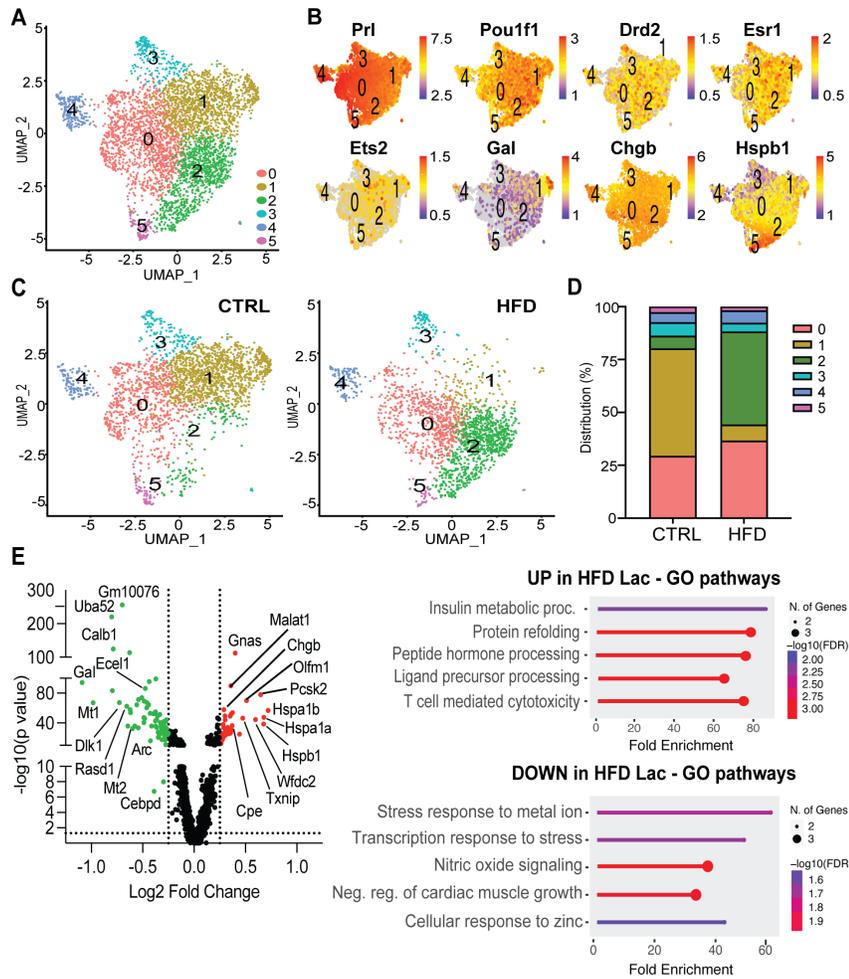
Fig 3.4 Lactotrope sub-cluster analysis identifies HFD-induced population changes. A. UMAP representation of lactotrope sub-clusters (CTRL and HFD); B. Feature plots of lactotrope enriched genes, expression scale represents Log2 expression of representative genes, scales differ for each gene depending on the expression level; C. UMAPS of CTRL (left) and HFD (right) sub-clusters: D. Sub-cluster cell number distributions in CTRL and HFD; E. Volcano plot highlighting select differentially expressed genes (DEGs) in HFD and CTRL lactotropes (left). Genes depicted as red dots represent significantly up-regulated genes in HFD (Log2FC ≥0.25, -Log10(p-value) >1.3) and genes depicted as green dots represent significantly down-regulated genes in HFD (Log2FC ≤0.25, -Log10(p-value) >1.3). Gene ontology (GO) analyses demonstrate significantly up-regulated and down-regulated pathways (right).

3.4.4 Diet-induced obesity down-regulates gonadotropin gene expression

Obese people and experimental animals have impaired gonadotropin production as well as sub-fertility. In agreement, our previous study indicated that male mice fed HFD have reduced LH, FSH and testosterone levels (9). We sought to investigate whether gonadotrope population was altered in HFD and if gene expression changes result in changes in hormone secretion (Fig. 3.5). Gonadotrope sub-cluster analysis revealed four sub-clusters (Fig. 3.5A). Expression of *Lhb* and *Fshb* showed the highest expression in sub-cluster 0, while *Cga* and *Gnrhr* were most highly expressed in sub-cluster 2, in addition to sub-cluster 0, suggesting that sub-cluster 0 represents a mature gonadotrope population, while sub-cluster 2 marks an immature committed gonadotrope population (Fig. 3.5B). *Nr5a1* and *Foxl2* that are important for *Lhb* and *Fshb* expression, respectively (39-44) were also expressed most highly in sub-clusters 0 and 2, while *Tgfbr3l,* a novel inhibin B co-receptor that has been shown to be specifically expressed in gonadotropes (45), was most highly expressed in sub-cluster 0 (Fig. 3.5B). Sub-cluster analysis between CTRL and HFD did not show any significant changes in cell numbers (Fig. 3.5C-D). Gonadotropes DEG analysis revealed 25 DEGs that were up-regulated in HFD and 253 DEGs that were significantly down-regulated in HFD (Fig. 3.5E). Of the DEGs that were up-regulated were *Grem1, Cga* and *Speer4e,* which has been implicated as a novel marker of gonadotropes (17). Genes that encode LH and GnRHR (*Lhb and Gnrhr)* as well as genes that are important in transcriptional regulation of gonadotropin hormones, such as *Fos, Jun, Egr1 and Atf3,* were significantly down-regulated in HFD (Fig. 3.5E). *Fshb*, *Tgfbr3l*, *Foxl2* and *Nr5a1* did not change with HFD. The top GO

pathways that were down-regulated in HFD correspond to transcriptional regulation as well as mRNA binding proteins (Fig 3.5E). This suggests that gonadotropin hormone transcriptional regulation and translation are down-regulated in diet-induced obesity. Because we determined significant suppression of genes important in the regulation of gonadotropin gene expression in the mature gonadotrope, we wanted to determine if HFD impairs gonadotrope differentiation (Fig. 3.5F). We performed pseudotime trajectory analysis, setting *Cga* expression as the root, and we did not see any significant differences between HFD and CTRL, suggesting that decreased gonadotropin gene expression is not due to impaired gonadotrope differentiation (Fig. 3.5F). Taken together, these data suggest that HFD does not induce population changes in the gonadotrope, however there are significant gene expression changes, primarily suppression of genes important in the transcriptional regulation of gonadotropin hormones, which may cause changes in hormone production and secretion in obesity.
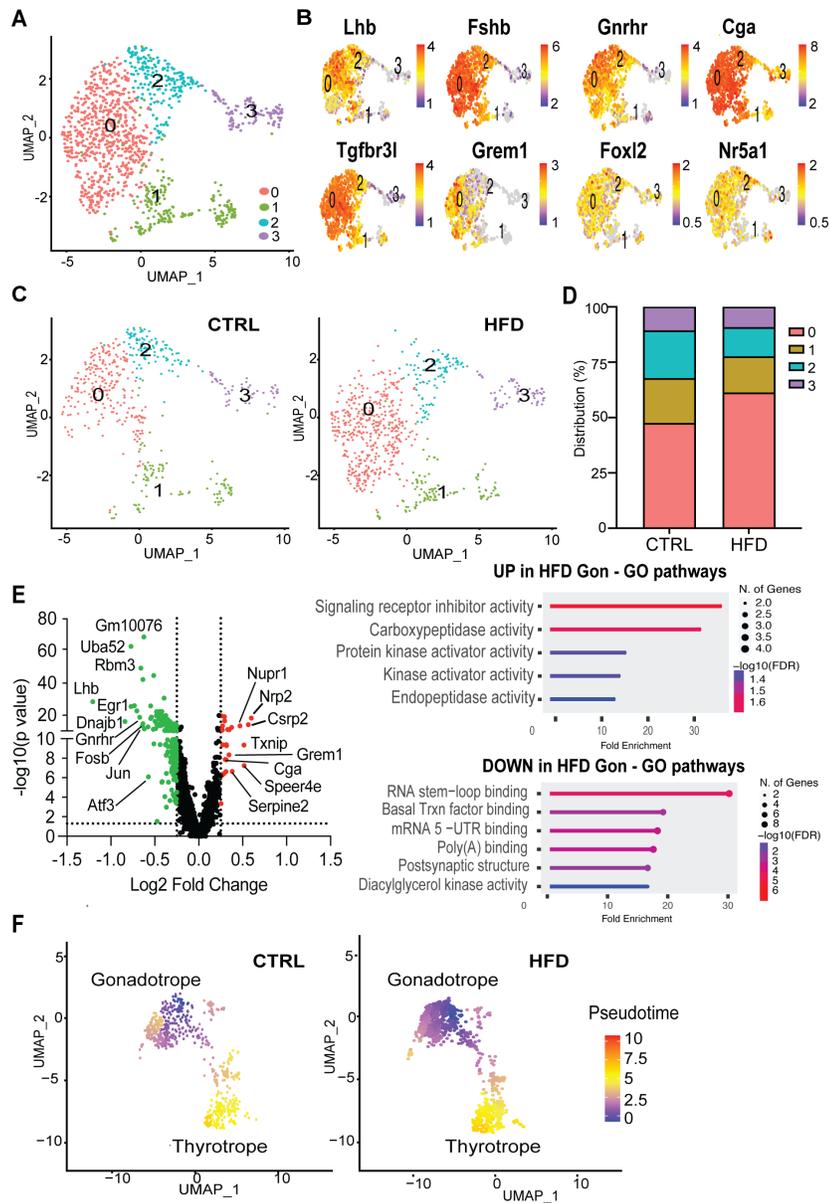
Fig 3.5 Gene expression changes in gonadotrope cells induced by HFD. A. UMAP representation of gonadotrope sub-clusters (CTRL and HFD, combined); B. Feature plots of gonadotrope genes, expression scale represents expression, scales adjusted for each gene expression level; C. UMAPS of CTRL (left) and HFD (right) sub-cluster analysis; D. Sub-clusters cell number proportions in CTRL and HFD; E. Volcano plot comparing DEGs in HFD and CTRL gonadotrope (left). Genes depicted as red dots represent significantly up-regulated genes in HFD (Log2FC ≥0.25, -Log10(p-value) >1.3) and genes depicted as green dots represent significantly downregulated genes in HFD (Log2FC ≤0.25, -Log10(p-value) >1.3). GO analyses demonstrate significantly up-regulated and down-regulated pathways (right). F. UMAPs of pseudotime trajectory analysis of gonadotrope and thyrotrope progression with Cga expression set as the root, CTRL (left) and HFD (right).

3.4.5 Corticotropes and thyrotropes are least affected by HFD

Obese individuals have dysregulated glucocorticoid production and secretion, as well as altered basal metabolism and thyroid function (46). Corticotrope and thyrotrope populations lacked changes in cell numbers in HFD (Fig. 3.6). Sub-cluster analysis of corticotropes identified three sub-clusters (Fig. 3.6A). *Pomc* expression was the highest in sub-cluster 0 (Fig. 3.6B). *Tbx19* and *Crhr1* were highly expressed in sub-clusters 0 and 1 (Fig. 3.6B). *Tnnt1,* which has been previously identified as a novel marker for corticotropes (17), showed the highest expression in sub-cluster 1 (Fig. 3.6B). There were no significant changes in sub-cluster cell numbers between HFD and CTRL (Fig. 3.6C-D). DEG analysis between CTRL and HFD corticotropes indicated 61 significantly up-regulated genes and 50 down-regulated genes (Fig. 3.6E). Genes that were significantly up-regulated include *Hspb1, Hspa1b and Hspa1a,* which are important in protein chaperone activity (Fig. 3.6E). Top down-regulated genes in HFD corticotropes include nuclear receptors, *Nr4a1 (Nur77) and Nr4a2* (Fig. 3.6E), indicating that transcriptional activity is decreased corresponding to its respective GO pathway down-regulation. *Tnnt1,* a novel marker highly expressed in sub-cluster 1, was significantly down-regulated in HFD corticotropes, without cell number changes (Fig. 3.6B-E). While the role of *Tnnt1* in corticotropes has not been elucidated, previous human GWAS studies identified hypermethylation of *Tnnt1* gene in blood samples of overweight and obese adults, and decreased expression in skeletal muscle in obese patients and patients with type 2 diabetes (47, 48), suggesting its role in obesity.

Thyrotrope sub-cluster analysis identified two sub-clusters (Fig. 3.6F). High expression of *Tshb* was identified in sub-cluster 1, suggesting that this sub-cluster marks a mature thyrotrope population (Fig. 3.6G). Other thyrotrope markers, such as, *Cga, Gata2, Pou1f1 and Foxl2* (49)*, were expressed in both sub-clusters 0 and 1, suggesting that sub-cluster 0 represents immature thyrotropes (Fig. 3.6G). Comparison of sub-cluster population numbers between CTRL and HFD showed no significant differences (Fig. 3.6H-I). DEG analysis between HFD and CTRL thyrotropes identified 30 DEGs that were up-regulated and 60 that were down-regulated in HFD, however genes involved in TSH transcriptional regulation and secretion, and marker genes highlighted in Fig. 3.6G did not change (data not shown). This suggests that thyroid hormone synthesis was not affected by HFD.
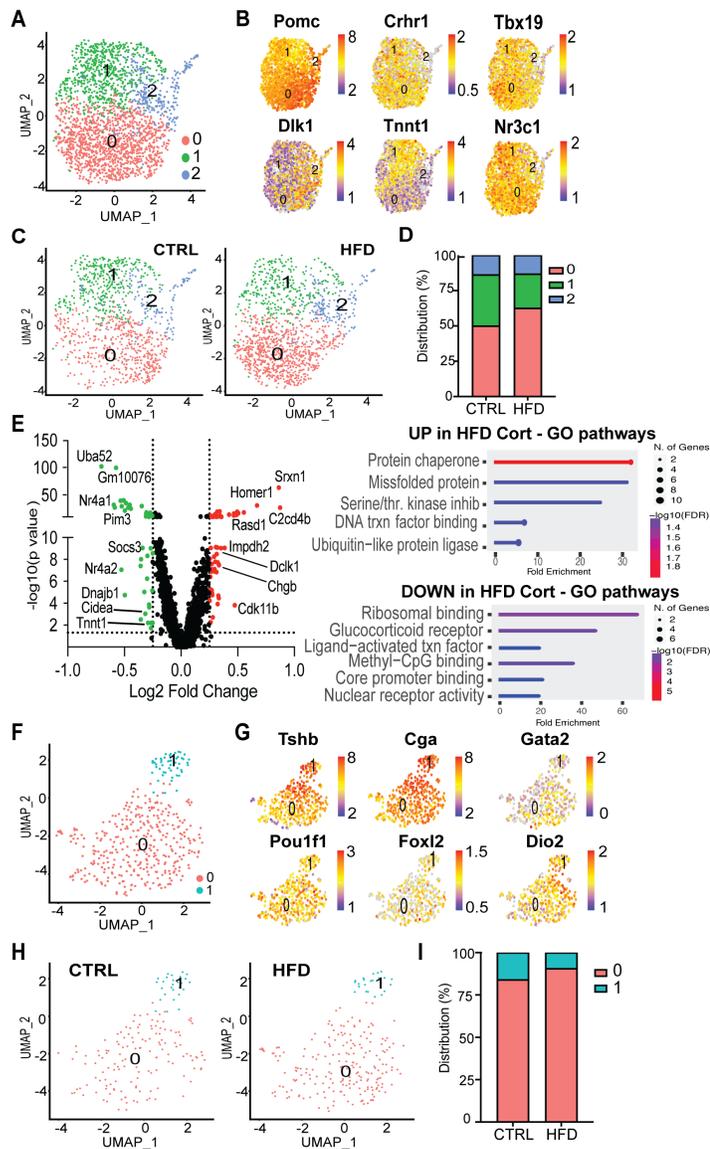
Fig 3.6 HFD does not induce population changes in corticotropes and thyrotropes. A. UMAP representation of corticotrope sub-clusters (CTRL and HFD); B. Feature plots of corticotrope marker genes, expression scale represents expression levels; C. UMAPs of CTRL (left) and HFD (right) sub-clusters; D. Sub-clusters cell number proportions in CTRL and HFD. E. Volcano plot comparing DEGs in HFD and CTRL corticotrope. Genes depicted as red dots represent significantly up-regulated genes in HFD (Log2FC ≥0.25, -Log10(p-value) >1.3) and genes depicted as green dots represent significantly down-regulated genes in HFD (Log2FC ≤0.25, -Log10(p-value) >1.3). GO analyses indicating up-regulated and down-regulated pathways; F. UMAP representation of thyrotrope cells sub-clusters (CTRL and HFD); G. Feature plots of thyrotrope marker genes, expression scale represents expression; H. UMAPs of CTRL (left) and HFD (right) sub-clusters; I. Cell type distributions of sub-clusters in CTRL and HFD.

3.4.6 Melanotrope cell number is decreased in HFD

Although melanotropes are not anterior pituitary hormone producing population, melanotropes showed significant population changes in response to HFD. Therefore, we analyzed melanotrope sub-clusters and identified four sub-clusters (Fig. 3.7A). *Pomc* and melanotrope-specific marker, *Oacyl,* expression was highest in sub-clusters 0 and 2 (Fig. 3.7B). Melanotrope-precursor genes, *Tbx19* and *Pax7* were expressed in all sub-clusters (Fig. 3.7B). Analyses of differences between CTRL and HFD, showed significantly fewer melanotrope cells in all sub-clusters in HFD compared to CTRL, however there were no differences in sub-cluster distribution (Fig. 3.7C-7D).

After performing DEG analysis between HFD and CTRL melanotropes, we identified 39 significantly upregulated DEGs and 61 significantly downregulated DEGs (Fig. 3.7E). Genes and GO pathways that were upregulated in HFD melanotropes include *Cidea*, *Ier3* and *Cd24a,* whose pathways correspond to negative regulation of tumor necrosis factor (TNF) production and apoptotic processes (Fig. 3.7E). GTP-Binding Protein (*Gem),* a regulatory protein in receptor mediated signal-transduction, was significantly increased in HFD melanotropes and showed highest expression in sub-cluster 1 (Fig. 3.7B, E). In addition, proprotein convertase subtilisin/kexin type 2 *(Pcsk2),* a serine endopeptidase that is hallmark of melanotrope identity and is responsible for the conversion of prohormone POMC (20), was up-regulated in HFD (Fig. 3.7E). *Pcsk2* expression was highest in sub-clusters 0 and 2 in melanotropes, and although we did not see significant changes in *Pomc* expression (data not shown), *Pcsk2* is important in the regulation of insulin and glucagon biosynthesis, with some reports demonstrated that point mutations

have been associated with obesity and type 2 diabetes (50, 51). Down-regulated genes, *Mt1* and *Mt2,* and pathways in HFD melanotropes correspond to stress response (Fig. 3.7E). Overall, this data suggests that while HFD diminishes the melanotrope numbers and causes gene expression changes compared to CTRL, overall cell type distribution between sub-clusters did not change.
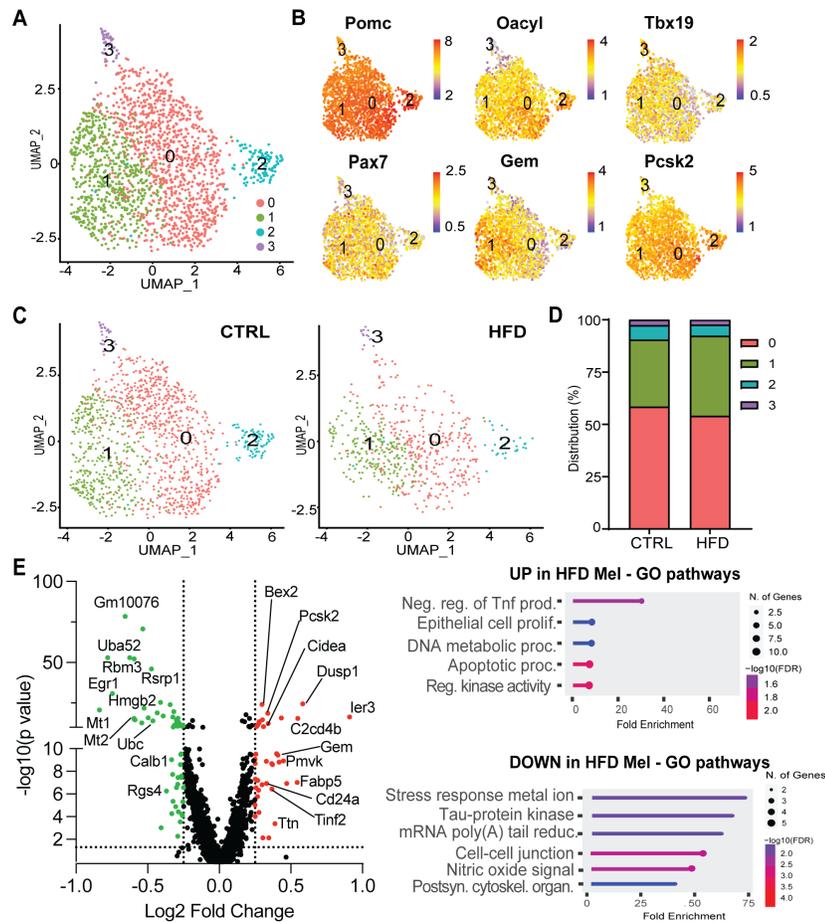
Fig 3.7 Fewer melanotrope cells in HFD. A. UMAP representation of melanotrope sub-clusters (CTRL and HFD combined); B. Feature plots of melanotrope genes, expression scale represents Log2 expression; C. UMSPD of CTRL (left) and HFD (right) sub-clusters; D. Cell type distributions of sub-clusters in CTRL and HFD; E. Volcano plot comparing DEGs in HFD and CTRL melanotropes (left). Genes depicted as red dots represent significantly upregulated genes in HFD (Log2FC ≥0.25, -Log10(p-value) >1.3) and genes depicted as green dots represent significantly downregulated genes in HFD (Log2FC ≤0.25, -Log10(p-value) >1.3). GO analyses indicating enriched pathways.

3.4.7 HFD-induced changes in the pituitary gland correspond to changes in hormone levels in the serum

Since diet-induced obesity leads to changes in cell numbers and gene expression in the pituitary gland, we determined if pituitary hormone levels were impacted by HFD. We performed Luminex and LH ELISA, in order to determine serum hormone levels (Fig. 3.8). There was no significant changes in GH, TSH and ACTH hormone levels between HFD and CTRL. On the other hand, prolactin levels were decreased with HFD. Decrease in the level of prolactin may correspond to fewer lactotropes, since prolactin mRNA expression did not significantly change. Consistent with previous reports from our and other studies (9, 52, 53), we determined decreased LH and FSH levels in serum of HFD animals compared to CTRL (Fig. 3.8). Decrease in LH corresponds to decreased gene expression in the gonadotrope. Taken together, our results demonstrate that HFD causes changes in population dynamics and gene expression that cause changes in hormone levels, with impact on physiology.
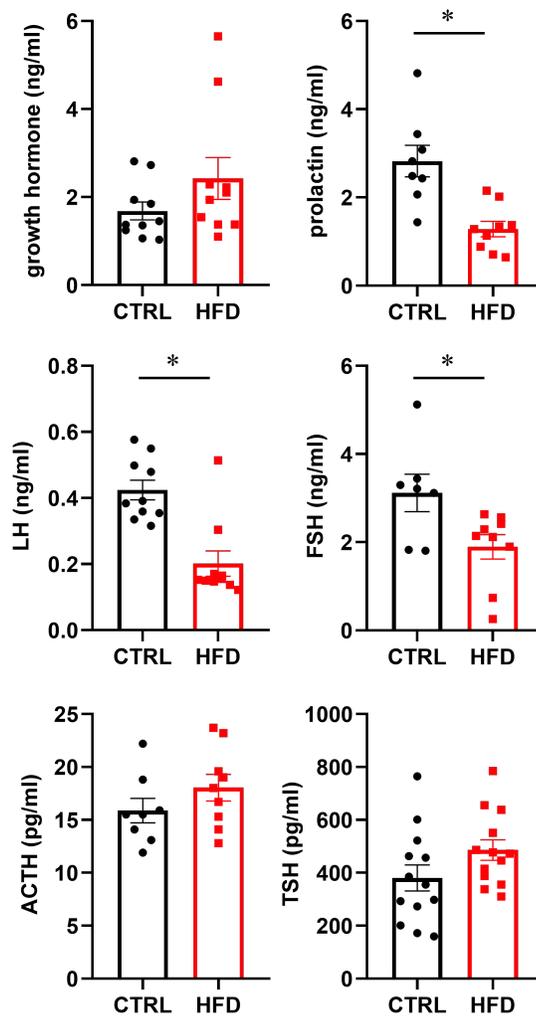
Fig 3.8 Obesity leads to changes in hormone levels. Serum hormone levels determined by Luminex and LH ELISA. Male mice on HFD have reduced levels of prolactin, luteinizing hormone (LH) and follicle stimulating hormone (FSH). No changes were observed in growth hormone, thyroid stimulating hormone (TSH) and adrenocorticotropic hormone (ACTH). Statistical differences between control (CTRL) and high fat diet (HFD) were determined by Student's T-test, followed by Tukey's HSD test (* $p < 0.05$).

3.5 Discussion

Single cell RNA sequencing (scRNA-seq) (17, 21, 22, 54) and single nuclei RNA sequencing (snRNA-seq) (23, 24) of pituitary cell was performed before to identify enriched genes in specific populations of pituitary cells. We performed scRNA-seq using 10X Genomics platform on dispersed pituitary cells from control-fed (CTRL) and high fat diet-fed (HFD) mice to determine changes in pituitary populations in obesity, since pituitary is a master gland that regulates homeostasis.

Our study identified many of the same markers previously associated with specific pituitary populations. Somatotropes in addition to *Gh*, show enrichment in other genes reported before (17, 21, 23, 54). For example, Pappalysin 2 (*Pappa2*), a metalloproteinase that regulates insulin-like growth factor (IGF) bioavailability, was enriched specifically in the somatotrope population and has been identified previously as a novel marker in somatotropes in mice and in rats (17, 21). *Pappa2* deficiency leads to shorter bone growth, impaired glucose tolerance, higher fat mass, and lower lean mass (55, 56). *Pappa2* mRNA was significantly decreased in HFD, and since *Pappa2* regulated bioactive IGF1 levels, it is possible that lower local IGF1 bioactivity diminishes negative feedback on somatotropes. *Rad18*, an E3 ubiquitin-protein ligase was highly enriched in somatotropes in our dataset, similarly to what has been previously reported (17, 21). We determined that this gene is significantly decreased in HFD, but how does this decrease affect its function in post-replication repair of damaged DNA, is not clear. Other somatotrope-enriched genes are *Dlk1*, involved in preadipocyte differentiation (57) and *Dapl1* that plays a role in amino-acid starvation and exhibits male

biased expression (54). As illustrated above, many of somatotrope enriched genes have roles in the metabolic tissues as well, and thus is may not be surprising that somatotrope population exhibits largest changes in obesity. Fraction of somatotropes increases after exposure to HFD, and although some of these genes do not change expression with obesity, increased number of cells may lead to increased levels. Sub-cluster analyses confirms this observation. Sub-cluster 0, terminally differentiated somatotropes with the highest expression of *Gh*, and sub-cluster 5, oxidative-stress, metabolically active somatotropes, increase proportion in obesity, while sub-clusters 1 characterized by immediate-early gene expression and heat-shock proteins, and sub-cluster 2, that has the highest expression of *Rad18* and *Pappa2,* decrease. Consistent with lack of changes in growth hormone serum levels, *Gh* mRNA levels do not change overall, since *Gh* is most highly expressed in subcluster 0, that enlarges in obesity, and in subcluster 2, that diminishes in obesity.

Prolactin is most highly expressed in sub-clusters 0 and 4, which do not change substantially in obesity. *Prl* mRNA expression decreases by 15%, but likely due to reduced numbers of lactotropes overall, prolactin serum levels are significantly lower in obese mice. The largest cell proportion changes in lactotrope subpopulation occur in sub-cluster 1, characterized by ribosomal mRNAs that is diminished in obesity, and in sub-cluster 2, characterized by lysosomal mRNA that is enlarged in obesity. Decrease in proportion of sub-cluster 1 combined with the decrease in serum prolactin may also indicate that prolactin translation is particularly affected in obesity.

As opposed to somatotrope and lactotropes that show changes in cell numbers, fraction of gonadotropes in the pituitary does not change with obesity. Interestingly, gonadotropes demonstrate the largest changes in gene expression, with vast majority of genes repressed by obesity. These include *Lhb* and *Gnrhr*, and transcription factors involved in their expression. We previously reported that during long-term obesity, *Gnrh* mRNA is diminished in the hypothalami of obese mice (9, 36, 58), which may lead to lower levels of *Lhb* and lower LH in the circulation, in addition to direct effects of obesity on the pituitary gland. On the other hand, *Fshb* expression does not significantly change with HFD, but FSH levels in the circulation are significantly lower, consistent with reports in mice and humans (9, 52, 59-62). This may indicate that obesity affects translation of *Fshb* mRNA or FSH glycosylation that may lead to lower half-life. Indeed, GO pathway analysis indicates a decrease in mRNA binding proteins.

Consistent with a lack of changes in ACTH and TSH levels in the circulation, corticotrope and thyrotrope population exhibit the fewest changes at the cell number or gene expression levels. Lack of significant changes in TSH levels in our study is in contrast with a previous study that demonstrated an increase in TSH (63), although reasons for this discrepancy are not clear. On the contrary, our previous study that reported a decrease in TRH mRNA levels in the hypothalamus (8) is in agreement with that study (63). Lack of changes in ACTH serum level in HFD diet animals at the basal level is in agreement with a previous study (64), which also demonstrated that HFD augments ACTH increase in response to stress, which we did not analyze. Corticotropes demonstrate some gene expression changes, up-regulation of stress pathways and

133

inhibitors of kinase signaling, and down-regulation of transcriptional activity and translation. Thyrotropes on the other hand do not show major changes in gene expression. Melanotropes exhibited significant changes is gene expression and overall cell number that determine their percentage that decreased in obesity.

In conclusion, we identified that diet-induced obesity leads to changes in pituitary gland plasticity and gene expression with downstream consequences on pituitary hormone levels in the circulation. Our scRNA-seq data demonstrates somatotrope and lactotrope population dynamics induced by HFD that may stem from altered differentiation of their progenitors based on trajectory analysis. We also identified gene expression changes in the gonadotrope that lead to changes in gonadotropin hormone levels. Therefore, we determined that some hormone changes may be due to the alternations in cell numbers, while others stem from changes in transcriptional activity.

References for Chapter Three

1. Trends in adult body-mass index in 200 countries from 1975 to 2014: a pooled analysis of 1698 population-based measurement studies with 19.2 million participants. Lancet (London, England) 2016; 387:1377-1396

2. The Lancet Public H. Tackling obesity seriously: the time has come. The Lancet Public health 2018; 3:e153

3. Le Thuc O, Stobbe K, Cansell C, Nahon JL, Blondeau N, Rovere C. Hypothalamic Inflammation and Energy Balance Disruptions: Spotlight on Chemokines. Frontiers in endocrinology 2017; 8:197

4. Agusti A, Garcia-Pardo MP, Lopez-Almela I, Campillo I, Maes M, Romani-Perez M, Sanz Y. Interplay Between the Gut-Brain Axis, Obesity and Cognitive Function. Frontiers in neuroscience 2018; 12:155

5. Li X, Li X, Fang F, Fu X, Lin H, Gao Q. Is Metabolic Syndrome Associated with the Risk of Recurrent Stroke: A Meta-Analysis of Cohort Studies. Journal of stroke and cerebrovascular diseases : the official journal of National Stroke Association 2017; 26:2700-2705

6. Nelson SM, Fleming R. Obesity and reproduction: impact and interventions. Current opinion in obstetrics & gynecology 2007; 19:384-389

7. Lainez NM, Coss D. Obesity, Neuroinflammation, and Reproductive Function. Endocrinology 2019; 160:2719-2736

8. Chen KE, Lainez NM, Nair MG, Coss D. Visceral adipose tissue imparts peripheral macrophage influx into the hypothalamus. Journal of neuroinflammation 2021; 18:140

9. Lainez NM, Jonak CR, Nair MG, Ethell IM, Wilson EH, Carson MJ, Coss D. Diet-Induced Obesity Elicits Macrophage Infiltration and Reduction in Spine Density in the Hypothalami of Male but Not Female Mice. Frontiers in immunology 2018; 9:1992

10. Kaprara A, Huhtaniemi IT. The hypothalamus-pituitary-gonad axis: Tales of mice and men. Metabolism: clinical and experimental 2018; 86:3-17

11. Mollard P, Hodson DJ, Lafont C, Rizzoti K, Drouin J. A tridimensional view of pituitary development and function. Trends Endocrinol Metab 2012; 23:261-269

12. Hodson DJ, Mollard P. Pituitary endocrine cell networks - 10 years and beyond. Ann Endocrinol (Paris) 2012; 73:56-58

13. Willis TL, Lodge EJ, Andoniadou CL, Yianni V. Cellular interactions in the pituitary stem cell niche. Cellular and molecular life sciences : CMLS 2022; 79:612

14. Fang Q, George AS, Brinkmeier ML, Mortensen AH, Gergics P, Cheung LY, Daly AZ, Ajmal A, Pérez Millán MI, Ozel AB, Kitzman JO, Mills RE, Li JZ, Camper SA. Genetics of Combined Pituitary Hormone Deficiency: Roadmap into the Genome Era. Endocrine reviews 2016; 37:636-675

15. Davis SW, Castinetti F, Carvalho LR, Ellsworth BS, Potok MA, Lyons RH, Brinkmeier ML, Raetzman LT, Carninci P, Mortensen AH, Hayashizaki Y, Arnhold IJ, Mendonca BB, Brue T, Camper SA. Molecular mechanisms of pituitary organogenesis: In search of novel regulatory genes. Mol Cell Endocrinol 2010; 323:4-19

16. Alatzoglou KS, Gregory LC, Dattani MT. Development of the Pituitary Gland. Comprehensive Physiology 2020; 10:389-413

17. Cheung LYM, George AS, McGee SR, Daly AZ, Brinkmeier ML, Ellsworth BS, Camper SA. Single-Cell RNA Sequencing Reveals Novel Markers of Male Pituitary Stem Cells and Hormone-Producing Cell Types. Endocrinology 2018; 159:3910-3924

18. Ho Y, Hu P, Peel MT, Chen S, Camara PG, Epstein DJ, Wu H, Liebhaber SA. Single-cell transcriptomic analysis of adult mouse pituitary reveals sexual dimorphism and physiologic demand-induced cellular plasticity. Protein & Cell 2020; 11:565-583

19. Chen Q, Leshkowitz D, Blechman J, Levkowitz G. Single-Cell Molecular and Cellular Architecture of the Mouse Neurohypophysis. eNeuro 2020; 7

20. Mayran A, Sochodolsky K, Khetchoumian K, Harris J, Gauthier Y, Bemmo A, Balsalobre A, Drouin J. Pioneer and nonpioneer factor cooperation drives lineage specific chromatin opening. Nature Communications 2019; 10:3807

21. Fletcher PA, Smiljanic K, Maso Prévide R, Iben JR, Li T, Rokic MB, Sherman A, Coon SL, Stojilkovic SS. Cell Type- and Sex-Dependent Transcriptome Profiles of Rat Anterior Pituitary Cells. Frontiers in endocrinology 2019; 10:623

22.   Cheung LYM, Menage L, Rizzoti K, Hamilton G, Dumontet T, Basham K, Daly AZ, Brinkmeier ML, Masser BE, Treier M, Cobb J, Delogu A, Lovell-Badge R, Hammer GD, Camper SA. Novel Candidate Regulators and Developmental Trajectory of Pituitary Thyrotropes. Endocrinology 2023; 164

23.   Ruf-Zamojski F, Zhang Z, Zamojski M, Smith GR, Mendelev N, Liu H, Nudelman G, Moriwaki M, Pincas H, Castanon RG, Nair VD, Seenarine N, Amper MAS, Zhou X, Ongaro L, Toufaily C, Schang G, Nery JR, Bartlett A, Aldridge A, Jain N, Childs GV, Troyanskaya OG, Ecker JR, Turgeon JL, Welt CK, Bernard DJ, Sealfon SC. Single nucleus multi-omics regulatory landscape of the murine pituitary. Nat Commun 2021; 12:2677

24.   Zhang Z, Zamojski M, Smith GR, Willis TL, Yianni V, Mendelev N, Pincas H, Seenarine N, Amper MAS, Vasoya M, Cheng WS, Zaslavsky E, Nair VD, Turgeon JL, Bernard DJ, Troyanskaya OG, Andoniadou CL, Sealfon SC, Ruf-Zamojski F. Single nucleus transcriptome and chromatin accessibility of postmortem human pituitaries reveal diverse stem cell regulatory mechanisms. Cell Rep 2022; 38:110467

25.   Ding J, Adiconis X, Simmons SK, Kowalczyk MS, Hession CC, Marjanovic ND, Hughes TK, Wadsworth MH, Burks T, Nguyen LT, Kwon JYH, Barak B, Ge W, Kedaigle AJ, Carroll S, Li S, Hacohen N, Rozenblatt-Rosen O, Shalek AK, Villani A-C, Regev A, Levin JZ. Systematic comparison of single-cell and single-nucleus RNA-sequencing methods. Nature biotechnology 2020; 38:737-746

26.   Lake BB, Codeluppi S, Yung YC, Gao D, Chun J, Kharchenko PV, Linnarsson S, Zhang K. A comparative strategy for single-nucleus and single-cell transcriptomes confirms accuracy in predicted cell-type expression from nuclear RNA. Scientific reports 2017; 7:6031

27.   Hao Y, Hao S, Andersen-Nissen E, Mauck WM, 3rd, Zheng S, Butler A, Lee MJ, Wilk AJ, Darby C, Zager M, Hoffman P, Stoeckius M, Papalexi E, Mimitou EP, Jain J, Srivastava A, Stuart T, Fleming LM, Yeung B, Rogers AJ, McElrath JM, Blish CA, Gottardo R, Smibert P, Satija R. Integrated analysis of multimodal single-cell data. Cell 2021; 184:3573-3587.e3529

28.   Xiong KX, Zhou HL, Lin C, Yin JH, Kristiansen K, Yang HM, Li GB. Chord: an ensemble machine learning algorithm to identify doublets in single-cell RNA sequencing data. Communications biology 2022; 5:510

29.   Hafemeister C, Satija R. Normalization and variance stabilization of single-cell RNA-seq data using regularized negative binomial regression. Genome biology 2019; 20:296

30.   Choudhary S, Satija R. Comparison and evaluation of statistical error models for scRNA-seq. Genome biology 2022; 23:27

31.   Ge SX, Jung D, Yao R. ShinyGO: a graphical gene-set enrichment tool for animals and plants. Bioinformatics (Oxford, England) 2020; 36:2628-2629

32.   Cao J, Spielmann M, Qiu X, Huang X, Ibrahim DM, Hill AJ, Zhang F, Mundlos S, Christiansen L, Steemers FJ, Trapnell C, Shendure J. The single-cell transcriptional landscape of mammalian organogenesis. Nature 2019; 566:496-502

33.   Steyn FJ, Wan Y, Clarkson J, Veldhuis JD, Herbison AE, Chen C. Development of a methodology for and assessment of pulsatile luteinizing hormone secretion in juvenile and adult male mice. Endocrinology 2013; 154:4939-4945

34.   Tordjman KM, Greenman Y, Ram Z, Hershkovitz D, Aizenstein O, Ariel O, Asa SL. Plurihormonal Pituitary Tumor of Pit-1 and SF-1 Lineages, with Synchronous Collision Corticotroph Tumor: a Possible Stem Cell Phenomenon. Endocrine pathology 2019; 30:74-80

35.   Li J, Ruggiero-Ruff RE, He Y, Qiu X, Lainez N, Villa P, Godzik A, Coss D, Nair MG. Sexual dimorphism in obesity is governed by RELMα regulation of adipose macrophages and eosinophils. eLife 2023; 12

36.   Chen KE, Lainez NM, Coss D. Sex Differences in Macrophage Responses to Obesity-Mediated Changes Determine Migratory and Inflammatory Traits. Journal of immunology 2021; 206:141-153

37.   Beattie JH, Wood AM, Newman AM, Bremner I, Choo KH, Michalska AE, Duncan JS, Trayhurn P. Obesity and hyperleptinemia in metallothionein (-I and -II) null mice. Proceedings of the National Academy of Sciences of the United States of America 1998; 95:358-363

38.   Wynick D, Small CJ, Bacon A, Holmes FE, Norman M, Ormandy CJ, Kilic E, Kerr NC, Ghatei M, Talamantes F, Bloom SR, Pachnis V. Galanin regulates prolactin release and lactotroph proliferation. Proceedings of the National Academy of Sciences of the United States of America 1998; 95:12671-12676

39.   Ongaro L, Schang G, Ho CC, Zhou X, Bernard DJ. TGF-beta Superfamily Regulation of Follicle-Stimulating Hormone Synthesis by Gonadotrope Cells: Is There a Role for Bone Morphogenetic Proteins? Endocrinology 2019; 160:675-683

40. Fortin J, Boehm U, Deng C-X, Treier M, Bernard DJ. Follicle-stimulating hormone synthesis and fertility depend on SMAD4 and FOXL2. The FASEB Journal 2014; 28:3396-3410

41. Tran S, Zhou X, Lafleur C, Calderon MJ, Ellsworth BS, Kimmins S, Boehm U, Treier M, Boerboom D, Bernard DJ. Impaired fertility and FSH synthesis in gonadotrope-specific Foxl2 knockout mice. Mol Endocrinol 2013; 27:407-421

42. Roybal LL, Hambarchyan A, Meadows JD, Barakat NH, Pepa PA, Breen KM, Mellon PL, Coss D. Roles of Binding Elements, FOXL2 Domains, and Interactions With cJUN and SMADs in Regulation of FSHβ. Molecular Endocrinology 2014; 28:1640-1655

43. Corpuz PS, Lindaman LL, Mellon PL, Coss D. FoxL2 is required for activin induction of the mouse and human follicle-stimulating hormone β-subunit genes. Mol Endocrinol 2010; 24:1037-1051

44. Zhao L, Bakke M, Krimkevich Y, Cushman LJ, Parlow AF, Camper SA, Parker KL. Steroidogenic factor 1 (SF1) is essential for pituitary gonadotrope function. Development 2001; 128:147-154

45. Brûlé E, Wang Y, Li Y, Lin YF, Zhou X, Ongaro L, Alonso CAI, Buddle ERS, Schneyer AL, Byeon CH, Hinck CS, Mendelev N, Russell JP, Cowan M, Boehm U, Ruf-Zamojski F, Zamojski M, Andoniadou CL, Sealfon SC, Harrison CA, Walton KL, Hinck AP, Bernard DJ. TGFBR3L is an inhibin B co-receptor that regulates female fertility. Science advances 2021; 7:eabl4391

46. Ylli D, Sidhu S, Parikh T, Burman KD. Endocrine Changes in Obesity. In: Feingold KR, Anawalt B, Blackman MR, Boyce A, Chrousos G, Corpas E, de Herder WW, Dhatariya K, Dungan K, Hofland J, Kalra S, Kaltsas G, Kapoor N, Koch C, Kopp P, Korbonits M, Kovacs CS, Kuohung W, Laferrère B, Levy M, McGee EA, McLachlan R, New M, Purnell J, Sahay R, Shah AS, Singer F, Sperling MA, Stratakis CA, Trence DL, Wilson DP, eds. Endotext. South Dartmouth (MA): MDText.com, Inc.

47. Hoffman NJ, Parker BL, Chaudhuri R, Fisher-Wellman KH, Kleinert M, Humphrey SJ, Yang P, Holliday M, Trefely S, Fazakerley DJ, Stöckli J, Burchfield JG, Jensen TE, Jothi R, Kiens B, Wojtaszewski JF, Richter EA, James DE. Global Phosphoproteomic Analysis of Human Skeletal Muscle Reveals a Network of Exercise-Regulated Kinases and AMPK Substrates. Cell metabolism 2015; 22:922-935

48. Samblas M, Milagro FI, Martínez A. DNA methylation markers in obesity, metabolic syndrome, and weight loss. Epigenetics 2019; 14:421-444

49. Ellsworth BS, Egashira N, Haller JL, Butts DL, Cocquet J, Clay CM, Osamura RY, Camper SA. FOXL2 in the pituitary: molecular, genetic, and developmental analysis. Mol Endocrinol 2006; 20:2796-2805

50. Chang TJ, Chiu YF, Sheu WH, Shih KC, Hwu CM, Quertermous T, Jou YS, Kuo SS, Chang YC, Chuang LM. Genetic polymorphisms of PCSK2 are associated with glucose homeostasis and progression to type 2 diabetes in a Chinese population. Scientific reports 2015; 5:14380

51. Winters A, Ramos-Molina B, Jarvela TS, Yerges-Armstrong L, Pollin TI, Lindberg I. Functional analysis of PCSK2 coding variants: A founder effect in the Old Order Amish population. Diabetes research and clinical practice 2017; 131:82-90

52. Fernandez MO, Sharma S, Kim S, Rickert E, Hsueh K, Hwang V, Olefsky JM, Webster NJ. Obese Neuronal PPARgamma Knockout Mice Are Leptin Sensitive but Show Impaired Glucose Tolerance and Fertility. Endocrinology 2017; 158:121-133

53. Sharma S, Morinaga H, Hwang V, Fan W, Fernandez MO, Varki N, Olefsky JM, Webster NJ. Free fatty acids induce Lhb mRNA but suppress Fshb mRNA in pituitary LbetaT2 gonadotropes and diet-induced obesity reduces FSH levels in male mice and disrupts the proestrous LH/FSH surge in female mice. Endocrinology 2013; 154:2188-2199

54. Hou H, Chan C, Yuki KE, Sokolowski D, Roy A, Qu R, Uusküla-Reimand L, Faykoo-Martinez M, Hudson M, Corre C, Goldenberg A, Zhang Z, Palmert MR, Wilson MD. Postnatal developmental trajectory of sex-biased gene expression in the mouse pituitary gland. Biol Sex Differ 2022; 13:57

55. Fujimoto M, Andrew M, Dauber A. Disorders caused by genetic defects associated with GH-dependent genes: PAPPA2 defects. Mol Cell Endocrinol 2020; 518:110967

56. Conover CA, Boldt HB, Bale LK, Clifton KB, Grell JA, Mader JR, Mason EJ, Powell DR. Pregnancy-associated plasma protein-A2 (PAPP-A2): tissue expression and biological consequences of gene knockout in mice. Endocrinology 2011; 152:2837-2844

57. Ansell PJ, Zhou Y, Schjeide BM, Kerner A, Zhao J, Zhang X, Klibanski A. Regulation of growth hormone expression by Delta-like protein 1 (Dlk1). Mol Cell Endocrinol 2007; 271:55-63

58. Lainez NM, Coss D. Leukemia Inhibitory Factor Represses GnRH Gene Expression via cFOS during Inflammation in Male Mice. Neuroendocrinology 2019; 108:291-307

59. Bakos HW, Mitchell M, Setchell BP, Lane M. The effect of paternal diet-induced obesity on sperm function and fertilization in a mouse model. International journal of andrology 2011; 34:402-410

60. Vendramini V, Cedenho AP, Miraglia SM, Spaine DM. Reproductive function of the male obese Zucker rats: alteration in sperm production and sperm DNA damage. Reproductive sciences (Thousand Oaks, Calif) 2014; 21:221-229

61. DiVall SA, Herrera D, Sklar B, Wu S, Wondisford F, Radovick S, Wolfe A. Insulin receptor signaling in the GnRH neuron plays a role in the abnormal GnRH pulsatility of obese female mice. PLoS One 2015; 10:e0119995

62. McGee WK, Bishop CV, Pohl CR, Chang RJ, Marshall JC, Pau FK, Stouffer RL, Cameron JL. Effects of hyperandrogenemia and increased adiposity on reproductive and metabolic parameters in young adult female monkeys. Am J Physiol Endocrinol Metab 2014; 306:E1292-1304

63. Swarnalatha NB, Roy N, Gouda MM, Moger R, Abraham A. High-fat, simple-carbohydrate diet intake induces hypothalamic-pituitary-thyroid axis dysregulation in C57BL/6J male mice. Applied physiology, nutrition, and metabolism = Physiologie appliquee, nutrition et metabolisme 2018; 43:371-380

64. Tannenbaum BM, Brindley DN, Tannenbaum GS, Dallman MF, McArthur MD, Meaney MJ. High-fat feeding alters both basal and stress-induced hypothalamic-pituitary-adrenal activity in the rat. American Journal of Physiology-Endocrinology and Metabolism 1997; 273:E1168-E1177

CHAPTER FOUR:

Sexual dimorphism in obesity is governed by RELMα regulation of adipose macrophages and eosinophils

Jiang Li[#1], Rebecca E. Ruggiero-Ruff [#1], Yuxin He[1], Xinru Qiu[2], Nancy M. Lainez[1], Pedro A. Villa[1], Adam Godzik[1], Djurdjica Coss[*1], Meera G. Nair[*1]

[1]Division of Biomedical Sciences; School of Medicine, University of California, Riverside; [2]Graduate Program in Genetics, Genomics and Bioinformatics, University of California, Riverside; Riverside, CA 92521

# equal contribution

* equal corresponding authorship

4.1 Abstract

Obesity incidence is increasing worldwide with the urgent need to identify new therapeutics. Sex differences in immune cell activation drive obesity-mediated pathologies where males are more susceptible to obesity co-morbidities and exacerbated inflammation. Here, we demonstrate that the macrophage-secreted protein RELMα critically protects females against high fat diet-induced obesity. Compared to male mice, serum RELMα levels were higher in both control and high fat diet-fed females and correlated with frequency of adipose macrophages and eosinophils. RELMα-deficient females gained more weight and had pro-inflammatory macrophage accumulation and eosinophil loss in the adipose stromal vascular fraction, while RELMα treatment or eosinophil transfer rescued this phenotype. Single cell RNA-sequencing of the adipose stromal vascular fraction was performed and identified sex and RELMα-dependent changes. Genes involved in oxygen sensing and iron homeostasis, including hemoglobin and lncRNA Gm47283/Gm21887, correlated with increased obesity, while eosinophil chemotaxis and response to amyloid-beta were protective. Monocyte-to-macrophage transition was also dysregulated in RELMα-deficient animals. Collectively, these studies implicate a RELMα-macrophage-eosinophil axis in sex-specific protection against obesity and uncover new therapeutic targets for obesity.

4.2 Rationale in elucidating mechanisms of sex-differences in diet-induced obesity

Obesity is an epidemic of significant public concern and contributes to the increased risk of several diseases, including type 2 diabetes, cardiovascular disease, nonalcoholic fatty liver disease, and COVID-19. Currently in the US, over 30% of men and women are classified as obese, with a body mass index (BMI) of $\geq 30\,\text{kg/m}^2$ (1). There are profound sex differences in adipose tissue deposition and obesity-associated diseases (2). Obese men are more at risk for metabolic syndrome, cardiovascular disease, and myocardial infarction than obese women (3). Male mice fed high fat diet (HFD) gain more weight and have an increased risk of insulin resistance than females (4). Despite these sex differences, most studies have historically focused on obesity mechanisms in males, since males gain weight more rapidly than females (5). Therefore, there remain many gaps in knowledge about the underlying mechanisms for obesity and whether these are sex-dependent, which can impact the development of therapeutics that are equally effective for both males and females. To address this gap, the focus of recent studies has been identifying mechanisms that provide protection in females ($6, 7$). Males and females accumulate fat into different adipose tissue depots; males deposit more fat into visceral adipose depots, while females deposit fat preferentially into subcutaneous depots ($7, 8$). Since visceral adiposity is associated with the metabolic syndrome (9), differential fat accumulation may explain male propensity for obesity-mediated pathologies.

An underlying immune component for obesity pathogenesis is well recognized, with obesity being regarded as a chronic inflammatory process. Macrophages are critical immune effectors in obesity. Increases in adipose tissue size correlate with macrophage

infiltration into the fat depots and proinflammatory cytokine production in both humans and mice (*10-12*). Obese adipose tissues produce increased levels of leptin (*6, 13*), and monocyte chemoattractant protein-1 (MCP-1, or CCL2 chemokine) that binds CCR2 (*14, 15*), which may serve as chemoattractant to recruit monocytes. In turn, they can be activated or differentiate into macrophages, initiating the secretion of cytokines and chemokines to exacerbate inflammation (*16, 17*). Given the role of macrophages in obesity, sex differences in macrophages are of particular interest and have been demonstrated before (*18, 19*). Visceral fat contains more infiltrating macrophages and higher expression of inflammatory cytokines than subcutaneous fat (*10, 20*), and male visceral adipose tissues accumulate more macrophages than females (*6, 21*). The presence of sex steroid hormones, specifically estrogen, was postulated to contribute to sex differences in obesity (*5, 8, 22*). (*23-26*) Alternatively, we and others have demonstrated intrinsic sex-specific differences in macrophages, independent of sex-steroid hormones (*6, 27, 28*). Male macrophages are more migratory and inflammatory, while protection in females is associated with higher production of anti-inflammatory cytokines, such as IL-10 (*6, 7*). Macrophage function and activation in the adipose tissue are guided by their ontogeny, the cytokine environment, as well as myriad factors such as hypoxia, metabolites, lipids (*29*). CD11c^{+} M1-like macrophages are activated through innate TLR2/4 receptors and produce proinflammatory mediators (e.g. TNFα, IL-6, CCL2) that drive metabolic changes. Adipose tissue macrophages or metabolically activated macrophages can be distinguished from other proinflammatory macrophages by several different cell surface markers, although they produce proinflammatory cytokines

as well (*30*). On the other hand, a T helper type 2 (Th2) cytokine environment within the adipose tissue promotes metabolic homeostasis and protective CD206$^+$ M2 macrophages that suppress inflammation. Immune drivers of the Th2 cytokine environment for M2 macrophage activation include IL-4-producing eosinophils and innate lymphoid cell (ILC)-2 (*31, 32*). It is now recognized that macrophage activation is far more complex than the M1/M2 paradigm (*29, 33, 34*). However, the M1/M2 macrophage paradigm is a useful framework to begin to address pathways that can be targeted for obesity pathogenesis, and whether these are influenced by sex.

The focus of this study was to identify sex-specific immune effectors that regulate obesity pathogenesis, focusing on the M2 macrophage signature gene Resistin-like molecule α (RELMα). RELMα is a small, secreted cysteine-rich protein that is expressed by macrophages primarily in response to Th2 cytokines but can also be induced by hypoxia (*35, 36*). RELMα has pleiotropic functions ranging from inflammatory or immunoregulatory to microbicidal roles (*37-39*). Within the myeloid population, RELMα is preferentially expressed in monocyte-derived macrophages, and is important for monocyte differentiation, infiltration into other tissues and survival (*40, 41*). In the adipose tissue, RELMα is a defining marker for perivascular macrophages and is co-expressed with CD206 and Lyve1 (*29, 34*). A beneficial function for RELMα in metabolic disorders has been proposed; CD301b$^+$ phagocytes promoted glucose metabolism and net energy balance through secretion of RELMα, and RELMα-overexpression promoted cholesterol homeostasis in hyperlipidemic low density lipoprotein receptor-deficient mice (*42, 43*). Based on these previous findings, the goal of

146

this study was to investigate how sex and RELMα regulate diet-induced obesity and inflammation by employing RELMα-deficient mice and utilizing flow cytometry and single-cell sequencing of visceral adipose stromal vascular fraction to identify sex-specific and RELMα-dependent targets of obesity.

4.3 Materials and methods

4.3.1 Animals

All experiments were performed with approval from the University of California (Riverside, CA) Animal Care and Use Committee (A-20210017; and A-20210034), in compliance with the US Department of Health and Human Services Guide for the Care and Use of Laboratory Animals. RELMα knockout mice were generated as previously described (37). RELMα and their WT controls were maintained under a 12-h light, 12-h dark cycle and received food and water *ad libitum*. After weaning and a week acclimatization on normal chow, animals were randomly distributed in groups and placed on either a high fat diet (HFD, D12492, 60% kcal from fat; 5.21 kcal/g (lard 0.32 g/g diet, soybean oil 0.03 g/g), 20% kcal from carbohydrate, 20% kcal from protein; Research Diet, New Brunswick, NJ) or control diet with matching sucrose levels to HFD (Ctr, D12450J, 10% kcal from fat 3.82 kcal/g (lard 0.02 g/g diet, soybean oil 0.025 g/g), 70% kcal from carbohydrate, 20% kcal from protein; Research Diet, New Brunswick, NJ) for 6-12 weeks, as indicated for each experiment. For all tissue and cell recovery mice were sacrificed between 8 and 9am.

4.3.2 Eosinophil and RELMα treatment

For adoptive transfer, peritoneal exudate cavity cells were recovered from

Heligmosomoides polygyrus-infected mice. Specifically, groups of 3-5 WT female BL/6

mice were infected by oral gavage of 200 *H.polygyrus* L3, which leads to adults in the

intestine and eosinophilia by day 10 post-infection, and a chronic infection in BL/6J for

at least at least 3 months (*76*). Infection was confirmed by egg count in feces. To ensure

sufficient eosinophil recovery, 2-3 *H.polygyrus*-infected female mice were euthanized

between days 14 and 20 post-infection for eosinophil recovery. Peritoneal exudate cavity

eosinophils were column-purified with biotinylated anti-SiglecF (BioLegend), followed

by anti-biotin MicroBeads then magnetic separation with MS columns according to

manufacturer's instructions (Miltenyi). 1×10^6 eosinophils were transferred to recipient

mice by i.p. injection every two weeks. Eosinophil purity was confirmed by flow

cytometry and by Diff-Quik stained-cytospins. For RELMα treatment, recipient RELMα

KO female mice were i.p. injected 2 ug RELMα every 14 days. Ctr mice were injected

with PBS.

4.3.3 Cytokine Quantification

RELMα and IL5 were measured by sandwich ELISA. IFN-γ, CXCL1 (KC), TNF-α,

CCL2 (MCP-1), IL-12p70, CCL5 (RANTES), IL-1β, CXCL10 (IP-10), GM-CSF, IL-10,

IFN-β, IFN-α and IL-6 were detected by the Mouse Anti-Virus Response Panel (13-plex)

(Cat# 740622 BioLegend, San Diego, CA) and analyzed on the NovoCyte Flow
Cytometer (Agilent, Santa Clara, CA) and LEGENDplexTM software (Biolegend, San
Diego, CA).

4.3.4 Histological analyses and immunohistochemistry

At the conclusion of diet exposure, mice were anesthetized, perfused with 20 ml cold
PBS, fat tissues were recovered and immersed in 4% PFA for 24 hours followed by 30%
sucrose for another 24 hours. Fat tissues were embedded with O.C.T (Sakura Finetek
USA) and sectioned at 10 μm. For immunofluorescent staining, sections were incubated
with APC-anti RELMα (DS8RELM, eBioscience, Santa Clara, CA), PE/Dazzle™ 594
anti-SiglecF (S17007L BioLegend, San Diego, CA) and Alexa Fluor® 488 anti-mouse
F4/80 (BM8 eBioscience, Santa Clara, CA) overnight at 4°C, then counterstained with
DAPI (BioLegend, San Diego, CA). For Hemoglobin staining, sections were incubated
with primary antibodies (rabbit anti-hemoglobin alpha (Invitrogen, catalog # MA5-
32328), F4/80 Monoclonal Antibody (Invitrogen, catalog # MA5-16624), TER-119
Monoclonal Antibody, APC, (eBioscience, catalog # 17-5921-81) overnight at 4°C.
Sections then washed with PBS-T three times, and then incubated fluorochrome-
conjugated secondary antibodies (chicken anti-Rabbit IgG (H+L) Cross-Adsorbed
Secondary Antibody, TRITC (Invitrogen, catalog # A15998), Goat anti-Rat IgG (H+L)
Cross-Adsorbed Secondary Antibody, Alexa Fluor™ 488(Invitrogen, catalog # A11006)
for 1h at RT. Sections were counterstained with DAPI (BioLegend, San Diego, CA).

Slides were examined with the Keyence microscope (BZ-X800; lense:BZ-PF10P, Plan

Fluorite 10X, WD 14.5 mm; BZ-PF40LP, Plan Fluorite 40X LD PH, WD 2.2 to 3.3mm).

4.3.5 Hemoglobin ELISA

The ELISA assay for Hemoglobin (Hba) was performed using a commercially

available ELISA kit, Mouse Hemoglobin Elisa Kit (abcam, Catalog # ab254517). Prior to

measurement, total protein samples were diluted 1:1250. The absorbance data of the

ELISA was acquired by a plate reader (BioTek Synergy HT).

4.3.6 Flow Cytometry

Tissues from each mouse were processed separately as part of a 3-4 mouse cohort per

group, with each experiment repeated 2-3 times. In brief, mice were perfused with ice

cold PBS, adipose tissue was collected from gonadal fat pads representing visceral fat

depot, or from inguinal fat pads representing subcutaneous fat depot, rinsed in cold PBS,

weighed, minced with razor blade and digested enzymatically with 3 mg/mL

collagenase/dispase (Roche) at 37 °C for 1 hour. Suspension was passed through 70 μm

cell strainer, cells pelleted, and red blood cells lysed using RBC lysis buffer (Biolegend,

San Diego, CA). Stromal vascular fraction cells were collected and counted, and 2

million cells labeled for flow cytometry analyses. Cells were Fc-blocked with anti-mouse

CD16/CD32 (1:100, Cat# 553141, BD Biosciences, San Jose, CA) followed by surface

marker staining with antibodies to MerTK (2B10C42, Biolegend), CD25 (PC61,

Biolegend), CD301 (LOM-14, Biolegend), CD36 (HM36, Biolegend), MHCII

(M5/114.15.2, Biolegend), CD45 (QA17A26, Biolegend), CXCR4 (L276F12, Biolegend), CD11b (M1/70, Biolegend), F4/80 (BM8, Biolegend), CD4 (RM4-5, Biolegend), CD206 (C068C2, Biolegend), SiglecF (S17007L, Biolegend), CD11c (N418, eBioscience), CD64 (X54-5/7.1, Biolegend), RELMα (DS8RELM, eBioscience). Dead cells were labeled with Zombie Aqua™ Fixable Viability Kit (Cat# 423102 Biolegend, San Diego, CA). Gating strategy was followed: macrophage ($CD45^+CD11b^+MerTK^+CD64^+$), eosinophils ($CD45^+CD11b^+SiglecF^+ MerTK^-CD64^-$), monocyte ($CD45^+CD11b^+MHCII^+CD11c^-MerTK^-CD64^-SiglecF^-$), dendritic cells ($CD45^+ MHCII^+CD11c^+MerTK^-CD64^-SiglecF^-$) and T cells ($CD45^+ CD4^+CD11b^-MHCII^-CD11c^- MerTK^-CD64^-SiglecF^-$). Cells were analyzed on the NovoCyte Flow Cytometer (Agilent, Santa Clara, CA) and FlowJo v10 software (Tree Star Inc.; Ashland, OR). tSNE analyses were performed using FlowJo v10 (Tree Star Inc.; Ashland, OR), following concatenation of samples (5000 cells per biological replicate) for each group, to generate plots consistent between groups. This was followed by analysis of the expression of desired markers in separated groups. The parameters used to run the tSNE analyses were FITC-MerTK, PerCP-CD25, Alexa Fluor 700-MHCII, Brilliant Violet 605-CD11b, Brilliant Violet 650-F4/80, Brilliant Violet 711-CD4, PE/Dazzle 594-SiglecF, PE Cy5-CD11c and PE Cy7-CD64. Cells were gated according to Supplemental Figure 4.1, clustering was done according to these gates, and annotation was performed with the FlowJo software.
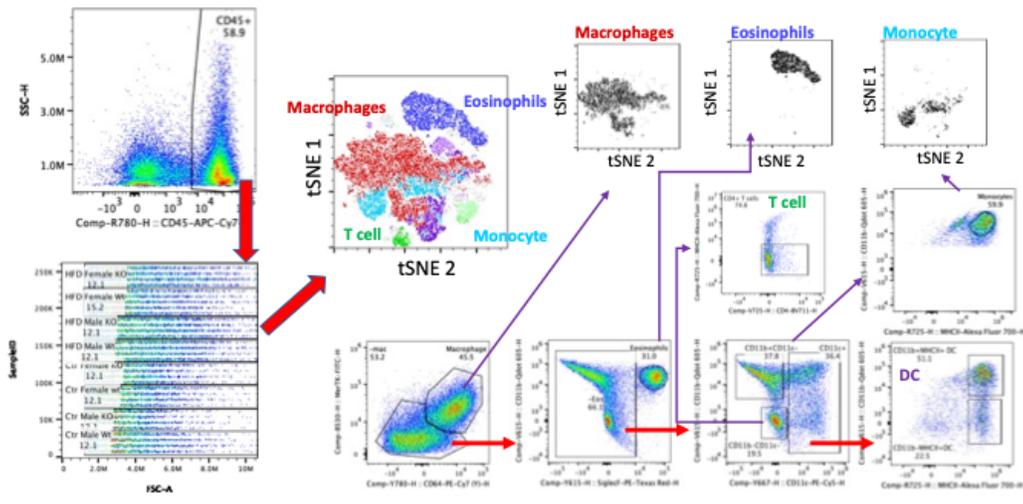
Supplemental Fig 4.1 Flow cytometry gating strategy. Representative flow cytometry plots of adipose immune cells from the stromal vascular fraction of visceral adipose tissue detailing gating strategy and subsequent tSNE analysis.

4.3.7 Stromal vascular fraction (SVF) isolation from adipose tissue

Adipose tissue was dissected, rinsed in ice cold PBS, and minced with a razor blade. Fat was digested enzymatically with 3 mg/ml collagenase/dispase (Roche) at 37 C for 1 hour. Suspension was passed through a 70 m strainer and centrifuged to pellet stromal vascular fraction. Cells were resuspended in PBS/0.04% BSA, counted, viability determined to be > 90% before proceeding to flow cytometry analysis or scRNA-seq.

4.3.8 Single cell RNA-seq (scRNA-seq)

ScRNA-seq was performed following the Chromium Next GEM Single Cell 3' v3.1 Dual Index with Feature Barcoding for Cell Multiplexing protocol. Each group consisted of three biological replicates. SVF single cell suspension from each mouse was labeled with the 10X Genomics Cell Multiplexing Oligos (CMOs) following manufacturer's protocol (10x Genomics, Demonstrated Protocol, CG000391). Cell suspensions from mice in the same group were pooled and processed for the Chromium Next GEM Single Cell 3' v3.1 Dual Index (10X Genomics, Demonstrated Protocol, CG000388). For generation of single-cell gel beads in emulsion (GEM), 50,000 cells were loaded on the Chromium Chip and barcoded, in order to reach a targeted cell recovery of 30,000 cells per group. GEM reverse-transcription was achieved in order to generate barcoded cDNA. GEMs were broken, and cDNA was cleaned up using DynaBeads MyOne Silane Beads (Thermofisher Scientific) and SPRIselect Reagent kit (Beckman Coulter). Full-length barcoded cDNA was amplified, cleaned up and fragmented in order to generate Illumina-

ready sequencing libraries. 3' single cell gene expression libraries were generated using a fixed proportion (25%) of the total cDNA per sample. Libraries were amplified by PCR, after which the library was split into two parts: one part for generating the 3' gene expression library and the other for the multiplexing library. Libraries were indexed for multiplexing (Chromium Dual Index Kit TT Set A, PN-1000215, 10x Genomics), quantified by Qubit 3 fluorometer (Invitrogen) and quality assessed by 2100 BioAnalyzer (Agilent). Equivalent molar concentrations of libraries were pooled and sequenced using Novaseq 6000 (Illumina) using 10x Genomics recommended sequencing depth and run parameters (sequencing depth of 20,000 read pairs per cell, paired end sequencing) at the UC San Diego (UCSD) Institute for Genomic Medicine (IGM) Center.

4.3.9 Data processing and analysis

Demultiplexed FASTQ files were provided and downloaded by a secure portal on the UCSD IGM core and were used for downstream processing. Raw scRNA-seq FASTQ files were aligned to the mouse mm10-2020-A genome with Cell Ranger v6.1.2 with default settings using STAR aligner in the Cell Ranger multi pipeline. The Cell Ranger multi pipeline specifically analyzes 3' Cell Multiplexing data combined with 3' Gene expression data. The reference genome was downloaded from the 10x Genomics website and built as per official release notes (https://support.10xgenomics.com/single-cell-gene-expression/software/release-notes/build#mm10_2020A). Every group was analyzed using the Cell Ranger multi pipeline, which allows multiplexing libraries to be processed together with the paired gene expression (GEX) libraries for each group. Cell

multiplexing oligo (CMO) deconvolution was performed using the Cell Ranger multi

pipeline. Briefly, a multi config CSV was created containing the library definitions and

experimental design variables (deposited on the Github repository:

https://github.com/rrugg002/Sexual-dimorphism-in-obesity-is-governed-by-RELM-

regulation-of-adipose-macrophages-and-eosinophils). These parameters contain sections

that specify parameters relevant to analysis of the gene expression library including the

10x Genomics-compatible reference genome, a samples section that specifies sample

information and CMO identity for cell multiplexing and a section that highlights the

identity and location of the input FASTQ file for each sample as well as the chemistry of

the assay. After generation of the multi config CSV, Cell Ranger multi was performed

with the output folder containing the main pipeline outputs, such as the generalized

multiplexing outputs and the demultiplexed outputs per sample. Dimensionality reduction

analysis was performed as an automated secondary analysis as part of the Cell Ranger

multi pipeline. Briefly, Cell Ranger performs principal component analysis (PCA) using

gene expression features as PCA features, using a python implementation of the IRLBA

algorithm. This data is then passed into the nonlinear dimensionality reduction method, t-

SNE (t-Stochastic Neighbor Embedding) analysis in order to visualize the data in a 2D

space. Unbiased clustering of the data was then performed in order to group cells together

that have similar expression profiles based on their principal components using a graph-

based method. Cell Ranger produces a table indicating differentially expressed features in

each cluster relative to other clusters, with the top hits being used to identify cell

populations. Sequencing reads for all 12 samples were then integrated using the Cell

Ranger aggr pipeline, which enables batch effect correction to be performed on the combined data set. Cell Ranger aggr pipeline generates a normalized integrated count matrix was generated by dividing the UMI count for each gene by the total number of UMIs in each cell, followed by log-transformation. To filter out poor quality cells, cells with threshold UMI count of >20,000 and <500 and mitochondrial fraction of >10% were filtered from analysis using the Loupe Browser software v 6.2. re-clustering tool.

4.3.10 Gene expression visualization and differential gene expression analysis

The 10x Genomics Loupe Browser software v 6.2 (10x Genomics, Pleasonton, Ca) was used to project tSNEs of the cell type clusters obtained after integration of all 12 samples (4 groups, WT Female, WT Male, KO Female, KO Male, n=3 per group) using the Cell Ranger aggr pipeline. Differential gene expression analysis for the myeloid cell, fibroblast, and ILC2 cell, sub-clustering analysis was calculated using the Loupe Browser's integrated locally distinguishing function, which determines the features that distinguish the selected groups from one another or by distinguishing cells from one selected cluster vs cells from another selected cluster. The locally distinguishing function of Loupe Browser utilizes the negative binomial test based on the sSeq method (*77*), with Benjamini-Hochberg correction for multiple tests and calculates log-normalized average expression values across the two samples or cell populations being compared. When performing pseudo bulk differential gene expression analysis between groups (WT female vs male, KO female vs male, KO female vs WT female KO male vs WT male), the globally distinguishing function on Loupe Browser was used to find features between

checked groups relative to all clusters in the dataset. Differential gene expression file outputs from Loupe Browser were downloaded and data were presented as volcano plots and average counts for select genes were plotted as histograms between both groups (Graphpad Prism). Heatmaps of differential gene expression data were plotted using Loupe Browser software and are generated using hierarchical clustering with Euclidian distance and average linkage.

Gene ontology (GO) enrichment analysis of the genes from DEG analysis was performed using the ShinyGo 0.76.3 platform (South Dakota State University (*78*)). ShinyGo 0.76.3 fold enrichment algorithm utilizes a hypergeometric distribution followed by false discovery rate (FDR) correction. Background gene-sets are all protein-coding genes in the mouse genome. The top 30 DEGs that were up- and downregulated for each respective comparison were visualized using a dotplot chart plotting fold enrichment for each respective enriched GO term for Biological Processes. For each GO enrichment analysis, false discovery rate (FDR) of <0.05 was applied, with the pathway minimum set to 10.

4.3.11 Trajectory Analysis

For Trajectory analysis, we utilized the Seurat package (Seurat_4.3.0) (*79*) and Monocle3 (v 3_1.2.9) (*80*) to process and analyze the scRNA-seq data. The raw data was initially read into R using the readMM function, with the matrices for features, barcodes, and counts extracted from the input files. The Seurat object was created by applying the

CreateSeuratObject function with a minimum of 3 cells per gene and 100 features per cell, which was then saved as an RDS file for subsequent analysis. Cell barcodes annotated from the 10x Genomics Loupe Browser were imported as separate CSV files. These annotations were subsequently integrated into the Seurat object's metadata. We then subset the data to focus on dendritic cells, macrophages, and monocytes for further trajectory analysis using Monocle3 (*81, 82*). The expression matrix, cell metadata, and gene annotations were extracted from the Seurat object and used to create a new CellDataSet (CDS) object in Monocle3. The CDS was preprocessed with a dimensionality reduction set at 100 dimensions, followed by an alignment step to adjust for batch effects using the Sample.ID variable. Lastly, a trajectory graph was constructed by applying the learn_graph function, which infers the developmental trajectories of the cell populations (*83*).

4.3.12 Statistical analyses

Data are presented as mean ± SEM and statistical analysis was performed by Graphpad Prism 9. Statistical differences between control and RELMα knockout mice (p < 0.05) were determined using t-test, or 2-way or 3-way ANOVA with Sidak multiple comparisons test . *, $p \leq 0.05$; **, $p \leq 0.01$; ***, $p \leq 0.001$ and **** $p \leq 0.0001$. 10x scRNA-seq experiment was performed once (3 mice per group). All other *in vivo* experiments were repeated 2-4 times with n=3-5 per group (combined n=6-20), based on sample size calculation by power analysis (Type I error<0.05 and Power (1-β).

4.4 Results

4.4.1 RELMα protects female mice from high fat diet-induced obesity and inflammation.

Studies investigating sex differences show that female mice are protected, or have delayed, diet-induced obesity, unless aged or challenged by ovariectomy (*7, 44*). In support of the critical role of macrophage polarization in sex-specific differences, previous studies demonstrated that protection in females is associated with Th2 cytokine-induced M2 polarization, for example CD206 expression, while males exhibit increased CD11c-positive 'proinflammatory' M1-like macrophages in the adipose tissue (*21*). The secreted protein RELMα is a signature protein expressed by M2 macrophages, with regulatory functions in downregulating inflammation and promoting tissue healing. A role for RELMα in promoting metabolic homeostasis has also been reported (*42, 43*). Based on these studies, we hypothesized that female-specific protection from high fat diet (HFD) may be influenced by RELMα. To examine systemic and local factors that may provide protection to females, serum and visceral adipose tissue homogenate were obtained from male or female mice on a control-fed (Ctr) or high fat diet-fed (HFD) for over 12 weeks. Under both Ctr and HFD conditions, female mice had significantly higher RELMα in the serum than males, and in adipose tissue under Ctr diet. Exposure to HFD diminished adipose RELMα levels in both sexes (Fig. 4.1A).

To determine the role of RELMα in obesity, we placed RELMα knockout (KO) mice on Ctr and HFD and compared their response to matched wild-type (WT) controls (Supplemental Figure 4.2). RELMα deficiency did not affect Ctr or HFD weight gain in males, however, RELMα deficiency in females led to significantly increased weight gain

159

on HFD compared to WT on HFD (Fig 4.1B). Whole-body weight, and visceral and subcutaneous adipose weights were similarly increased in WT and KO males on HFD (Fig 4.1C-D). However, RELMα deficiency only affected HFD-fed females, with significantly increased body weight, and visceral and subcutaneous adipose tissue mass compared to HFD WT females. Chemokines that change with exposure to HFD were assessed in the adipose tissue of these mice (Fig 4.1E). The monocyte chemoattractant CCL2 was significantly elevated in WT and KO HFD-males, while it remained low in females regardless of diet, as demonstrated before (6). On the other hand, females had higher levels of the anti-inflammatory IL-10 than males, as demonstrated before (6, 7), as well as the regulatory T cell growth factor GM-CSF, and the Th2 cytokine IL-5. The higher level of IL-10 and GM-CSF in females were dependent on RELMα and were further decreased with exposure to HFD, while IL-5 was not detected with HFD. Inflammatory cytokines such as TNFα, IL-6 and IL-1β were also measured, but no RELMα-dependent differences with HFD exposure were observed. A larger animal cohort size may have provided more powered analysis and identified more adipose protein differences between groups especially with CCL2, which demonstrated the greatest variability. Nonetheless, the adipose protein profile indicates sex and RELMα-dependent effects of diet-induced obesity, which correlates with increased proinflammatory CCL2, and decreased anti-inflammatory and Th2 cytokines, IL-10, GM-CSF and IL-5, respectively.

Adipose tissue inflammation was next examined by flow cytometry of the stromal vascular fraction (SVF) from the visceral adipose tissue (Fig. 4.1F). RELMα deficiency

and HFD resulted in significantly higher leukocyte frequency in the male SVF, demonstrating a role of RELMα in males (Fig 4.1G). WT females did not exhibit increased leukocyte frequency in adipose tissues with HFD, as shown previously (*6*). Compared to HFD-fed WT females, RELMαKO females fed HFD had significantly more SVF leukocytes, specifically macrophages (Fig 4.1H). In contrast, the proportion of eosinophils was lower in HFD-fed males compared to females with the same diet (Fig 4.1I), suggesting a reduction in the protective type 2 immune response. This was consistent with the reduction in IL-5 in the adipose tissue following HFD (see Fig 4.1E). The contribution of diet, sex and genotype to body weight and adipose tissue inflammation was assessed by 3-way ANOVA (n=4-5 per group) (Supplemental Table 4.1). Diet, followed by sex, then genotype, were all significant factors accounting for the variance in body weight, at both 6 and 12-weeks post diet. While diet was the greatest factor in adipose tissue inflammation, evaluated as SVF leukocyte frequency, RELMα deficiency was a greater factor accounting for variance than sex. For SVF macrophage frequency, diet then sex were the significant factors accounting for variance, while for eosinophil frequencies, sex differences were the main driving factor. Together, these data show that female-specific protection from diet-induced obesity is associated with elevated RELMα expression, and that RELMα deficiency selectively affects females, leading to increased weight gain, adipose tissue mass and adipose tissue inflammation.
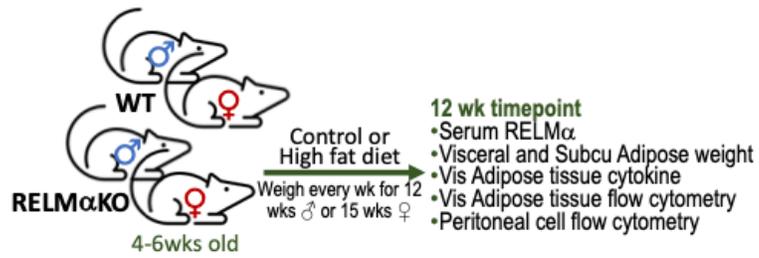
Supplemental Figure 4.2 Experimental model figure. Model figure overviewing experimental design and important timepoints for this study**.**
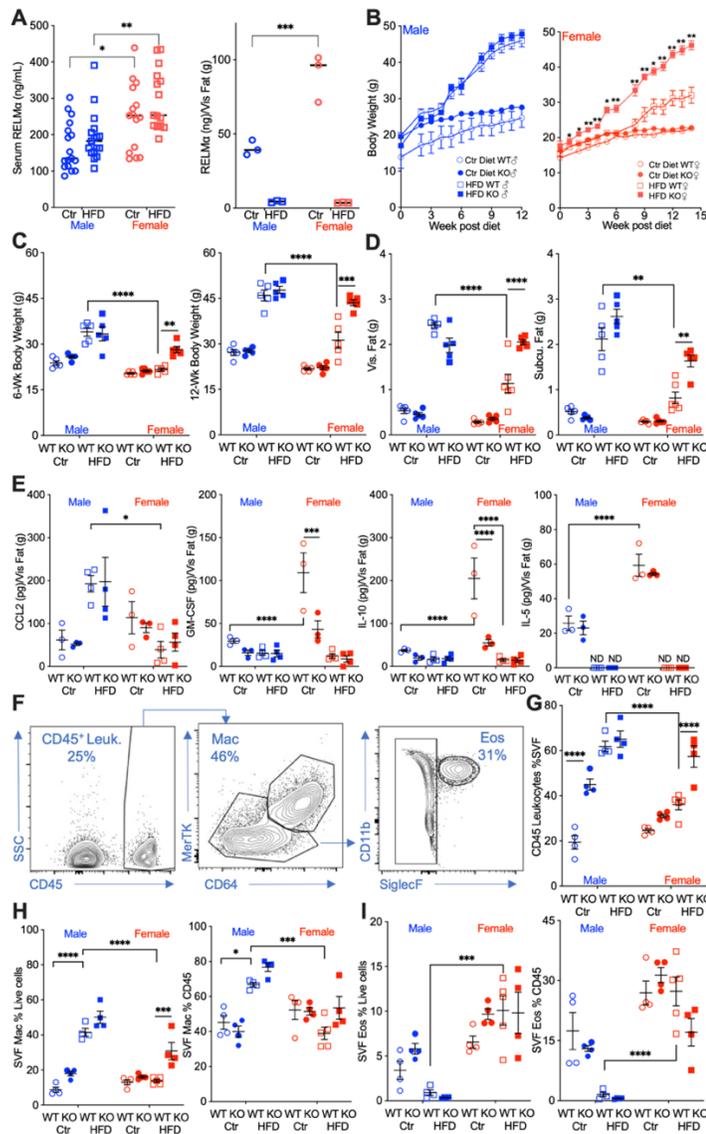
Fig 4.1 RELMα protects females from diet-induced obesity. (A) RELMα levels in serum and visceral adipose tissue from 18-week old male (♂) and female (♀) C57BL/6 mice after exposure to control (Ctr) or high fat diet (HFD) for 12 weeks. (B) WT or RELMα KO mice were weighed for 12-15 weeks of diet exposure. After 6-week diet and 12-week diet exposure (C), whole body, visceral and subcutaneous fat pad weights were recorded (D). (E) CCL2, GM-CSF, IL10, and IL5 levels in protein extracts from visceral fat pad after 12-week diet exposure. (F) Gating strategy for flow cytometric analysis of the visceral adipose stromal vascular fraction (SVF). (G-I) Proportion in the SVF of CD45+ leukocytes (G), CD45+CD64+Mertk+ macrophages (H), and CD45+SiglecF+CD11b+ eosinophils (I). Males (blue), females (red), WT (open symbols), RELMα KO (filled symbols), control diet (Ctr, circles), high fat diet (HFD, squares); data for (B) is presented as mean +/- S.E.M., data for (H) is representative of one animal, all other data are presented as individual points for each animal, where lines represent group means +/- S.E.M. Statistical significance between HFD WT females and HFD RELMα KO females was determined by two or three-way ANOVA with Sidak's multiple comparisons tests. (ND, not detected; *, p < 0.05; **, p<0.01; ***, p<0.001; ****, p<0.0001 are indicated for functionally-relevant comparisons). Data are representative of 3 experiments with 4-6 mice per group.

4.4.2 RELMα deficiency results in dysregulated macrophage activation and impaired eosinophil homeostasis in the adipose tissue

We performed flow cytometry followed by t-distributed stochastic neighbor embedding (tSNE) analysis to evaluate immune cell heterogeneity and surface marker expression in the visceral adipose SVF (Fig. 4.2A). tSNE analysis was performed based on gating strategies detailed in Supplemental Fig 4.1. Within the groups, eosinophils demonstrated the greatest changes; Ctr-fed male and female mice had high eosinophil numbers (see Fig 4.1I), and this eosinophil population disappeared in male mice upon HFD (Fig. 4.2B, red outline). WT female mice retained their eosinophil subset even with HFD. In contrast, RELMα KO females had decreased eosinophil population following HFD. Within the eosinophil subset, heterogeneity is observed in females, with Ctr mice exhibiting a different cell distribution compared to the HFD mice. The macrophage population also exhibited changes; Ctr-fed female mice, had a smaller macrophage subset compared to males, regardless of genotype (Fig. 4.2B, green outline). In both sexes, HFD led to an increase in this macrophage subset, and in their heterogeneity, especially in RELMα KO mice. Within the CD64$^+$MerTK$^+$ macrophage subset, expression of CD11c, a marker for proinflammatory M1-like macrophages, was evaluated. There was an increase in both number of CD11c+ macrophages and surface expression of CD11c on a per macrophage cell basis, in response to HFD in both males and females, however males had higher levels of CD11c than females under both diet conditions (Fig. 4.2C). RELMα deficiency exacerbated the increase in CD11c, particularly in the HFD-fed females (Fig. 2D). This may indicate that the increase in CD11c arises due to the abrogation of RELMα

levels in the visceral fat after HFD (see Fig. 4.1A). On the other hand, anti-inflammatory 'M2' macrophage marker, CD206, decreased with HFD, but was not dependent on the presence of RELMα (Supplemental Fig 4.3). CD301b, another M2 marker that is upregulated by IL-4, also decreased with HFD in both males and females (Fig. 4.2E). Specifically, in HFD females, CD301b was further decreased with a loss of RELMα. Although the number of eosinophils decreased in HFD-fed males of both genotypes, eosinophils in all groups maintained high expression of SiglecF, which was further increased with HFD specifically in RELMα KO females but not WT females (Fig. 4.2F). SiglecF is a paralogue of human Siglec-8, and in mice is expressed on eosinophils and alveolar macrophages. The function of SiglecF appears to be context-dependent, with reported evidence of stimulatory and inhibitory roles on eosinophils (45, 46). One study showed that SiglecF stimulation induced apoptosis (47). It is possible that the higher expression of SiglecF on the RELMα-deficient eosinophils from HFD KO female mice may contribute to their susceptibility to apoptosis, explaining their reduced frequency. We evaluated if eosinophil surface marker expression changed based on sex, diet, and genotype (Supplemental Fig. 4.3B-D). CXCR4 and MHCII expression was reduced following HFD in both WT and KO females but not males, which may account for the subset heterogeneity (see Fig. 4.2B). Overall, these data identify that sex-specific and RELMα-dependent protection against diet-induced obesity is associated with changes in adipose macrophages and eosinophils.
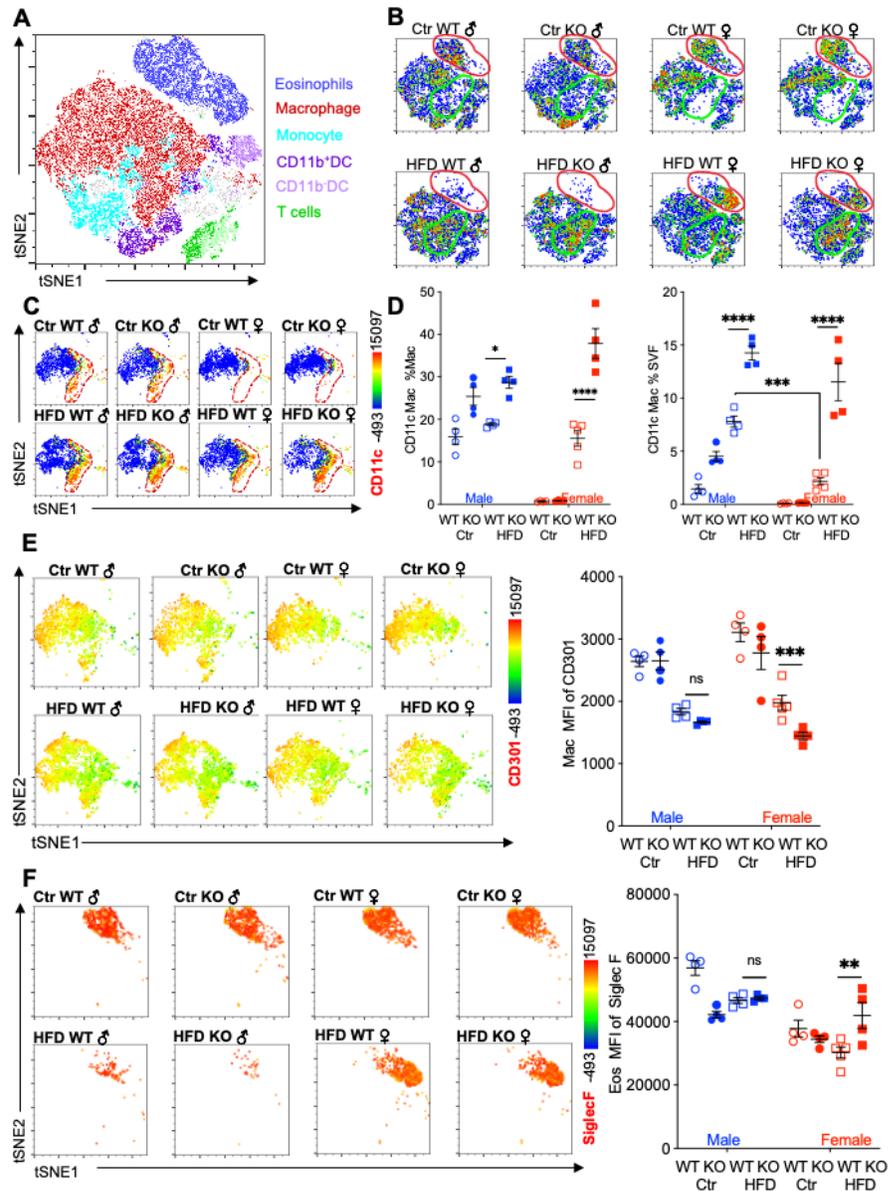
Fig 4.2 Adipose eosinophil and macrophage populations are influenced by sex, diet and RELMα. (A) tSNE analysis to identify SVF leukocyte populations. (**B**) tSNE analyses of SVF from the different groups (Male ♂, Female ♀, WT or RELMα KO) after 12 weeks of diet exposure (Ctr or HFD) revealed changes in eosinophil RELMα-dependent and diet-induced changes in eosinophil (red outline) and macrophage (green outline) subsets. (**C-D**) CD11c surface expression in $CD45^+MerTK^+CD64^+$ macrophages was analyzed by tSNE, where dashed red outline shows $CD11c^{Hi}$ cells, and quantified. **(E)** CD301b surface expression on SVF macrophages was examined by tSNE and quantified by mean fluorescent intensity (MFI). **(F)** Siglec-F surface expression on $CD45^+SiglecF^+CD11b^+$ SVF eosinophils was examined by tSNE and quantified by mean fluorescent intensity (MFI). tSNE data are one representative animal per group. All other data are presented as individual points for each animal, where lines represent group means +/- S.E.M. Statistical significance was determined by three-way ANOVA Sidak's with multiple comparisons test. (ns, no significant; *, $p < 0.05$; **, $p<0.01$; ***, $p<0.001$; ****, $p<0.0001$). Data are representative of 3 experiments with 4-6 mice per group.
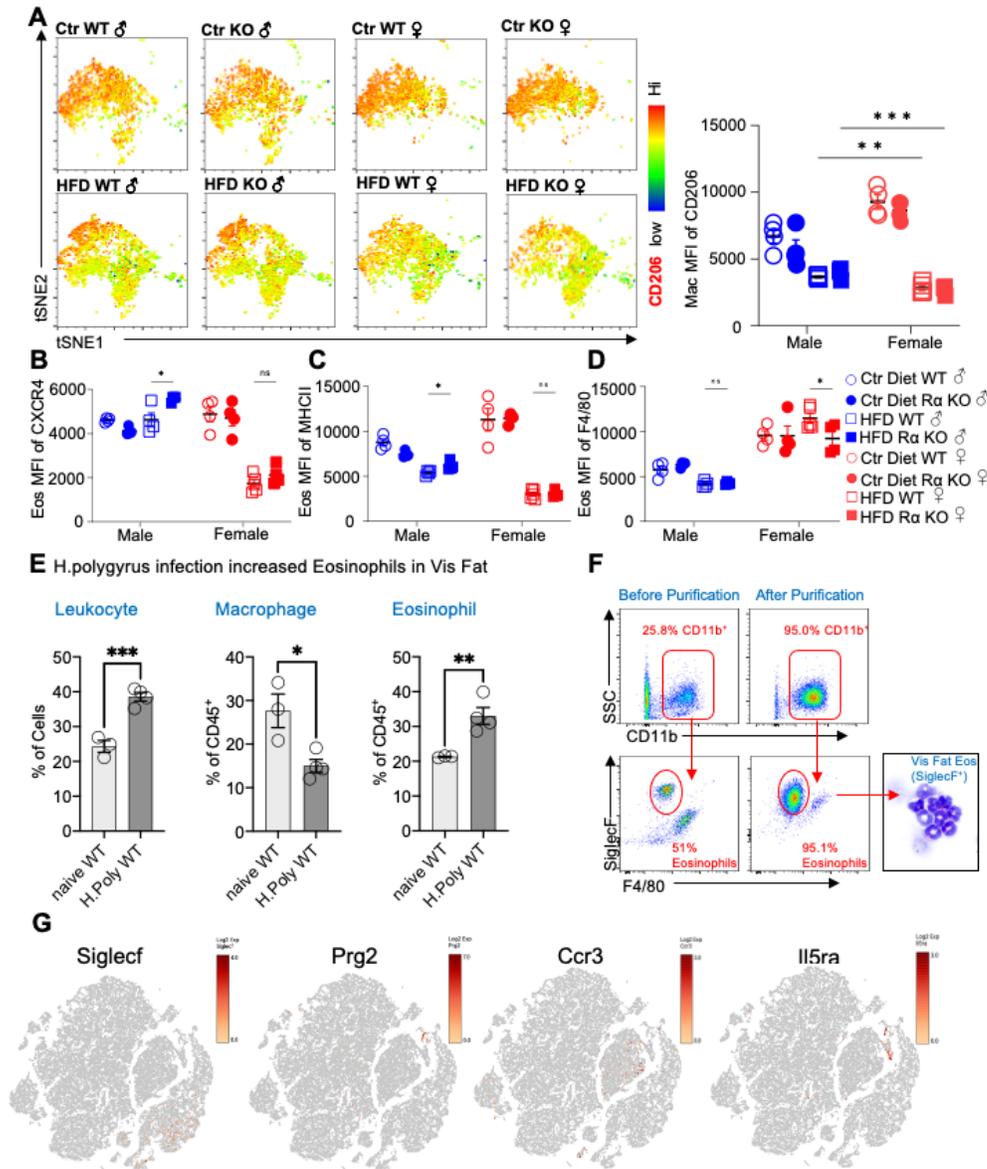
Supplemental Fig 4.3 Flow cytometric analysis of adipose immune cells. (A-D) Flow cytometry analysis of the visceral adipose stromal vascular fraction of 12-week diet exposed mice for CD206 surface expression on CD45+CD64+Mertk+ macrophages by tSNE plot and mean fluorescent intensity (MFI) (A) and surface expression by CD45+SiglecF+CD11b+ eosinophils of CXCR4 (B), MHCII (C) and F4/80 (D). (E-F) Visceral fat leukocytes from naïve or *H. polyrus*-infected mice were quantified (E), and eosinophils were column purified and analyzed for purity by flow and cytocentrifuge (F). (G) Feature plots of Log2Fold expression of eosinophil markers (*SiglecF, Prg2, Ccr3* and *Il5ra)* in all clusters of scRNA-seq data. Statistical significance was determined by unpaired t-test (*, p < 0.05; **, p<0.01). tSNE plot analysis and flow plots are representative of one animal per group, all other data are presented as individual points for each animal, where lines represent group means +/- S.E.M. Statistical significance for (A-D) was determined by two-way ANOVA with Sidak's multiple comparisons test. (ns, no significant; *, p < 0.05; **, p<0.01; ***, p<0.001) and by unpaired t-test for (E). Data are representative of two experiments with 3-6 mice per group.

167

4.4.3 Protection against diet-induced obesity in females is mediated by RELMα and eosinophils

We evaluated whether associations existed between adipose immune cells and obesity by performing correlation analysis of body weight with adipose macrophage or eosinophil frequencies (Fig. 4.3A-B). Across mice from all groups, there was a significant, positive correlation between macrophage frequency and body weight in the visceral SVF. In contrast, SVF eosinophil frequencies were negatively correlated with body weight. RELMα expression has been reported by many immune cell subsets, including macrophages, eosinophils, B cells (*35, 48*), although expression in the adipose tissue is less clear. Given that RELMα protein was present in the visceral adipose tissue, especially of females (see Fig 4.1A), flow cytometry analysis of intracellular RELMα in the SVF cells was performed in Ctr or HFD-fed female mice. SVF macrophages expressed RELMα, especially in the CD11c-negative subset, which was reduced with HFD (Fig 4.3C-D). RELMα$^+$ SVF macrophage frequency was negatively correlated with body weight in females (Fig. 4.3E), supporting the protective role of 'M2' macrophages in obesity. Focused comparisons between HFD vs Ctr-fed female mouse groups showed that significant, negative correlation between RELMα$^+$ macrophages and body weight occurred only in HFD-fed and not Ctr-fed mice (Fig. 4.3F-G). These data raise the possibility that diet, rather than obesity per se, may be responsible for these significant correlations. Immunofluorescent staining of visceral adipose tissue sections was consistent with the flow cytometry analysis (Fig. 4.3H-I); HFD-fed male mice had increased F4/80$^+$ macrophage crown-like structures (green), while HFD-fed females had

fewer F4/80$^+$ macrophages but had more detectable SiglecF$^+$ eosinophils (magenta). In contrast, eosinophils and RELMα were absent from HFD-fed RELMα KO females, which had increased F4/80$^+$ cells compared to HFD-fed WT females. These data implicate RELMα-driven eosinophils as the underlying mechanism of female-specific protection from HFD-induced obesity and adipose tissue inflammation. This hypothesis was tested next by adoptive eosinophil transfer and recombinant RELMα treatment.
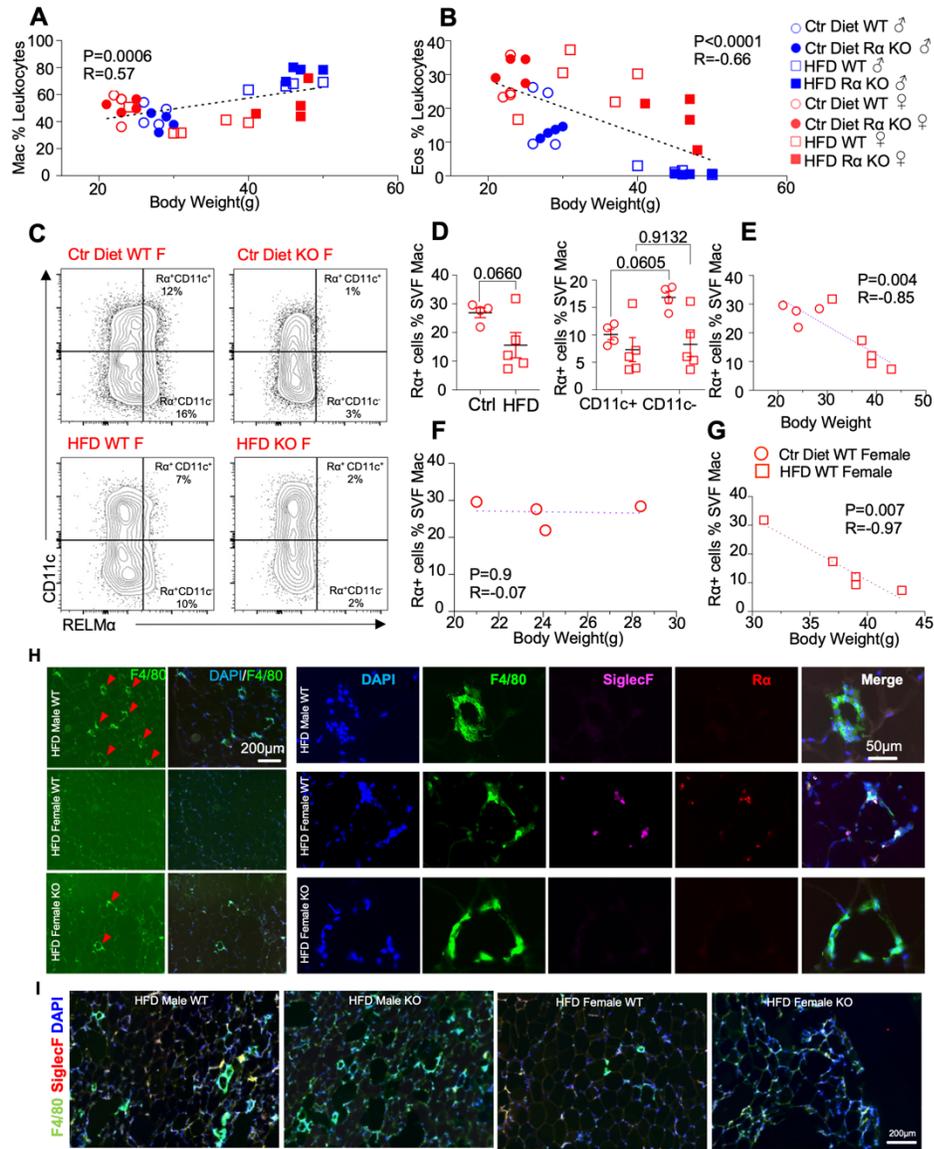
Fig 4.3 High fat diet-induced obesity is correlated with RELMα levels, eosinophils and macrophages.
(A-B) Pearson correlation analysis of adipose SVF macrophage **(A)** or eosinophil **(B)** frequency against body weight of mice from all groups. **(C)** Representative flow plots of RELMα intracellular staining against CD11c surface staining of SVF Mac from WT and KO ♀ mice. **(D)** Frequency of RELMα+ SVF Mac in Ctr and HFD WT ♀ (left) or CD11c+ and CD11c- Mac (right). **(E-G)** Pearson correlation analysis of RELMα+ cells against body weight of Ctr or HFD WT ♀ mice. **(H)** Immunofluorescent staining for F4/80 (green), SiglecF (magenta), RELMα (red) and DAPI (blue) was performed on visceral fat tissue sections (Bar, 200μM; red arrows indicate F4/80+cells). **(I)** IF staining was performed for F4/80 (green), SiglecF (red), and DAPI (blue) for all groups. Flow plots (C) and IF images (H, I) are one representative animal per group. All other data are presented as individual points for each animal, where lines represent group means +/- S.E.M. Statistical significance was determined by unpaired t test (D), or Pearson correlation analysis for other data and p values are provided. Data are representative of 2 experiments with 4-6 mice per group.

Following previously published methodologies for eosinophil adoptive transfer to protect against obesity (*31, 32*), SiglecF$^+$ eosinophils were column-purified from WT female mice that were chronically infected with helminth *Heligmosomoides polygyrus*, to increase eosinophil frequency (Fig. 4.4A). PBS or eosinophils (Eos) were intraperitoneally transferred into HFD-fed WT or RELMα KO female mice every 14 days, and weight gain monitored for 7 weeks, followed by analysis of the peritoneal and visceral adipose tissue. As an alternative approach, RELMα KO female mice were treated with recombinant RELMα with the same timeline. As expected, PBS-treated RELMα KO females gained significantly more weight than PBS-treated WT mice, however, this was rescued by either eosinophil adoptive transfer or RELMα treatment, with the KO+Eos and KO+RELMα having equivalent body weight to WT+PBS and WT+Eos (Fig. 4.4A-C). Flow cytometry analysis of the peritoneal cavity and visceral fat SVF confirmed reduced eosinophils in RELMα KO compared to WT mice, which was rescued by eosinophil transfer or recombinant RELMα treatment (Fig. 4.4D-E). Evaluation of CD11c+ M1-like macrophages in the visceral fat confirmed that RELMα KO mice had more M1-like macrophages compared to WT mice, which were significantly decreased by either eosinophil transfer or RELMα treatment (Fig. 4.4F). These data identify a RELMα-eosinophil-macrophage axis underlying female-specific protection from diet-induced obesity and inflammation; and strongly suggest that macrophage production of RELMα is necessary to promote adipose eosinophil homeostasis and inhibit M1-like macrophage activation, which is protective against HFD in females but not males.
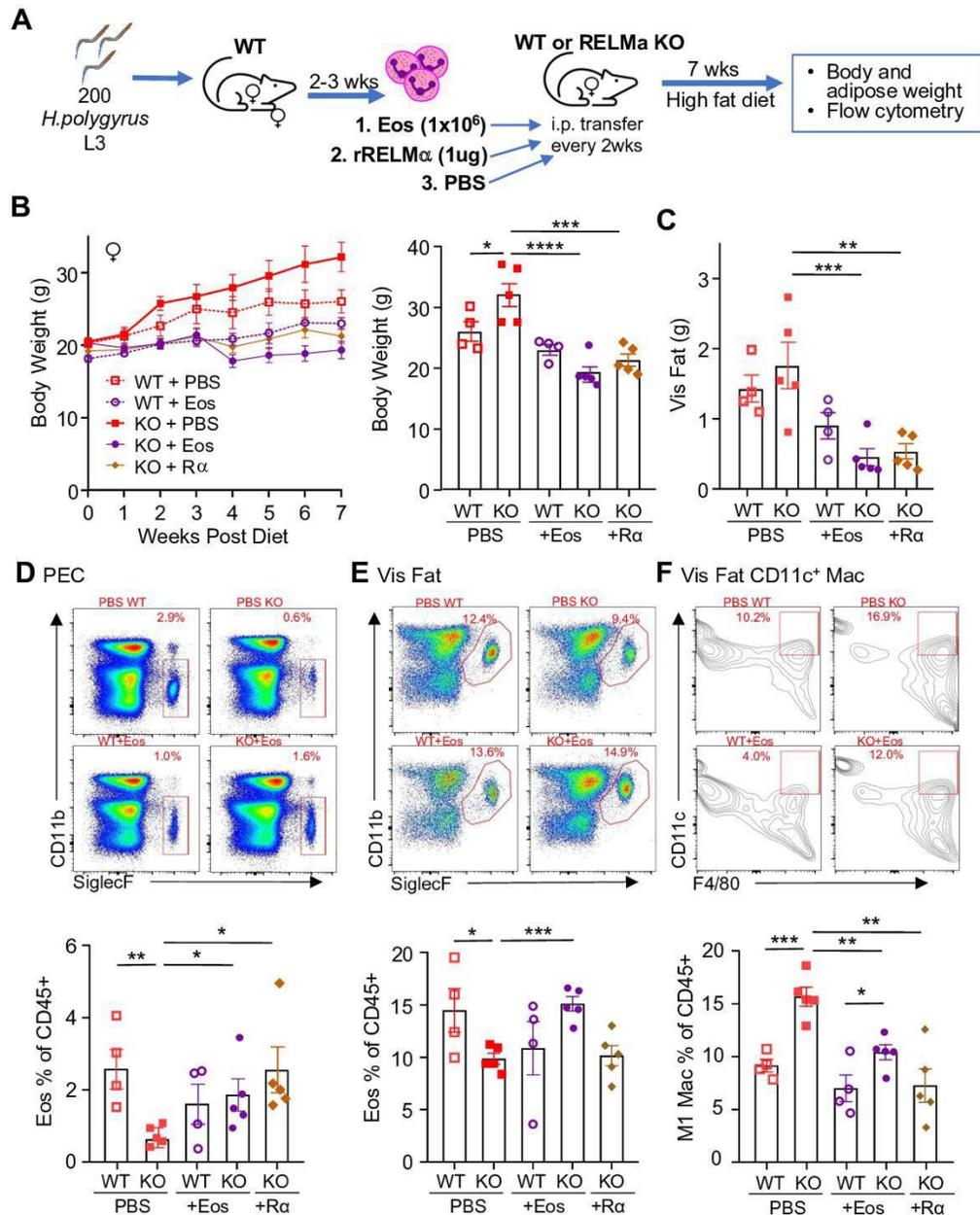
Fig 4.4 RELMα and eosinophils protect against diet-induced obesity. WT or RELMα KO female (♀) mice were exposed to HFD for 7 weeks, during which they were intraperitoneally injected every two weeks with PBS, RELMα (2μg) or SiglecF⁺ eosinophils (1x10⁶) recovered from helminth-infected WT ♀ mice (A). (B) Body weight was recorded every week. Mice were sacrificed at 7 weeks post diet, and body and visceral fat weight (C) were recorded. (D-F) Flow cytometric analysis and quantification of eosinophils from the peritoneal exudate cells (PEC) (D), visceral fat SVF (E) and quantification of the % of CD11c⁺ Macs in the visceral fat SVF (F). Data for (B) is presented as mean +/- S.E.M., flow plots for (D-F) are representative of one animal per group, all other data are presented as individual points for each animal, where lines represent group means +/- S.E.M. Statistical significance was determined by one-way ANOVA with Sidak's multiple comparisons test. (ns, no significant; *, p < 0.05; **, p<0.01; ***, p<0.001; ****, p<0.0001). Data are representative of 2 experiments with 4-6 mice per group**.**

172

4.4.4 Single cell RNA sequencing of the adipose stromal vascular fraction uncovers sex-specific and RELMα-specific heterogeneity

To identify cell-specific gene expression changes underlying RELMα-dependent and sex-dependent adipose effects, the 10x Genomics platform was used for single cell RNA-sequencing (scRNA-seq) of the visceral adipose SVF from 6-week HFD-fed WT *vs.* RELMα KO, and males *vs.* females. At 6-weeks HFD, WT females were protected from weight gain, compared to the other groups (see Fig. 4.1B), therefore this timepoint was chosen to define functionally relevant gene expression and pathway changes associated with weight gain. SVF single cell suspensions from each mouse per group were labeled with Cell Multiplexing Oligos (CMOs) to allow for pooling of biological replicates, prior to performing the single cell 3' library generation and sequencing (Fig. 4.5A). Principal component analysis of all differentially expressed genes (DEG) confirmed clustering of biological replicates by group (Fig. 4.5B). A histogram of all DEG comparisons in all clusters between sex and genotype determined that WT male *vs.* WT female had the most DEG (Supplemental Fig 4.4A). Because WT females are protected from diet-induced changes, we sought to analyze gene expression changes in all clusters in WT females compared to WT males, KO females, and KO males (Supplemental Fig 4.4B). A heatmap of the top 30 genes showed that WT females have increased expression of serine/threonine kinase and proto-oncogene *Pim3*, and of anti-apoptotic gene *Bag3*, compared to the other three groups (Supplemental Fig 4.4C). A Venn diagram of the top 100 genes in WT females compared to WT males, KO females and KO Males revealed that WT females uniquely upregulated 75 genes compared to the other three groups. The

enriched pathways in the top 75 genes that were upregulated in WT females compared to the three other groups were sex-specific (e.g. ovulation, sex differentiation, gonads, reproduction) (Supplemental Fig 4.5A-B). Non-sex specific pathways that were enriched in protected WT females included vasculogenesis and response to lipids, providing molecular hints to genes that are associated with protection from obesity and inflammation, e.g. TGFβ (Tgfb1, Tgfbr2, Tgfbr3), Th2 cytokine signaling (Il4, Il4ra, Il13) and matrix remodeling (connexins, metallopeptidases).

   The top differentially expressed genes and gene ontology (GO) pathways between males and females or WT and KO mice for all cells were examined (Fig. 4.5C-F). Comparison of WT females *vs.* WT males showed that most highly differentially expressed genes are as expected *Xist* (the X inactivation gene in females) and *Ddx3y* (unique to males, expressed on the Y chromosome). Other most highly differentially expressed genes upregulated in females include *Il4ra*, suggesting M2 macrophage responsiveness, and genes involved in extracellular matrix, such as *Spon2,* which promotes macrophage phagocytic activity (Fig. 4.5C). Males had higher levels of the sulfotransferase *Sult1e1*, and higher expression of inflammatory genes (e.g. *Lcn2*, lipocalin 2, and C7, complement 7). GO pathway analyses revealed that WT females upregulate genes in cellular responses to amyloid-beta. Compared to WT females, WT males had over-represented genes in terpenoid and isoprenoid biosynthetic pathway, which are involved in cholesterol synthesis. Comparison between KO males and KO females revealed shared sex-specific DEG compared to WT mice (Fig. 4.5D); upregulated *Xist*, *IL4ra*, and downregulated *Sult1e1* in KO females). Unique female-

specific genes that were also enriched were hemoglobin genes and oxygen binding pathways. These were upregulated in KO female mice compared to KO males. In KO males, genes involved in extracellular matrix (Collagen 4 genes) and vascularization (*Ccn2*) were over-represented.

We then evaluated the RELMα-dependent genes that were associated with the loss of protection from diet-induced obesity in KO females (Fig. 4.5E). Genes related to the negative regulation of amyloid proteins were the most enriched pathways in WT females compared to KO females, following a similar trend to the WT female *vs.* WT male comparison. The downregulation of this pathway in WT males and KO females suggest that sex and RELMα contribute to protection through this shared pathway. On the other hand, RELMα KO females compared to WT females upregulated hemoglobin genes and oxygen-binding genes. Of note, these RELMα-driven differences were unique to females since they were not identified in the comparison between WT *vs.* KO males. Instead, RELMα-regulated genes in males mapped to innate inflammatory response pathways (e.g. increased genes related to MHC Class 2, chemokine/chemokine receptor signaling in the KO males), while genes in cholesterol synthesis pathway were over-represented in WT males compared to KO males (Fig. 4.5F). Of interest, long non-coding RNA *Gm47283/ Gm21887*, located in the syntenic regions of both sex chromosomes (annotated as Gm47283 on Y chromosome, and Gm21887 on X chromosome), is the most upregulated RNA in both male and female RELMα KO mice compared to their WT counterparts (Fig. 4.5E-F; Log2 fold change of 3.3 in KO males vs Log2 fold change of 2.4 in KO females).

Together, these data suggest that female-specific genes regulated by RELMα map to non-immune but hypoxic and iron stress-related pathways (hemoglobin, oxygen binding, and ferroptosis).
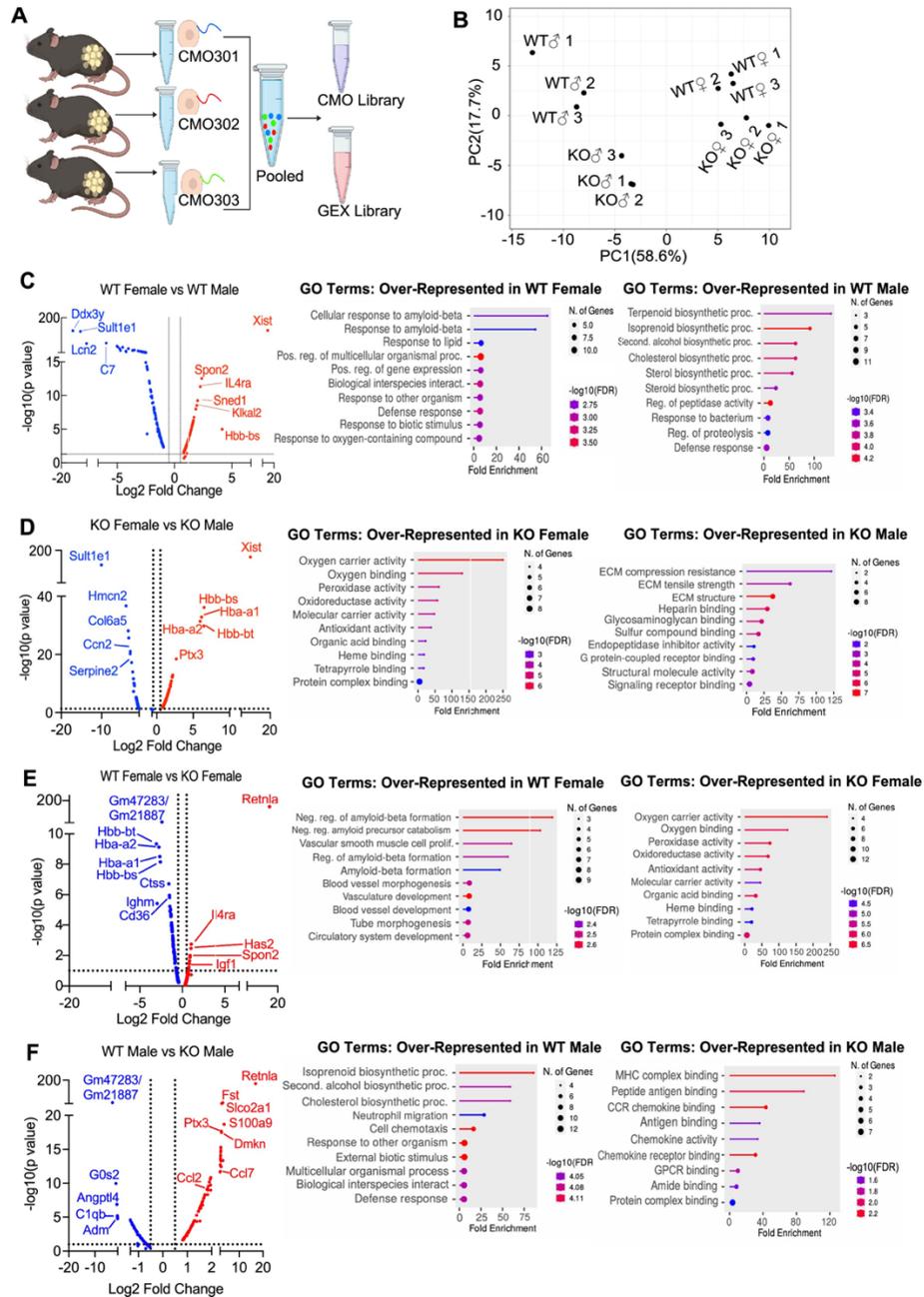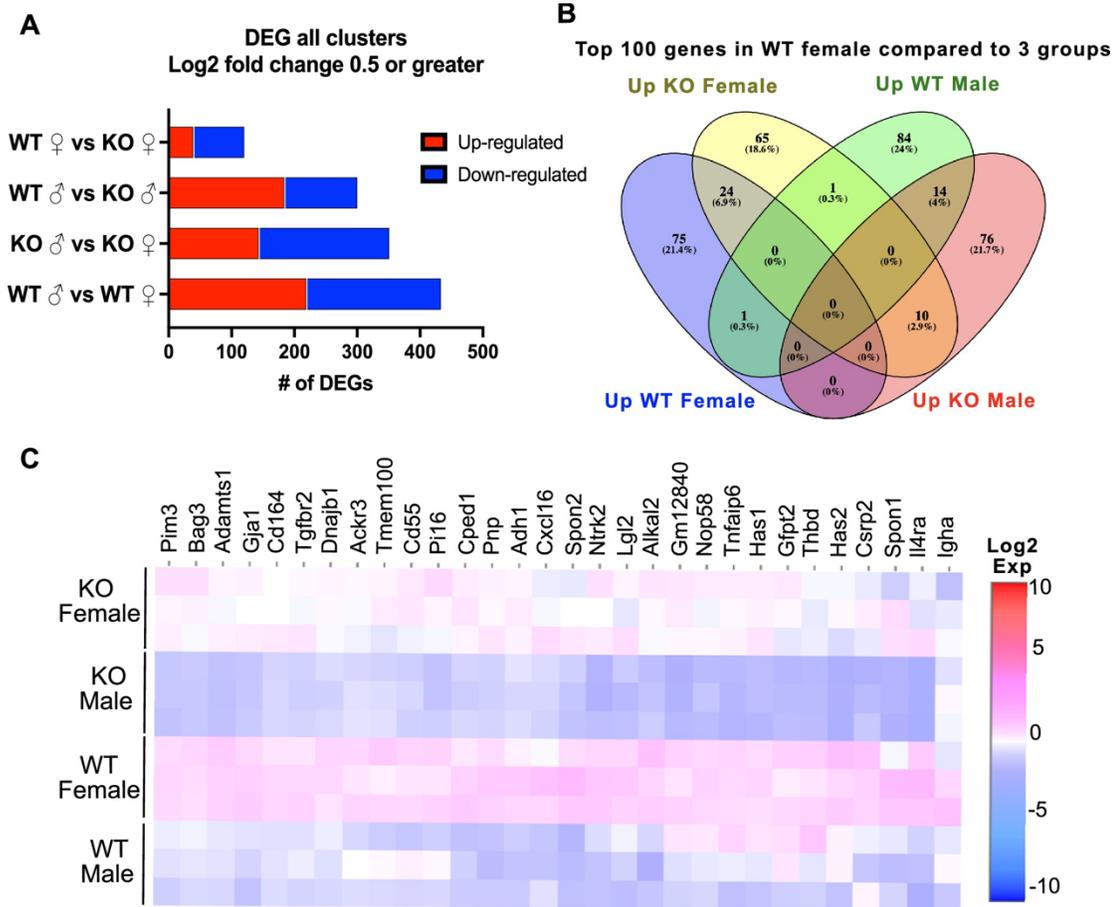
Fig 4.5 Single cell RNA-sequencing (scRNA-seq) of adipose stromal vascular fraction reveals genes associated with protection from diet-induced obesity. WT or RELMα KO male (♂) or female (♀) mice were exposed to HFD for 6 weeks, following which cells from the adipose stromal vascular fraction were recovered for single cell sequencing. **(A)** Schematic protocol of scRNA-seq cell multiplexing oligo (CMO) labeling and library preparation workflow. **(B)** Principal component analysis (PCA) assay of individual mice. Volcano plot comparing the top 100 DEGs in all clusters between: WT females and. WT males **(C)**, KO females and KO males **(D)**, WT females and KO females **(E)**, WT males and KO males **(F)**. The most significant genes (-log10(p-value) >1, Log2 Fold change >0.5) are indicated. GO terms indicating enriched pathways for the top 30 upregulated genes are plotted as histograms. Data are from 1 experiment with 3 mice per group.

Supplemental Fig 4.4 Single cell RNA-sequencing (scRNA-seq) of adipose stromal vascular fraction reveals differential gene expression between all four groups in all clusters. A) Histogram of differentially expressed gene (DEG) analysis with Log2 fold change of 0.5 or greater from all clusters comparing sex and genotype. (B) Venn diagram of the Top 100 genes in all clusters comparing WT female to KO female, WT male and KO male. (C) Heatmap of top 30 DEGs in WT female compared to all other groups in all clusters.

Supplemental Fig 4.5 Differentially expressed genes in fibroblast and ILC2 cell populations from scRNA-seq analysis. (A) Gene ontology (GO) pathways of the top 75 genes that were upregulated in WT females vs other three group in all clusters. **(B)** Pathway network analysis of the top 75 genes upregulated in WT females vs other three groups. **(C)** Population-shift in fibroblasts between WT female, WT male, KO female and KO male. **(D-L)** Differentially expressed genes in fibroblast population between WT female vs. WT male, WT female vs KO female, WT male vs KO male as associated GO terms for top DEG. **(M-P)** ILC2 cell clusters and DEG between WT females and WT males. Heatmaps indicate DEGs between WT female, WT male, KO female and KO males.

4.4.5 Cell-specific gene expression changes in fibroblasts, ILC2 and myeloid subsets correlate with sex-specific and RELMα-dependent protection against diet-induced obesity

Cell-specific gene expression changes were evaluated. Based on expression of known marker genes, twelve clusters were identified, consisting of immune and non-immune cells, displayed as tSNE plots and histograms (Fig. 4.6A-B). Eosinophils were not detected in any of the clusters. This was also shown in other SVF scRNA-seq studies, which concluded that eosinophils do not have sufficiently different transcriptomes from other leukocytes, or that there was a bias in the software, or technical difficulty such as low RNA content, or degranulation that leads to RNA degradation, which precluded eosinophil identification (*49*). At the same time as our ongoing analysis, the first publication of eosinophil single cell RNA-seq was published, using a flow cytometry-based approach rather than 10X, that included RNAse inhibitor in the sorting buffer, and prior eosinophil enrichment (*50*). We employed targeted approaches to identify eosinophil clusters according to eosinophil markers (e.g. *Siglecf, Prg2, Ccr3, Il5r*), and relaxed the scRNA-seq cutoff analysis to include more cells and intronic content, but still could not detect eosinophils (Supplemental Fig 4.3G). We concluded that eosinophils may be absent due to the enzyme digestion required for SVF isolation and processing for single cell sequencing, which could lead to specific eosinophil population loss due to low RNA content, RNases or cell viability issues. Future experiments would be needed to optimize eosinophil single cell sequencing, based on the recent publication of eosinophil single cell sequencing.

The main population in the SVF, accounting for 50-75% of cells, were non-immune cells identified as *Pdgrfa+* fibroblasts (green). They were significantly more abundant in WT females compared to the other groups (p<0.01, S2C). We investigated if any sub-cluster in the fibroblast cell population expressed pre-adipocyte marker genes (Ppara, Pparg, Foxo1, Sirt1, Cebpa and Cebpb) but no cluster-specific expression of these genes was observed (data not shown). Compared to WT males, SVF fibroblasts from WT females exhibited over-represented pathways involved in inhibition of cell proliferation and M2 macrophage responses (e.g. IL-4R, Insulin growth-like factor, IGF-R) (Supplemental Fig 4.5C-L). On the other hand, WT male fibroblasts upregulated genes involved in vasculogenesis and extracellular matrix deposition, such as collagen genes and *Ccn2,* which contributes to chondrocyte differentiation. Similar trends were observed between WT and KO females, indicating again that RELMα deficiency results in females that are more similar to males by adipose tissue gene expression. KO females had increased levels of fatty acid binding proteins, *Fabp4* and connective tissue development, *Ccn3* and *Mmp3* (Supplemental Fig 4.5G-I). In males, WT males SVF fibroblasts increased expression of prostaglandin transporter, *Slco2a1* and stromal chemokine *Cxcl12,* while KO males upregulated pathways involved in the inhibition of the antioxidative functions, resulting in the accumulation of reactive oxygen species and oxidative stress, such as *Txnip.* Innate lymphoid cell (ILC)-2 are drivers of Th2 cytokine responses and are protective in obesity (*32, 51, 52*). ILC2 were present at small frequencies in the SVF in all groups (Supplemental Fig 4.5M-P). Gene expression analysis revealed that ILC2 from WT female mice expressed significantly higher Th2

cytokines (*Il13*, *Il5*) and *Csf2*, encoding for GM-CSF, which fits the increased adipose protein levels of IL-5 and GM-CSF in females (see Fig. 4.1). Functional pathway analysis revealed that fatty acid metabolism genes were over-represented in WT females compared to males. When comparing WT and RELMα KO female mice, there was a reduction in *Csf2* in the KO females compared to WT females. These data indicate that ILC2 in females are functionally distinct from males and may contribute to the protective Th2 cytokine environment and metabolic homeostasis in the adipose tissue.

Myeloid cells/macrophages were the main immune cell subset that changed in the SVF in response to sex and RELMα deficiency; macrophage proportions were lowest in WT females, but expanded in the other groups (Fig 4.6A, orange). Gene ontology analysis revealed that the IGF pathway, chemokine and cytokine activity pathways were over-represented in WT female myeloid cells, while innate immune activation (e.g. TLR-4, RAGE receptor) and extracellular matrix remodeling were higher in WT males (Supplemental Fig 4.6A). This data matches macrophage polarization signatures where protective M2 macrophages produce and are responsive to IGF, while M1 macrophages respond to danger signals (e.g. LPS, RAGE). RELMα-dependent changes were observed in both females and males (Supplemental Fig 4.6B). Upregulated pathways in WT myeloid cells all involved innate chemokines and migration. Counterintuitively, downregulated pathways in WT compared to KO myeloid cells in females were associated with adipose tissue browning (e.g. brown fat cell differentiation, cold-induced thermogenesis), which are generally associated with protection from obesity. These data implicate RELMα in promoting innate immune cell migration and inhibiting adaptive

thermogenesis. Overall, these scRNA-seq data identify sex-specific and RELMα-dependent changes in the adipose tissue that are associated with obesity-induced inflammation. Drivers of obesity included increased macrophages and innate immune activation. On the other hand, protection from obesity involved more fibroblasts, Th2 cytokine expression by ILC2, and chemokine expression by myeloid cells.
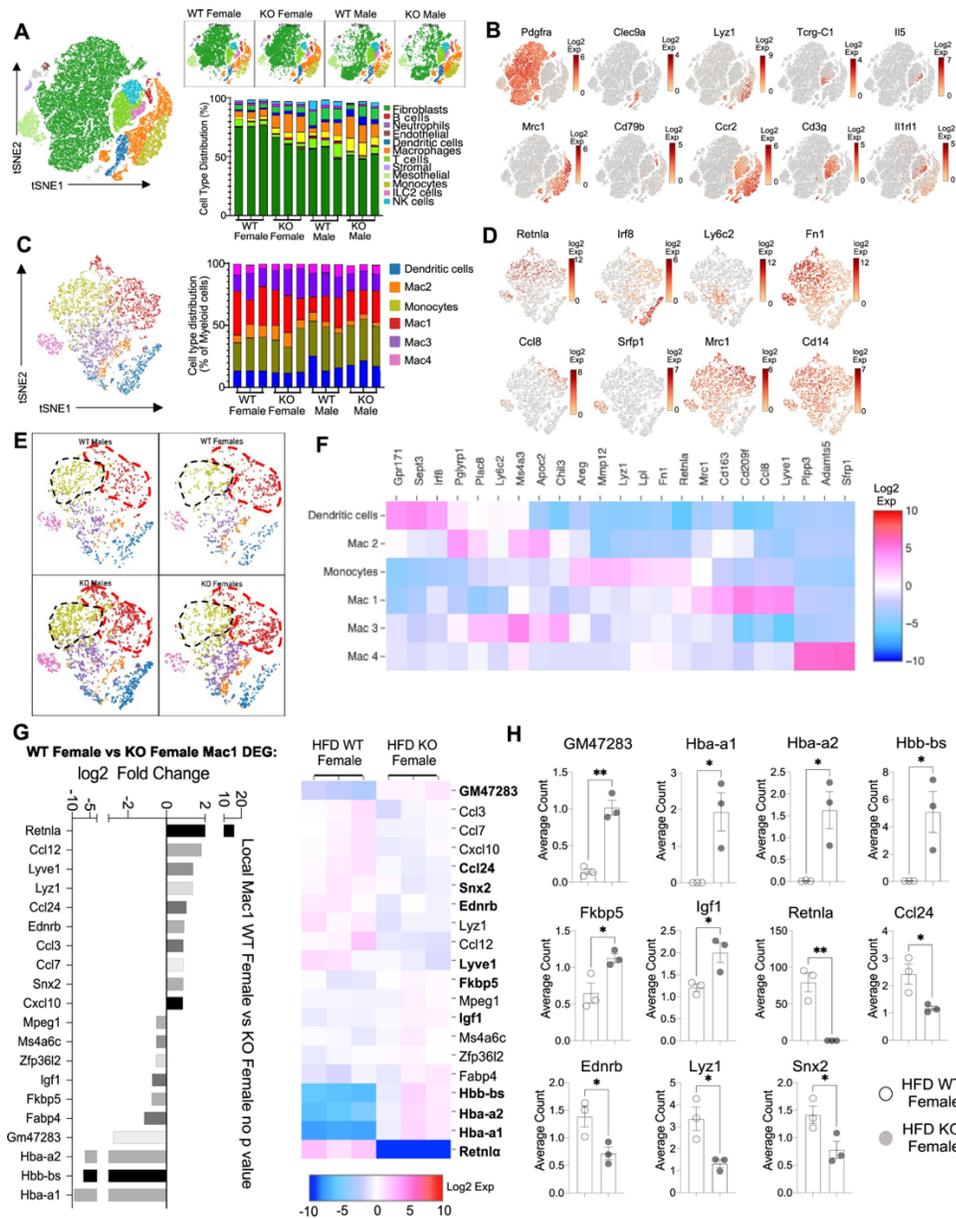
Fig 4.6 Sex-specific and RELMα-dependent gene expression changes in the SVF myeloid subsets in response to high fat diet. (A) tSNE plot showing cell populations from stromal vascular fraction (SVF) from all four groups of mice fed HFD for 6 weeks, with a histogram plotting cell type distribution per animal per group in all clusters. **(B)** Log2 fold change of candidate marker genes for each cell population across all clusters. **(C)** tSNE plot of re-clustered myeloid cell populations with a histogram plotting cell type distribution per animal per group. **(D)** Log2 fold change of candidate marker genes across myeloid cell populations. **(E)** tSNE plot highlighting population changes in Monocyte and Mac1 clusters between WT male, WT female, KO male and KO female in myeloid cells. **(F)** Heatmap of the top DEG that define each Mac subset. **(G)** WT female vs. KO female top DEG in Mac1 cluster. **(H)** Histograms of the average UMI count change of select candidate genes between WT female and KO female in Mac1 cluster. Data in **(H)** is presented as individual points for each animal, where lines represent group means +/- S.E.M. Statistical significance was determined by unpaired t-test (*, p < 0.05; **, p<0.01). Data are from 1 experiment with 3 mice per group.

184

Myeloid cells (pathway analysis for top 30 hits):
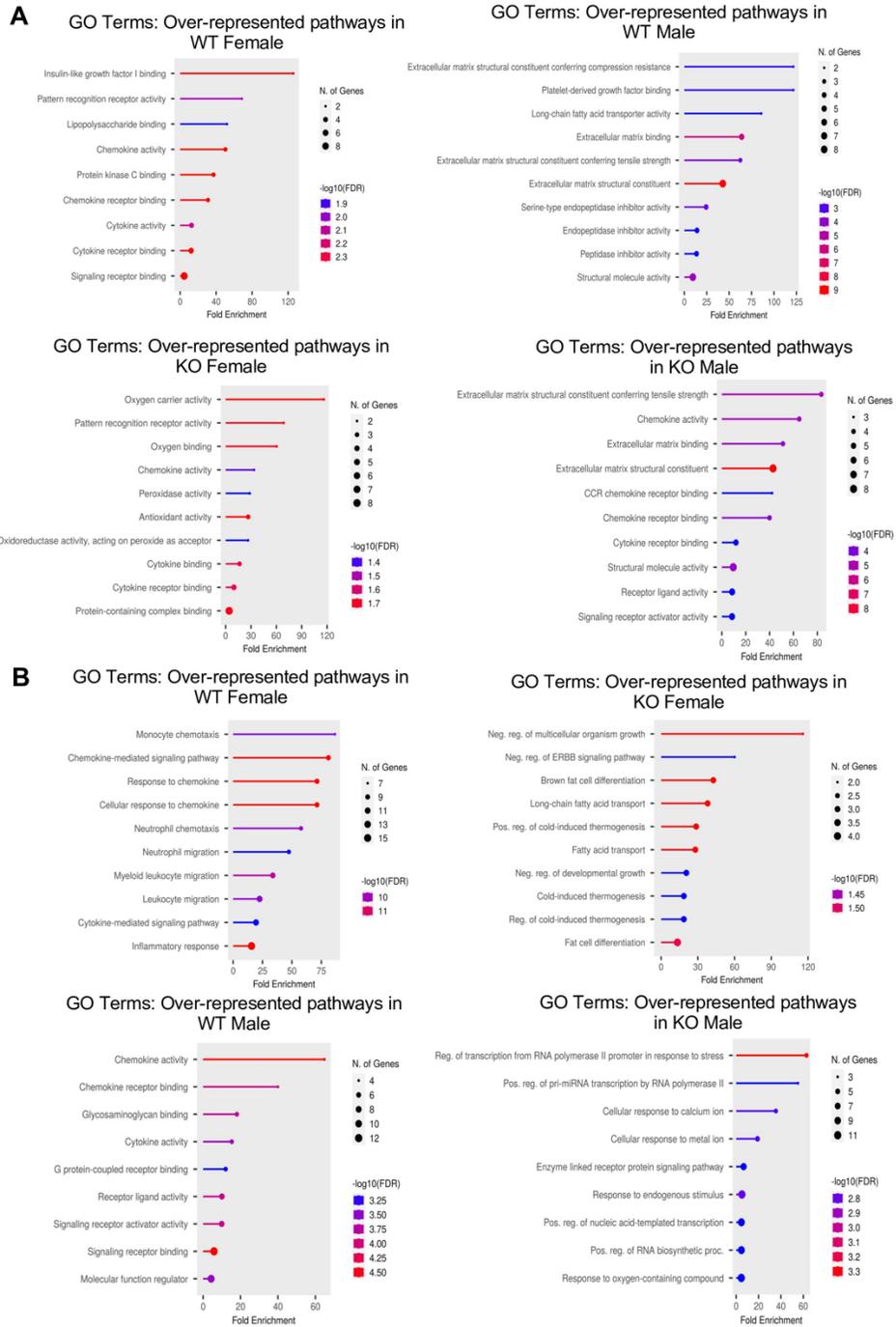
Supplemental Fig 4.6 Gene ontology pathway analysis for the top 30 hits in myeloid cell subsets.
(A) GO pathway analyses comparing the top 30 genes between WT female vs WT male, and KO female vs KO male in myeloid cell subsets. **(B)**: GO comparing the top 30 genes between WT female vs KO female and WT male vs KO male in myeloid cell subsets.

4.4.6 Monocyte to Mac1 macrophage transition and functional pathways are dysregulated in RELMα deficient mice

Based on previous studies, macrophage sub-clusters were defined and enumerated according to the Jaitin *et al.* study (*34*), and subset-specific gene expression was examined (Fig. 4.6C-D). Comparison of the genes unique to each myeloid subset *vs.* the other subsets showed that monocytes were enriched for *Lyz1*, while Mac1 were lymphatic vessel-associated macrophages expressing *Lyve1* (Fig. 4.6F). These two subsets in particular, were more abundant in WT males than WT females, and in KO males compared to KO females, but further increased in both sexes with a lack of RELMα (Fig. 4.6E, black contour, monocytes; red contour, Mac1). Determined by scRNA-seq data from WT mice, RELMα *(Retnla)* exhibited higher expression in the Mono and Mac1 clusters (Fig. 4.6D, F). We evaluated cell-intrinsic effects of RELMα on these subsets. Gene ontology analysis revealed strong enrichment for genes involved in leukocyte migration in both the Mono and Mac1 subsets from WT females, specifically eosinophil chemotaxis (Supplemental Fig 4.7A). Evaluation of the top DEG indicated similar gene expression by sex rather than genotype (Supplemental Fig 4.7B). Focused chemokine analyses identified sex and genotype-specific eosinophil-recruitment chemokines. In particular, the eosinophil-recruiting chemokine *Ccl24* was significantly reduced in Mono and Mac subsets from KO females compared to WT females. We examined the Mac1 subset in females, to identify RELMα-regulated genes within this population that typically expresses RELMα under normal conditions (Fig. 4.6G, H).
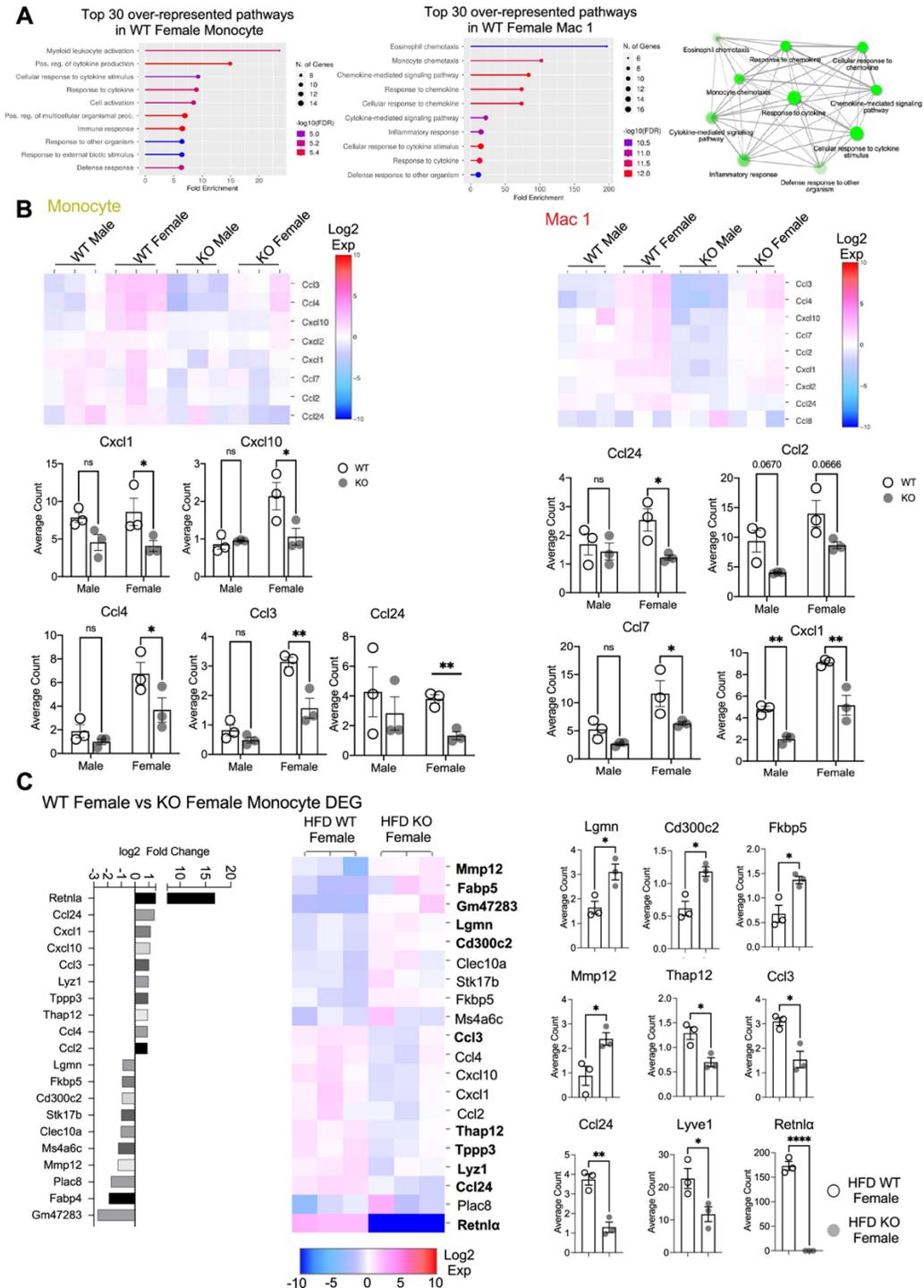
Supplemental Fig 4.7 Monocyte and Mac1 DEG (A) GO pathway analyses of top 30 DEG in WT female monocytes and Mac1 compared to other groups. **(B)** Heatmaps indicating DEGs in Monocyte and Mac1 and average UMI count analysis between all groups for key marker genes. **(C)** WT female vs KO female on HFD monocyte subcluster DEG presented as Log2 fold changes in a heatmap and average UMI count comparisons

Hemoglobin genes were the most highly upregulated genes in KO female Mac1 cells compared WT females (5-10 log2fold change). The hypoxia-induced lncRNA *Gm47283/Gm21887* was also upregulated in KO female Mac1. The hemoglobin expression was not due to red blood cell (RBC) contamination for several reasons: first, mice were perfused and then RBC lysis was performed on the single cell suspension; second, filtering was performed to remove doublets (see methods); third, single cell analysis of the myeloid subsets for an RBC-specific gene (Gypa/CD235a) showed no expression, in contrast to the hemoglobin genes, which were expressed in the KO females (Fig. 4.7A-B). To further validate that hemoglobin expression in macrophages was not tied to RBC contamination, IF staining for F4/80, hemoglobin, and RBC-specific marker Ter119, was performed on perfused adipose tissue sections from HFD-fed mice (Fig. 4.7C). Hemoglobin protein was present (magenta), especially in RELMα KO females (white arrows), and co-localized with F4/80 (green). In contrast, there was little Ter119 staining, and minimal co-localization with hemoglobin, even at higher magnification (Fig. 4.7D). Last, analysis of hemoglobin protein concentration in the adipose tissue lysates of WT and KO females was performed by ELISA and determined significantly upregulated hemoglobin protein in KO females (Fig. 4.7D). Together, these data indicate that RELMα deficiency induces hemoglobin genes in adipose tissue macrophages. Previous studies have shown that macrophages can upregulate hemoglobin genes during inflammation and hypoxia (*53, 54*). Macrophage-specific upregulation of hemoglobin protein might indicate a response to hypoxia or oxidative stress in KO female Mac1 cells.
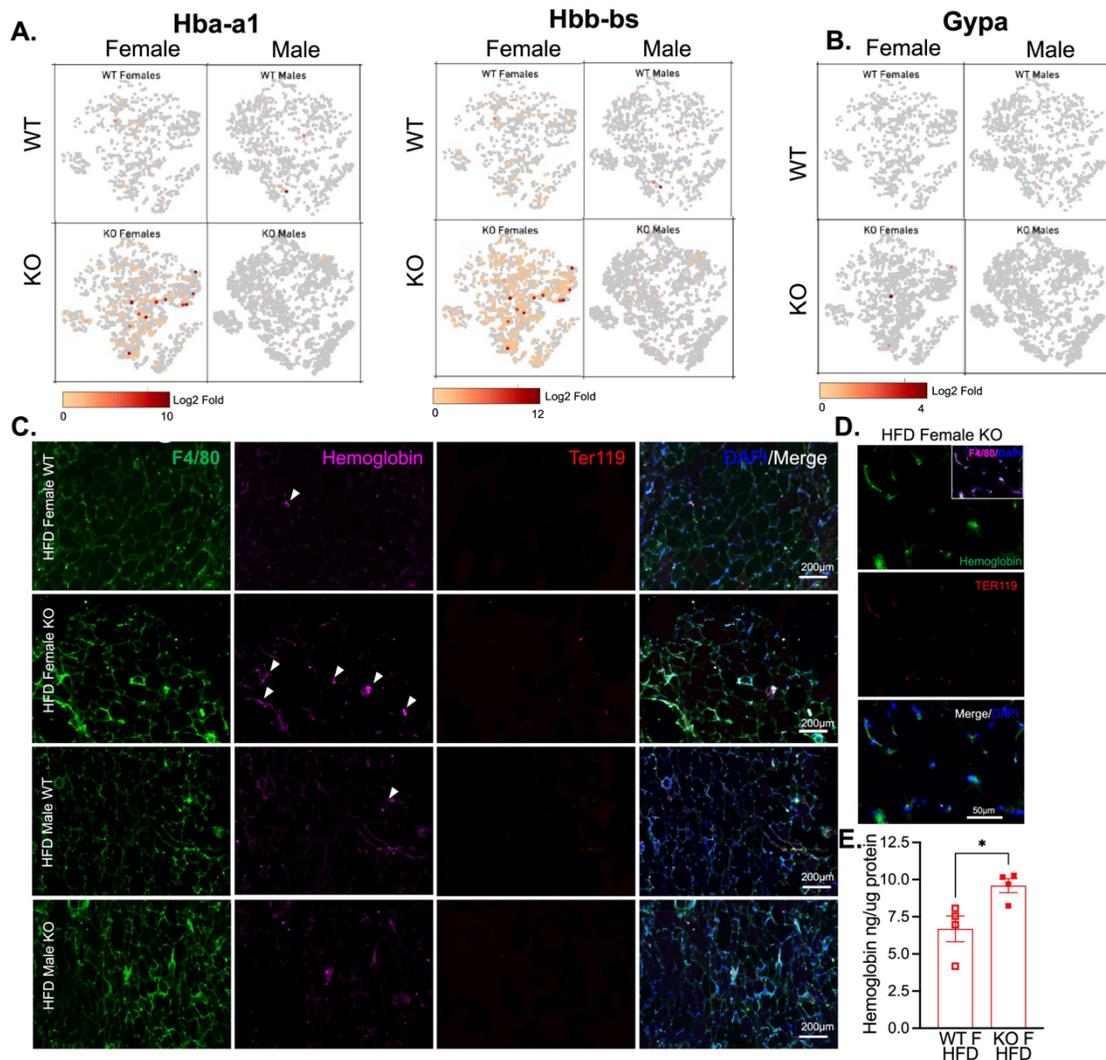
Fig 4.7 Hemoglobin expression in RELMα KO myeloid cells. (A) tSNE feature plots of Hba-a1 and Hbb-bs Log2 fold expression in myeloid clusters in WT female, KO female, WT male and KO male. **(B)** tSNE feature plot of Gypa Log2 fold expression in myeloid clusters of KO female. **(C)** Immunofluorescent staining for F4/80 (green), Hemoglobin (magenta), Ter119 (red) and DAPI (blue) was performed on visceral fat tissue sections (Bar, 200μM; arrows indicate Hemoglobin+ cells). **(D)** High magnification of HFD KO female. F4/80 (magenta,inset), Hemoglobin(green), Ter119 (red) and DAPI (blue). Bar, 50μM). **(E)** Visceral adipose tissue homogenate hemoglobin ELISA in HFD WT or KO females. Data in **(E)** is presented as individual points for each animal, where lines represent group means +/- S.E.M. Statistical significance was determined by unpaired t-test (*, $p < 0.05$; **, $p<0.01$). Data are from 1 experiment with 3-4 mice per group.

A trajectory analysis was performed to assess the relationships between the myeloid clusters, and whether they changed based on sex or genotype (Fig. 4.8A). In WT females, monocytes were the point of origin, leading to the generation of Mac1 subsets. Mac2 and Mac3 were related but separate clusters. Dendritic cells (DC) and Mac4 were even more distinct from monocytes suggesting that they are resident and not monocyte derived. These trajectories were similar in WT males. However, in KO males and females, the clusters were no longer distinct, and the Mac1 cluster was able to become Mac2/3 clusters, suggesting that loss of RELMα leads to dysregulated differentiation of monocytes to Mac1 or Mac2/3 subsets. We evaluated Mono to Mac1 transition in WT females and observed enriched pathways in IL-4 responsiveness and chemotaxis (Fig. 4.8B). In contrast, Mono to Mac1 transition in RELMα KO females involved proton transport and ATP synthesis pathways, suggesting dysregulated differentiation leading to metabolically active, inflammatory Mac1 subsets. Together, these data implicate a critical function for RELMα in myeloid cell function and differentiation in the adipose tissue. First, we uncover a RELMα cell-intrinsic mechanism whereby RELMα-expressing Mono and Mac1 cells mediate leukocyte recruitment, and Mac1 preferentially recruits eosinophils. Second, RELMα is necessary to drive functional Mac1 differentiation; in the absence of RELMα, Mac1 cells become metabolically active and increase their oxygen binding capacity by upregulating hemoglobin genes. Given that Mac1 in the normal setting are defined as the protective, vascular-associated, and anti-inflammatory subset, the loss of function of this myeloid population may be the underlying mechanism for increased inflammation in RELMα KO mice.
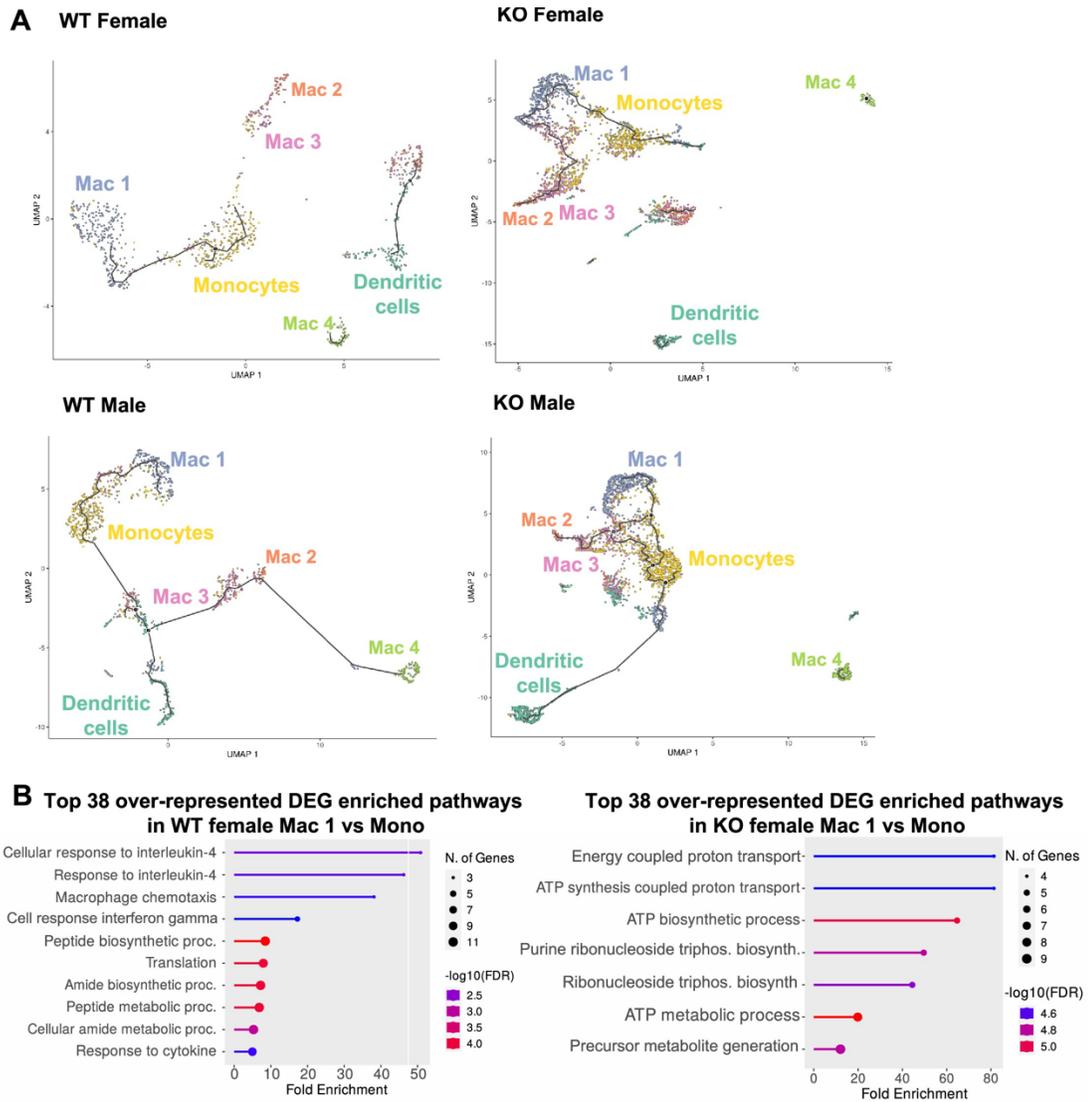
Fig 4.8 Trajectory analysis reveals dysfunctional myeloid differentiation in RELMα KO females. (A) UMAP plots of trajectory analysis with monocytes set as the root were made for the myeloid subsets within each group (WT female, WT male, KO female, and KO male fed HFD for 6 weeks). **(B)** Histogram of top 38 DEG with enriched GO terms that were upregulated in WT female Mac 1 vs. Monocyte population and KO female Mac 1 vs. Monocyte population. Data are from 1 experiment with 3 mice per group.

4.5 Discussion

The goal of this study was to investigate sex differences in obesity pathogenesis and elucidate immune mechanisms underlying female-specific protection from adipose inflammation, cardiovascular disease, and the metabolic syndrome. Herein, we uncover an eosinophil-macrophage axis in females that is driven by RELMα and protects from diet-induced obesity and inflammation. A role for RELMα in whole body metabolism has been investigated (*42, 43, 55*), but none of these studies delineated sex-specific differences in chronic obese conditions. Here, by performing side-by-side comparisons between male and female RELMα KO or WT mice we identify sex-specific and RELMα-specific immune mechanisms of obesity pathogenesis. While C57BL/6J females are protected from obesity compared to males, we show that loss of RELMα abrogates this protection. RELMα deficiency also had significant effects in males, but to a lesser extent than females. For instance, RELMα KO males had increased proportions of leukocytes and CD11c$^+$ macrophages in the stromal vascular fraction (SVF) to the same degree as exposure to high fat diet (HFD). Compared to WT females, RELMα KO females exhibited more diet-induced inflammatory changes than their male counterparts did. Under control and obese conditions, females had higher levels of RELMα than males, which likely explains why RELMα deficiency affected females more than males.

Several studies demonstrated the protective role of estrogen in obesity-mediated inflammation and in weight gain, as discussed above. Whether estrogen protection occurs via estrogen regulation of RELMα levels is a focus of our future studies. Alternatively, intrinsic sex differences in immune system have been demonstrated as well (*6, 28*) that

192

are dependent on sex chromosome complement and/or *Xist* expression (*56, 57*), and RELMα may be regulated by these as well. Additionally, ageing-mediated increase in inflammation (including of adipose tissue, recently reviewed in (*58*)), may also occur via changes in RELMα levels. Our studies used young but developmentally mature mice (4-6 weeks old when placed on diet, 18 weeks old at sacrifice), and future work on aged mice would be needed to investigate aging-mediated inflammation. Furthermore, there are sex differences in fat deposition, metabolic rates and oxidative phosphorylation (reviewed in (*59*)), and adipokine expression (*6, 21*) which regulate cytokine and chemokines levels, and therefore may regulate levels of RELMα as well. These possibilities will be addressed in future studies.

A significant strength of this study was the use of single cell sequencing to identify adipose tissue SVF heterogeneity and detect new targets and pathways to alleviate obesity. We first examined the top differentially expressed genes in protected WT females compared to the other groups and identify *Pim3* as protective. *Pim3* encodes a kinase that is a negative regulator of insulin secretion (*60*). *Pim3* is functionally responsive to forskolin, a cAMP activator that is also dietary supplement for weight loss and heart disease (*61, 62*). Our data indicate that forskolin's effectiveness through Pim3 might be sex-dependent. As the most significantly upregulated gene in the protected WT females, our data also point to cAMP activation as a promising target to alleviate diet-induced obesity. Gene ontology (GO) pathway analyses revealed that WT females upregulate genes in cellular responses to amyloid-beta. Amyloid-beta synthesis is elevated in obesity in humans (*63*). In adipose tissue, it plays a role in lipolysis and

secretion of adipokines (*64*). The increased cellular response to amyloid-beta specifically in females may explain female resistance to obesity-mediated changes. On the other hand, obese males had increased expression of *Sult1e1*, a sulfotransferase that leads to the inactivation of many hormones, including estrogen. *Sult1e1* is associated with increased BMI in humans (*65*). Males also had higher expression of inflammatory genes (e.g. *Lcn2*, lipocalin 2, and C7, complement 7). WT males also upregulated genes in terpenoid and isoprenoid biosynthetic pathway, such as *Aldh1a3*, *Fdps*, and *Hmgcs1* that regulate cholesterol synthesis, triacylglycerol absorption and fat deposition. Their association with insulin resistance and metabolic syndrome may explain the male propensity to develop these diseases (*66*).   Examination of RELMα-dependent genes within the SVF led to the discovery of lncRNA *Gm47283/Gm21887*, which is the most significantly induced RNA by RELM deficiency in both males and females. This lncRNA is located in the syntenic region of sex chromosome; *Gm47283* on Y chromosome, while 100% identical *Gm55594* and *Gm21887*, are located on the X chromosome. Very little is known about *Gm47283*, apart from one recent paper indicating it is a biomarker for myocardial infarction that is induced in hypoxia and involved in prostaglandin 2 synthesis and ferroptosis (*67*). It is also called erythroid differentiation regulator 1 (Erdr1), which may correlate increase in this lncRNA in RELMα KO with hemoglobin gene induction (*68*). Our findings indicate that RELMα potently downregulates this lncRNA, and future research is warranted to investigate whether *Gm47283/Gm21887* is a downstream effector of RELMα.

Both control and HFD-fed females had a higher proportion of eosinophils in adipose tissues than males, and furthermore, males lost their eosinophil subset after exposure to high fat diet. Correlation analyses implicated that higher RELMɑ levels in females contributed to the higher proportion of eosinophils in female adipose tissues and female protection. This protection was lost in RELMɑ KO HFD-fed females, associated with the loss of eosinophils. Eosinophil transfer and RELMɑ treatment experiments confirmed this mechanistic link whereby RELMɑ recruits eosinophils with the overall outcome of reduced weight gain, decreased adipose tissue inflammation, and decreased CD11c$^+$ proinflammatory macrophages. These findings support the potential for RELMɑ treatment in males to protect from obesity-mediated inflammation by driving eosinophils. A critical function for eosinophils in establishing a Th2 cytokine environment in the adipose tissue has been reported (*31, 69*). Specifically, through use of eosinophil-deficient mice or transgenic mice that have increased eosinophils, these studies demonstrate that eosinophils produce IL-4 to promote M2 macrophages, which in turn mediate adipose tissue beiging and other protective pathways against obesity. In the context of helminths, studies also identified eosinophils as the underlying mechanism whereby helminth infection protects from obesity. Our studies uncover further complexity to eosinophil function by demonstrating that females have significantly increased adipose eosinophils, and that eosinophilia is critically dependent on RELMɑ. Since females do not gain weight compared to males, investigation of female-specific pathways in murine models of obesity is an understudied area. However, there is an urgent need to determine what mechanisms are protective in females and whether these

195

change with age or menopause. These would allow the identification of new therapeutic targets and will also distinguish whether treatments may differ in their effectiveness according to sex. Our findings open a new area of investigation into RELM proteins, which are produced in humans, and whether they regulate eosinophils to protect from obesity. Another study investigated whether IL-5-induced eosinophils could protect obese male mice from metabolic impairments but reported no protective effects (*70*). They concluded that physiological levels of eosinophils are not protective, in contrast to the previous studies that used transgenic mice to delete or artificially expand eosinophils. By additionally examining female mice and performing adoptive eosinophil transfer, our findings support a protective function for eosinophils even at physiologic levels, but also identify eosinophil heterogeneity. tSNE plot flow cytometric analysis of adipose SVF cells indicated that eosinophils were heterogeneous and different in females compared to males. These included changes in surface expression of CXCR4 and MHCII with HFD in females but not in males. In addition, single cell sequencing analyses of the adipose SVF indicated striking sex-specific or RELMα-specific changes in multiple eosinophil chemoattractants such as IL-5, produced by ILC2, and myeloid cell-derived eotaxin-2 (CCL24) and CXCL10. Eotaxin-2 was produced by myeloid cells in the SVF female WT mice but was significantly decreased with the loss of RELMα. Our data implicates female-specific and RELMα-dependent immune mechanisms in the adipose environment, whereby ILC2 and myeloid cells recruit eosinophils that function to downregulate obesity-induced inflammation.

Myeloid cells are critical for adipose tissue homeostasis, and monocyte recruitment and differentiation to proinflammatory macrophages are associated with obesity. Strikingly, RELMα deletion led to induction of hemoglobin genes in SVF female KO mice compared to WT females and KO male mice. This may have significant health implications. The importance of hemoglobin in erythrocytes is well accepted, but the presence of hemoglobin in non-erythroid cells is less well known with limited studies. Hemoglobin gene induction was first detected in RAW264 and isolated peritoneal macrophages (*53*). Alternatively, hemoglobin genes can be induced by iron-recycling macrophages, derived from Ly6c$^+$ monocytes during hemolysis, after erythrophagocytosis. Hemoglobin synthesis in cells other than erythroid lineage occurs in hypoxic conditions to increase oxygen binding and compensate for low oxygen (*71*). Therefore, it is possible that the lack of RELMα in females leads to hypoxia in adipose tissues. Alternatively, hemoglobin may be induced in KO females in response to macrophage activation and nitric oxide (NO) production, since hemoglobin can bind NO in addition to oxygen (*72*), which is produced by activated macrophages (*73*). Induction of hemoglobin genes may lead to dysregulation in iron handling and anemia, which have been associated with obesity. While obesity-increased incidence of anemia is not conclusive, iron deficiency is correlated with obesity (*74*). Macrophages normally recycle iron, but lack of RELMα in obese females may have disrupted this ability. Increase in hemoglobin gene expression may lead to iron sequestration and would explain iron deficiency that is observed in obesity especially in women. Hemoglobin components include heme and iron, which can be cytotoxic. Overexpression of hemoglobin genes in

197

the RELMα myeloid cells may not only act as a sink to deplete iron, oxygen and heme with consequences for the SVF environment, but could also constitute cytotoxic stress for the myeloid cells themselves, in a positive feedback cycle spurring further adipose dysfunction. To our knowledge, this is the first evidence of a hemoglobin pathway in myeloid cells during metabolic dysfunction and may point to new therapeutic targets and biomarkers for adipose tissue inflammation and obesity pathogenesis.

RELMα function in peritoneal macrophages was previously demonstrated to be sexually dimorphic, where peritoneal macrophage replenishment from the bone marrow is lower in females, and macrophage differentiation in females, but not males, is RELMα-dependent (*41, 75*). Our data further reveal that RELMα expression is sex-dependent and has critical functions in the adipose tissue through macrophage and eosinophil-driven mechanisms. We also demonstrate RELMα-specific effects on monocyte to macrophage transition in the adipose tissue that occur in both males and females. Whether these effects may be influenced by sex-specific differences in myeloid cell ontogeny from the bone marrow is unclear and an important avenue for future research. The importance of monocyte expression of RELMα for survival and differentiation has recently been reported (*40*). Trajectory analysis of the myeloid subsets revealed that WT animals of both sexes followed expected trajectories of monocyte differentiation to either Mac1 or to Mac2/3 clusters. Mac2/3 clusters express markers of proinflammatory macrophages, such as Ly6c, while Mac1 expresses markers of anti-inflammatory macrophages, such as *Mrc1* (CD206). The lack of RELMα in KO animals of both sexes led to dysregulated monocyte differentiation, where the 'protective' Mac1 cluster could become Mac2/3 cells. This

trajectory change implies that lack of RELMα disrupts myeloid differentiation leading to a more proinflammatory profile. Genes enriched in monocyte to Mac1 transition in WT vs. RELMα KO female mice were examined to determine cell-intrinsic functions for RELMα. These analyses revealed that RELMα expression is critical for monocyte differentiation into IL-4 responsive macrophages, but in its absence, monocytes begin to increase expression of genes associated with high metabolic activity, which could result in oxidative stress.

In conclusion, these studies demonstrate a previously unrecognized role for RELMα in modulating metabolic and inflammatory responses during diet-induced obesity that is sex-dependent. Results from these studies highlight a critical RELMα-eosinophil-macrophage axis that functions in females to protect from diet-induced obesity and inflammation. Promoting these pathways could provide novel therapies for obesity pathology.

References for Chapter Four

1.   H. The Lancet Public, Tackling obesity seriously: the time has come. *The Lancet. Public health* **3**, e153 (2018).

2.   J. C. Link, K. Reue, Genetic Basis for Sex Differences in Obesity and Lipid Metabolism. *Annual review of nutrition* **37**, 225-245 (2017).

3.   E. Gerdts, V. Regitz-Zagrosek, Sex differences in cardiometabolic disorders. *Nature medicine* **25**, 1657-1666 (2019).

4.   B. W. Parks *et al.*, Genetic architecture of insulin resistance in the mouse. *Cell metabolism* **21**, 334-347 (2015).

5.   J. P. Camporez *et al.*, Anti-inflammatory effects of oestrogen mediate the sexual dimorphic response to lipid-induced insulin resistance. *The Journal of physiology* **597**, 3885-3903 (2019).

6.   K. E. Chen, N. M. Lainez, D. Coss, Sex Differences in Macrophage Responses to Obesity-Mediated Changes Determine Migratory and Inflammatory Traits. *Journal of immunology* **206**, 141-153 (2021).

7.   N. M. Lainez *et al.*, Diet-Induced Obesity Elicits Macrophage Infiltration and Reduction in Spine Density in the Hypothalami of Male but Not Female Mice. *Frontiers in immunology* **9**, 1992 (2018).

8.   B. F. Palmer, D. J. Clegg, The sexual dimorphism of obesity. *Mol Cell Endocrinol* **402**, 113-119 (2015).

9.   B. L. Wajchenberg, Subcutaneous and visceral adipose tissue: their relation to the metabolic syndrome. *Endocrine reviews* **21**, 697-738 (2000).

10.   S. P. Weisberg *et al.*, Obesity is associated with macrophage accumulation in adipose tissue. *The Journal of clinical investigation* **112**, 1796-1808 (2003).

11.   C. A. Curat *et al.*, Macrophages in human visceral adipose tissue: increased accumulation in obesity and a source of resistin and visfatin. *Diabetologia* **49**, 744-747 (2006).

12.   J. M. Olefsky, C. K. Glass, Macrophages, inflammation, and insulin resistance. *Annu Rev Physiol* **72**, 219-246 (2010).

13.   M. L. Gruen, M. Hao, D. W. Piston, A. H. Hasty, Leptin requires canonical migratory signaling pathways for induction of monocyte and macrophage

chemotaxis. *American Journal of Physiology-Cell Physiology* **293**, C1481-C1488 (2007).

14.   H. Kanda *et al.*, MCP-1 contributes to macrophage infiltration into adipose tissue, insulin resistance, and hepatic steatosis in obesity. *The Journal of clinical investigation* **116**, 1494-1505 (2006).

15.   J. L. Kaplan *et al.*, Adipocyte progenitor cells initiate monocyte chemoattractant protein-1-mediated macrophage accumulation in visceral adipose tissue. *Molecular metabolism* **4**, 779-794 (2015).

16.   D. E. Lackey, J. M. Olefsky, Regulation of metabolism by the innate immune system. *Nat Rev Endocrinol* **12**, 15-28 (2016).

17.   J. C. McNelis, J. M. Olefsky, Macrophages, immunity, and metabolic disease. *Immunity* **41**, 36-48 (2014).

18.   S. T. Gal-Oz *et al.*, ImmGen report: sexual dimorphism in the immune system transcriptome. *Nat Commun* **10**, 4295 (2019).

19.   M. Varghese *et al.*, Monocyte Trafficking and Polarization Contribute to Sex Differences in Meta-Inflammation. *Frontiers in endocrinology* **13**, 826320 (2022).

20.   K. J. Strissel *et al.*, Adipocyte death, adipose tissue remodeling, and obesity complications. *Diabetes* **56**, 2910-2918 (2007).

21.   K. E. Chen, N. M. Lainez, M. G. Nair, D. Coss, Visceral adipose tissue imparts peripheral macrophage influx into the hypothalamus. *Journal of neuroinflammation* **18**, 140 (2021).

22.   A. Keselman, X. Fang, P. B. White, N. M. Heller, Estrogen Signaling Contributes to Sex Differences in Macrophage Polarization during Asthma. *Journal of immunology* **199**, 1573-1583 (2017).

23.   K. L. Grove, S. K. Fried, A. S. Greenberg, X. Q. Xiao, D. J. Clegg, A microarray analysis of sexual dimorphism of adipose tissues in high-fat-diet-induced obese mice. *International journal of obesity (2005)* **34**, 989-1000 (2010).

24.   R. E. Stubbins, V. B. Holcomb, J. Hong, N. P. Nunez, Estrogen modulates abdominal adiposity and protects female mice from obesity and impaired glucose tolerance. *European journal of nutrition* **51**, 861-870 (2012).

25. E. L. Sullivan, A. J. Daniels, F. H. Koegler, J. L. Cameron, Evidence in female rhesus monkeys (Macaca mulatta) that nighttime caloric intake is not associated with weight gain. *Obesity research* **13**, 2072-2080 (2005).

26. P. A. Heine, J. A. Taylor, G. A. Iwamoto, D. B. Lubahn, P. S. Cooke, Increased adipose tissue in male and female estrogen receptor-alpha knockout mice. *Proceedings of the National Academy of Sciences of the United States of America* **97**, 12729-12734 (2000).

27. B. B. Shenoda *et al.*, Xist attenuates acute inflammatory response by female cells. *Cellular and molecular life sciences : CMLS*, (2020).

28. K. Singer *et al.*, Differences in Hematopoietic Stem Cells Contribute to Sexually Dimorphic Inflammatory Responses to High Fat Diet-induced Obesity. *The Journal of biological chemistry* **290**, 13250-13262 (2015).

29. S. Chakarov, C. Blériot, F. Ginhoux, Role of adipose tissue macrophages in obesity-related disorders. *The Journal of experimental medicine* **219**, (2022).

30. M. Kratz *et al.*, Metabolic Dysfunction Drives a Mechanistically Distinct Proinflammatory Phenotype in Adipose Tissue Macrophages. *Cell metabolism* **20**, 614-625 (2014).

31. D. Wu *et al.*, Eosinophils sustain adipose alternatively activated macrophages associated with glucose homeostasis. *Science* **332**, 243-247 (2011).

32. J. R. Brestoff *et al.*, Group 2 innate lymphoid cells promote beiging of white adipose tissue and limit obesity. *Nature* **519**, 242-246 (2015).

33. D. A. Hill *et al.*, Distinct macrophage populations direct inflammatory versus physiological changes in adipose tissue. *Proceedings of the National Academy of Sciences* **115**, E5096-E5105 (2018).

34. D. A. Jaitin *et al.*, Lipid-Associated Macrophages Control Metabolic Homeostasis in a Trem2-Dependent Manner. *Cell* **178**, 686-698.e614 (2019).

35. G. M. Pine, H. M. Batugedara, M. G. Nair, Here, there and everywhere: Resistin-like molecules in infection, inflammation, and metabolic disorders. *Cytokine* **110**, 442-451 (2018).

36. M. Lv, W. Liu, Hypoxia-Induced Mitogenic Factor: A Multifunctional Protein Involved in Health and Disease. *Frontiers in cell and developmental biology* **9**, 691774 (2021).

37. J. Li, S. Y. Kim, N. M. Lainez, D. Coss, M. G. Nair, Macrophage-Regulatory T Cell Interactions Promote Type 2 Immune Homeostasis Through Resistin-Like Molecule α. *Frontiers in immunology* **12**, 710406 (2021).

38. T. A. Harris *et al.*, Resistin-like Molecule α Provides Vitamin-A-Dependent Antimicrobial Protection in the Skin. *Cell host & microbe* **25**, 777-788.e778 (2019).

39. B. Krljanac *et al.*, RELMα-expressing macrophages protect against fatal lung damage and reduce parasite burden during helminth infection. *Science immunology* **4**, (2019).

40. D. E. Sanin *et al.*, A common framework of monocyte-derived macrophage activation. *Science immunology* **7**, eabl7482 (2022).

41. C. C. Bain *et al.*, CD11c identifies microbiota and EGR2-dependent MHCII(+) serous cavity macrophages with sexually dimorphic fate in mice. *European journal of immunology* **52**, 1243-1257 (2022).

42. Y. Kumamoto *et al.*, CD301b(+) Mononuclear Phagocytes Maintain Positive Energy Balance through Secretion of Resistin-like Molecule Alpha. *Immunity* **45**, 583-596 (2016).

43. M. R. Lee *et al.*, The adipokine Retnla modulates cholesterol homeostasis in hyperlipidemic mice. *Nat Commun* **5**, 4410 (2014).

44. A. E. Salinero, B. M. Anderson, K. L. Zuloaga, Sex differences in the metabolic effects of diet-induced obesity vary by age of onset. *International journal of obesity (2005)* **42**, 1088-1091 (2018).

45. R. Willebrand, D. Voehringer, IL-33-Induced Cytokine Secretion and Survival of Mouse Eosinophils Is Promoted by Autocrine GM-CSF. *PLoS One* **11**, e0163751 (2016).

46. S. Westermann *et al.*, Siglec-F Promotes IL-33-Induced Cytokine Release from Bone Marrow-Derived Eosinophils Independently of the ITIM and ITIM-like Motif Phosphorylation. *Journal of immunology* **208**, 732-744 (2022).

47. M. Zhang *et al.*, Defining the in vivo function of Siglec-F, a CD33-related Siglec expressed on mouse eosinophils. *Blood* **109**, 4280-4287 (2007).

48. F. Chen *et al.*, B Cells Produce the Tissue-Protective Protein RELMα during Helminth Infection, which Inhibits IL-17 Expression and Limits Emphysema. *Cell Rep* **25**, 2775-2783.e2773 (2018).

49. A. Weinstock, H. Moura Silva, K. J. Moore, A. M. Schmidt, E. A. Fisher, Leukocyte Heterogeneity in Adipose Tissue, Including in Obesity. *Circulation research* **126**, 1590-1612 (2020).

50. A. Gurtner *et al.*, Active eosinophils regulate host defence and immune responses in colitis. *Nature* **615**, 151-157 (2023).

51. M. Ikutani, S. Nakae, Heterogeneity of Group 2 Innate Lymphoid Cells Defines Their Pleiotropic Roles in Cancer, Obesity, and Cardiovascular Diseases. *Frontiers in immunology* **13**, 939378 (2022).

52. M. W. Lee *et al.*, Activated type 2 innate lymphoid cells regulate beige fat biogenesis. *Cell* **160**, 74-87 (2015).

53. L. Liu, M. Zeng, J. S. Stamler, Hemoglobin induction in mouse macrophages. *Proceedings of the National Academy of Sciences of the United States of America* **96**, 6643-6647 (1999).

54. D. Saha *et al.*, Hemoglobin Expression in Nonerythroid Cells: Novel or Ubiquitous? *International Journal of Inflammation* **2014**, 803237 (2014).

55. A. Munitz *et al.*, Resistin-like molecule alpha decreases glucose tolerance during intestinal inflammation. *Journal of immunology* **182**, 2357-2363 (2009).

56. C. M. Syrett *et al.*, Diversity of Epigenetic Features of the Inactive X-Chromosome in NK Cells, Dendritic Cells, and Macrophages. *Frontiers in immunology* **9**, 3087 (2018).

57. S. Pyfrom *et al.*, The dynamic epigenetic regulation of the inactive X chromosome in healthy human B cells is dysregulated in lupus patients. *Proceedings of the National Academy of Sciences of the United States of America* **118**, (2021).

58. Y. X. Zhang *et al.*, Adipose tissue aging is regulated by an altered immune system. *Frontiers in immunology* **14**, 1125395 (2023).

59. F. Mauvais-Jarvis, Sex differences in metabolic homeostasis, diabetes, and obesity. *Biology of Sex Differences* **6**, 14 (2015).

60. G. Vlacich, M. C. Nawijn, G. C. Webb, D. F. Steiner, Pim3 negatively regulates glucose-stimulated insulin secretion. *Islets* **2**, 308-317 (2010).

61. M. P. Godard, B. A. Johnson, S. R. Richmond, Body composition and hormonal adaptations associated with forskolin consumption in overweight and obese men. *Obesity research* **13**, 1335-1343 (2005).

62. N. Mukaida, Y. Y. Wang, Y. Y. Li, Roles of Pim-3, a novel survival kinase, in tumorigenesis. *Cancer science* **102**, 1437-1442 (2011).

63. W. G. Tharp *et al.*, Effects of glucose and insulin on secretion of amyloid-β by human adipose tissue cells. *Obesity (Silver Spring, Md.)* **24**, 1471-1479 (2016).

64. Z. Wan, D. Mah, S. Simtchouk, A. Kluftinger, J. P. Little, Role of amyloid β in the induction of lipolysis and secretion of adipokines from human adipose tissue. *Adipocyte* **4**, 212-216 (2015).

65. C. A. Ihunnah *et al.*, Estrogen sulfotransferase/SULT1E1 promotes human adipogenesis. *Molecular and cellular biology* **34**, 1682-1694 (2014).

66. J. M. Castellano, J. M. Espinosa, J. S. Perona, Modulation of Lipid Transport and Adipose Tissue Deposition by Small Lipophilic Compounds. *Frontiers in cell and developmental biology* **8**, (2020).

67. F. Gao *et al.*, Suppression of lncRNA Gm47283 attenuates myocardial infarction via miR-706/ Ptgs2/ferroptosis axis. *Bioengineered* **13**, 10786-10802 (2022).

68. Y. K. Houh, K. E. Kim, H. J. Park, D. Cho, Roles of Erythroid Differentiation Regulator 1 (Erdr1) on Inflammatory Skin Diseases. *International journal of molecular sciences* **17**, (2016).

69. Y. Qiu *et al.*, Eosinophils and type 2 cytokine signaling in macrophages orchestrate development of functional beige fat. *Cell* **157**, 1292-1308 (2014).

70. W. R. Bolus *et al.*, Elevating adipose eosinophils in obese mice to physiologically normal levels does not rescue metabolic impairments. *Molecular metabolism* **8**, 86-95 (2018).

71. C. L. Grek, D. A. Newton, D. D. Spyropoulos, J. E. Baatz, Hypoxia up-regulates expression of hemoglobin in alveolar epithelial cells. *American journal of respiratory cell and molecular biology* **44**, 439-447 (2011).

72. D. A. Gell, Structure and function of haemoglobins. *Blood cells, molecules & diseases* **70**, 13-42 (2018).

73. M. Orecchioni, Y. Ghosheh, A. B. Pramod, K. Ley, Macrophage Polarization: Different Gene Signatures in M1(LPS+) vs. Classically and M2(LPS-) vs. Alternatively Activated Macrophages. *Frontiers in immunology* **10**, 1084 (2019).

74. A. C. Cepeda-Lopez, K. Baye, Obesity, iron deficiency and anaemia: a complex relationship. *Public Health Nutrition* **23**, 1703-1704 (2020).

75. C. C. Bain *et al.*, Rate of replenishment and microenvironment contribute to the sexually dimorphic phenotype and function of peritoneal macrophages. *Science immunology* **5**, (2020).

76. A. Ariyaratne *et al.*, Trickle infection with Heligmosomoides polygyrus results in decreased worm burdens but increased intestinal inflammation and scarring. *Frontiers in immunology* **13**, 1020056 (2022).

77. D. Yu, W. Huber, O. Vitek, Shrinkage estimation of dispersion in Negative Binomial models for RNA-seq experiments with small sample size. *Bioinformatics (Oxford, England)* **29**, 1275-1282 (2013).

78. S. X. Ge, D. Jung, R. Yao, ShinyGO: a graphical gene-set enrichment tool for animals and plants. *Bioinformatics (Oxford, England)* **36**, 2628-2629 (2020).

79. T. Stuart *et al.*, Comprehensive Integration of Single-Cell Data. *Cell* **177**, 1888-1902.e1821 (2019).

80. J. Cao *et al.*, The single-cell transcriptional landscape of mammalian organogenesis. *Nature* **566**, 496-502 (2019).

81. X. Qiu *et al.*, Reversed graph embedding resolves complex single-cell trajectories. *Nature methods* **14**, 979-982 (2017).

82. L. Haghverdi, A. T. L. Lun, M. D. Morgan, J. C. Marioni, Batch effects in single-cell RNA-sequencing data are corrected by matching mutual nearest neighbors. *Nature biotechnology* **36**, 421-427 (2018).

83. C. Trapnell *et al.*, The dynamics and regulators of cell fate decisions are revealed by pseudotemporal ordering of single cells. *Nature biotechnology* **32**, 381-386 (2014).

CHAPTER FIVE:

Conclusions and future directions

The work in this dissertation identified new genetic and environmental targets and mechanisms in hypothalamic function and pituitary gland homeostasis in obesity. In addition, this work also demonstrated a role for RELMα in modulating metabolic and inflammatory responses during diet-induced obesity that is protective for females. In chapter two, using a mouse model for Fragile X Syndrome (FXS), my work determined that male Fmr1 KO mice, but not female mice, exhibited increased body weight when compared to wild-type controls, similarly to humans with FMR1 mutations. This increase in body weight was due to decreased olfactory-induced food foraging behavior. Fmr1 KO male mice had decreased locomotor activity in their dark cycle, which is their active circadian phase. Male KO mice had olfactory dysfunction determined by buried food test, and since olfactory regions communicate with hypothalamic regions that regulate energy homeostasis and POMC neurons regulate locomotion, we examined POMC neuron innervation, neuronal number and activity. We determined that POMC neurons in male KO mice had increased inhibitory innervation, lower neuronal activity based on cFOS expression, and decreased neuronal number in the rostral arcuate nucleus (ARC), compared to controls. These results suggest that Fmr1 gene is critical in POMC neuronal function and regulation of locomotion and suggest an etiology for obesity in FXS patients. POMC neurons are a heterogenous population. In future studies, addressing regional heterogeneity in the rostral ARC, where there is a decrease in POMC neuronal number in male KO mice, could address which sub-population of neurons that are affected in Fmr1-linked obesity as well as the sub-population that is important in the regulation of locomotion. In addition, future studies determining if differences between

KO males and controls in neurotransmitter and neuropeptide receptor composition also cause POMC neuronal functional heterogeneity. Future studies using chemogenetic approaches in order to determine if Fmr1 gene in POMC neurons is necessary in the regulation of locomotor activity and POMC prohormone processing will provide a new genetic target in POMC neuronal homeostasis.

In chapter three, my work investigated an important environmental factor in obesity pathogenesis, diet, and how that impacts pituitary gland plasticity and hormone gene regulation. My work utilized single cell RNA-seq (scRNA-seq) in order to determine if high fat diet (HFD) induced obesity alters pituitary population plasticity and hormonal gene expression that would lead to changes in hormone secretion. My work determined that somatotrope and lactotrope populations, which are important in the production and secretion of growth hormone and prolactin, respectfully, are drastically changed by HFD. Sub-cluster analysis revealed dynamic population shifts that were induced by HFD. In somatotropes, my work determined enrichment of genes associated with cellular respiration and downregulation in genes important in cholesterol biosynthesis, suggesting that HFD makes somatotropes more metabolically active. While population shifts were the most evident in somatotrope and lactotrope populations, the gonadotropes, which are responsible for the synthesis and secretion of luteinizing hormone (LH) and follicle-stimulating hormone (FSH), did not have changes in cell number but demonstrated the largest changes in gene expression, with a vast majority of genes that are repressed in obesity. Of the genes that were repressed, included *Lhb* and *Gnrhr,* and transcription factors that are involved in their expression. Obese males suffer from reduced LH and

FSH, leading to infertility. Decreases in genes that are important in the regulation of gonadotropins, as indicated by my scRNA-seq data, as well as decreased hormones in serum by Luminex, could explain why obese males are infertile. This work suggests that the pituitary gland is subjected to changes by HFD and is extremely plastic to changes in diet, leading to changes in gene expression and downstream hormone secretion.

Lastly in chapter four, my studies investigated diet and a gene target, the macrophage-secreted protein, resistin-like molecule alpha (RELMα), in sex differences in obesity mediated inflammation. Obese males and females exhibit sex differences in adipose tissue deposition as well as obesity-mediated pathologies. Obesity is a state of chronic inflammation, where adipose tissue homeostasis is disrupted by the increase in pro-inflammatory macrophages to white adipose tissue depots. Obese males are more at risk for metabolic syndrome, cardiovascular disease and stroke, than obese women. The goal of this chapter was to determine immune mechanisms underlying female-specific protection from adipose tissue inflammation in diet-induced obesity. This work determined a previously unrecognized role for RELMα in modulating metabolic and inflammatory responses that is sex-dependent in obesity. Loss of RELMα in female mice on HFD diminished protection from diet-induced obesity, and KO females exhibited more diet-induced inflammatory changes than their male counterparts. Both control and HFD-fed females had a higher proportion of eosinophils in adipose tissue than males. Correlation analysis implicated higher RELMα levels in females contributed to the higher proportion of eosinophils in female adipose tissue, and the protection that was lost in HFD KO females was associated with the loss of eosinophils. Using scRNA-seq of the

stromal vascular fraction (SVF) of visceral adipose tissue, we aimed to uncover adipose tissue heterogeneity, as well as sex-dependent and RELMα-depdenent changes in diet-induced obesity. We discovered the lncRNA, Gm47283, which was the most significantly induced RNA by RELMα deficiency in both males and females. Future work to investigate whether Gm47283 is a downstream effector of RELMα, could explain a potential mechanism on how RELMα-eosinophil-macrophage axis regulates adipose tissue homeostasis in females.

Taken together, the data in this dissertation implicate new genetic and environmental targets of obesity that mediate hypothalamic function and pituitary plasticity with potential new mechanisms for endocrine dysfunction in obesity.